High temperature sensors

based on hydrogen loaded fiber Bragg gratings

Bowei Zhang

A Thesis

in

The Department

of

Electrical and Computer Engineering

Presented in Partial Fulfilment of the Requirements

for the Degree of Master of Applied Science (Electrical and Computer Engineering) at

Concordia University

Montreal, Quebec, Canada

March 2004

Your file Votre référence
ISBN: 0-612-91153-5
Our file Notre référence
ISBN: 0-612-91153-5

Abstract

High temperature sensors based on hydrogen-loaded fiber Bragg gratings

Bowei Zhang

The different topics of this thesis include temperature sensors based on the hydrogen-loaded fiber Bragg gratings, and the thermal stability of hydrogen loaded fiber Bragg gratings in the high temperature range.

The aim of this thesis is to investigate a new type of high temperature fiber Bragg grating. We have fabricated the hydrogen loaded fiber Bragg gratings for high temperature sensor applications. These gratings differ from other types of fiber Bragg gratings, because their refractive index structure is attributed to the change in the hydroxyl groups and germanium oxygen-deficient centers. An annealed hydrogen loaded fiber Bragg grating has shown to survive at temperatures in excess of 936 $^{\circ}$C. The gratings of the sensors retained their reflectivity up to 70%, when they were kept at 700°C for 90 minutes. The annealed fiber Bragg grating can be stabilized at temperatures in excess 700°C for sensor applications.

The main results of this thesis provide a better understanding of the thermal response of the hydrogen-loaded fiber Bragg gratings and their decay behavior at elevated temperatures. It is demonstrated that temperature annealing treatment of these fiber Bragg gratings is able to enhance effectively the grating's thermal stability.

Finally, photosensitivity of pure silica and germanium-doped optical fibers at the presence of hydroxyl groups was also studied.

Acknowledgements

There are a number of people whom have been both directly and indirectly responsible for the successful completion of my thesis. I would like to give special thanks to my supervisor, Professor Mojtaba Kahrizi, for his guidance, encouragement and support. He not only introduced me to the experimental techniques in optics, but also showed me how to present my work more effectively and professionally. He has spent a significant amount of time supervising this work and always had time for my questions over these two years at Concordia University.

I would also like to thank the Faculty of Electrical and Computer Engineering at Concordia University and the Natural Sciences and Engineering Research Council (NSERC) of Canada for their financial support.

A special acknowledgement must also be made to the faculty members of Electrical and Computer engineering who have ever taught me during these two years of graduate studies, especially, Professor Leslie M. Landsberger, Professor Victor Rossokhaty and Professor Chunyan Wang. I would also like to express my thanks to Mr. Shailesh Prasad at the Microelectronics Fabrication Lab for his help during the course of this thesis.

I would also like to thank all the people that I have had the honor to collaborate with over these two years. My thanks go to Jun Li, Steven Mu and all the members of the MEMs research group.

Finally, I would like to express my gratitude to all my friends and family for their tireless love and support over the years, most notably: to my dearest wife, Ning, and to my son, Oliver, who have been supporting me during these years, allowing me to stay in the lab until late nights and during weekends, listening to my problems, encouraging me, and understand me. Their supports provide me a solid foundation for both mind and heart so that I can have the freedom and opportunity to chase my dreams.

Many thanks to all of you!

Bowei Zhang

Table of Contents

List of Figures

List of Tables

List of publications and conference contributions

1. Bowei Zhang, Mojtaba Kahrizi, "Wide range periodic waveguide temperature sensor," Proceeding of the Canadian Conference on Electrical and Computer Engineering (CCECE) 2003, pp. 117-121, Montreal, Canada, 2003
2. Bowei Zhang, Mojtaba Kahrizi, "High-Temperature Bragg Grating Waveguide Sensor," International Conference on MEMS, NANO and Smart Systems (ICMENS'03), pp. 400-404, Banff, Alberta, Canada, 2003
3. Bowei Zhang, Mojtaba Kahrizi, "High-Temperature Bragg Grating Waveguide Sensor," Sensor Letters, submitted.
4. Bowei Zhang, Mojtaba Kahrizi, "Hydrogen loaded Bragg grating in high temperature sensor applications," Conferences of Photonics North 2004, Ottawa, Canada, 2004. The abstract was submitted.

Chapter 1
Introduction

As one of the seven basic quantities used in the SI (International System of Units) system, temperature is probably the most measured physical parameter since the most process in nature and in industry is temperature dependent. Its accurate measurement is essential for the safe and efficient operation and control of a vast range of industrial processes. Appropriate techniques and instrumentation are needed depending on temperature measurement requirements in different industrial processes and working environments.

The aim of this thesis is to develop a simply temperature sensor based on hydrogen loaded fiber Bragg grating (FBG) capable of operation at high temperature environment. Over the past ten years, there has been a large quantity of development and research in the field of low temperature fiber optic sensors but the area of high temperature fiber optic sensors is comparatively immature. Due to the decay of the reflectivity of the fiber Bragg gratings, especially the decay of the reflectivity of hydrogen loaded fiber Bragg gratings [1], the grating based temperature sensors are usually used under 200 °C. This thesis presents details of the sensor design and brings forth some important issues during the development process that ranging from materials concerns to implementation details.

Chapter 1 briefly introduces the concepts of optical fiber sensors and the temperature sensors based on the fiber Bragg grating.

1.1. The role of the fiber Bragg gratings

Fiber Bragg gratings are emerging as very important elements for both the optical fiber communications and sensing fields. Applications include used in a wide range of devices for wavelength routing, filtering, gain flattening, dispersion compensation in communications systems, a range of distributed strain [2], and temperature sensing systems. The inherent advantages of fiber optical sensors areas follow:

1. Lightweight, tiny, passive, low-power and resistant to electromagnetic interference.
2. High sensitivity.
3. Huge bandwidth.
4. Environmental ruggedness.

The concept fiber optic sensing is based on the modulation in the sensing head, by a particular measurand, of one or more of the parameters of the light, which is guided by an optical fiber, being possible the measurand to act directly on a particular section of the fiber, in case the light never exits the fiber (intrinsic sensor), or acting on a structure illuminated by light guided by the fiber (extrinsic sensor).

The light parameters that can be modulated are intensity (energy), polarization state, phase, and wavelength. Each of these parameters gives to the correspondent class of fiber optic sensors. Conceptually, the intensity based sensors are the one that requires more accessible fiber technology (multimode technology); therefore, the intensity based sensors was the first being researched and also the first having more deeply penetrated the market. Later on, considerable work was directed to polarization and phase based fiber optic sensors essentially due to the possibility of measuring large electric currents

(polarization modulation via Faraday Effect) and the possibility of measurement to a large range of parameters with very high sensitivity (phase modulation). In parallel, substantial effort was concentrated with the objective of studying the criteria for the most efficient multiplexing of these sensors.

Fiber Bragg gratings are simple, intrinsic sensing elements, which can be "writing" in to a photosensitive fiber using the UV light and have all the advantage attributed to fiber sensors. Fiber Bragg gratings behave like "flake mirrors" in fiber that reflect specific wavelengths due to periodic changes in the index of refraction of the fiber core. The small reflections from these "flake mirrors" add together in a phenomenon known as the Bragg reflection, where a single large reflection results from the coherent addition of many small reflections spaced a multiple of half the wavelength apart ($m\lambda = 2L$) (See chapter 2). The wavelength that is reflected by the fiber Bragg grating can be changed in two ways, changing the ambient temperature of the fiber grating, or inducing strain in the fiber grating along the direction of the fiber.

In principle, wavelength modulation should be the most favorable sensing method owing to its absolute nature and basically unaffected by environmental noise or power loss; however, in the past several years, research on fiber sensing dodged this type of sensors, because of lacking of fiber components with appropriated performance. In recent years, fiber Bragg gratings proved a breakthrough being an almost ideal component for the in-fiber localized monitoring of physical parameters, of notably strain and temperature (See chapter 4). It can be stated that a large effort of research in fiber optic sensors will be directed to the application of these devices in functional sensing structures in the future.

An emerging technological field of great importance, where fiber sensing has a crucial role to play, is fiber optic smart structures. This area developed from new advances in the technology of composite materials. The needs of monitor certain parameters soon demanded the incorporation of sensors in these materials. Buildings and bridges that can call up central maintenance depots and report on their status as well as aircrafts that monitor, communicate and correct for structural changes in flight are examples of applications, which require materials that are lighter in weight, have superior strength and have the ability to change dynamically the shape and the degree of stiffness; therefore, the new materials must be "smart", with the ability to sense environmental changes within or around the structure and to communicate with a central system, so is able to interpret and react to these changes. The realization of these objectives requires a "nervous system" capable of sensing changes in the material while being itself part of the structure.

Fiber optic sensor technology, particularly fiber Bragg gratings, has enabled the implementation of this type of systems by providing sensors that are small and rugged enough that they can be integrated and consolidated directly into materials; therefore, these sensors brings with them weight reduction, minimization of points of ingress into materials, electrical isolation and immunity to electromagnetic interference.

In addition, the devices have an inherent self-referencing capability and easily multiplexed in a serials fashion along single fiber. Grating based sensors appear to be useful for a variety of applications. In particular the area of distributed embedded sensing in materials for creating "smart structures" is of primary interest. Fibers with sensor arrays can be embedded into the materials to allow measurement of parameters such as

load, strain, temperature, and vibration. As an example [3], Figure 1.1 shows the Stork Bridge in Winterthur, Switzerland, in which of carbon fibre reinforced plastics (CFRP) cables were used instead of the conventional steel cables. Each CFRP equipped with an array of seven Bragg gratings as well as other types of regular sensors.

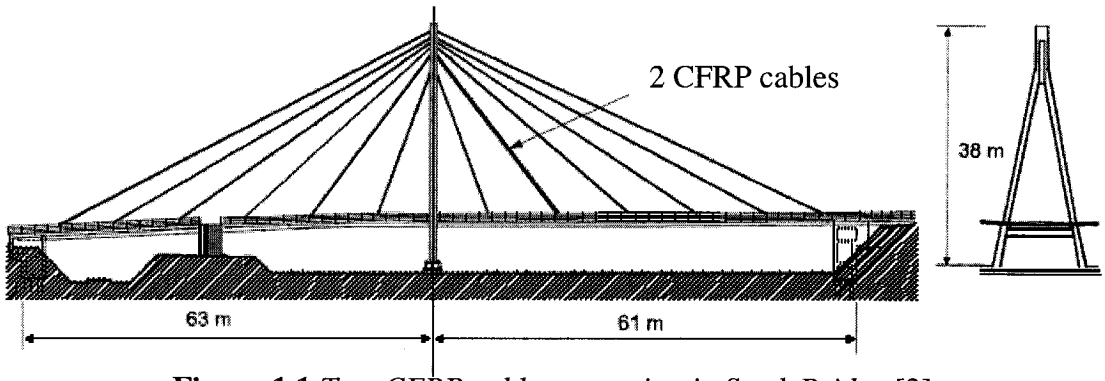

Figure 1.1 *Two CFRP cables are using in Stork Bridge* [3].

Fiber Bragg gratings may also prove to be useful as the optical sensing element in the other fiber sensor configurations: grating based chemical sensors, pressure sensors, and accelerometers are examples.

The major disadvantages associated with using fiber optic sensors are [4]:

- May need to isolate sensor from unwanted parameters
- Availability of optical sources
- Cost and availability of suitable instrumentation
- Long term stability needs to be examined
- Low general awareness of fiber optic sensor technology

1.2. The role of temperature sensors based on fiber Bragg grating

For the fiber Bragg grating based temperature sensor, a variation in temperature causes a modification of the grating period and an induced modification of the refractive index of the material. The variations in the period and refractive index of the grating cause a shift in its reflected peak wavelength. And by measuring this shift, the applied temperature can be measured. The change of the temperature induces variations in the wavelength of the grating, which can be observed in either optical spectrum analyzers (OSA) or wavelength interrogators. The over change is ~6.8pm/°C near the Bragg wavelength of 830 nm, ~10pm/°C near 1300 nm, and ~13pm/°C near 1550nm although the values depend on FBG types [5]. The Bragg wavelength with temperature has been widely used for temperature sensing or temperature compensation over a lower temperature range [6] because Type I grating is erased within seconds when exposed to temperature of the order of 500 °C [7]. The accuracy of these temperature sensors depend on the wavelength detector. As an example [8], Figure 1.2 shows fiber Bragg grating based temperature sensors into the stator bars of a two pole air cooled turbo generator.

Using fiber Bragg gratings as sensor heads has a series of advantages that make it very attractive for smart structures over the other conventional fiber optic and electrical sensors. Firstly, the Bragg wavelength shifting is a linear function of the measurands over large ranges. Secondly, the measurand information is encoded as the wavelength change; hence, the sensor signal are basically unaffected by environmental noise or power loss. Thirdly, fiber Bragg gratings are absolutely light in weight. Due to their small diameters, they can be inserted into composite materials without disturbance. Finally, various types of sensor multiplexing such as Time Division Multiplexing (T.D.M.), Wavelength

Division Multiplexing (W.D.M.), Spatial Division Multiplexing (S.D.M.), and code division multiple accesses (CDMA) etc., as well as their combinations, can be implemented to form quasi-distributed or quasi-point sensor array systems.

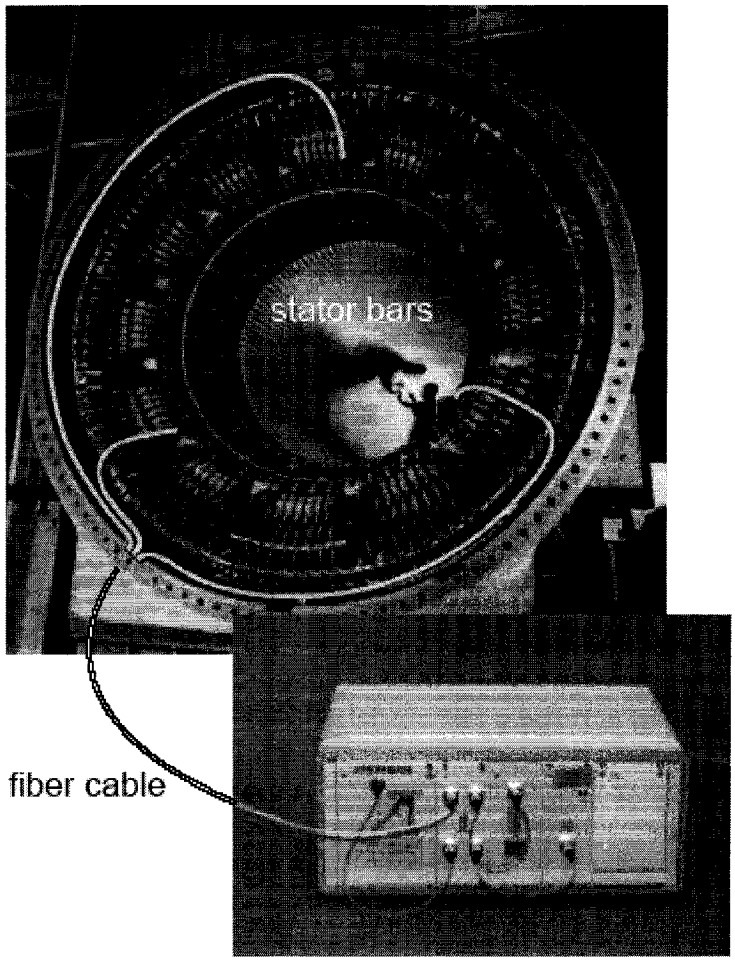

Figure 1.2 *Fiber Bragg grating based temperature sensor system built into the stator bars of a two-pole air-cooled turbo generator* [8].

Bragg gratings are refractive index structures manufactured by exposing the core of an optical fiber to intense periodic ultraviolet radiation. The ability of change the refractive index with radiation is referred to as photosensitivity (See chapter 2). Although photosensitivity in optical fiber has been extensively studied over several decades, no unified theory for the physical and chemical mechanisms responsible for the changes in refractive index has been provided. One explanation of the lack of a unified theory is that

the photosensitive response may differ significantly depending on several factors such as the type of fiber, prior treatment of the fiber, UV writing wavelength, and the UV laser writing power.

In most cases, the ideal situation would be to inscribe gratings into the low-loss standard telecommunications fiber that is used in optical networks today. This would enable 100 % fiber compatibility and the use of low-cost mass-produced fibers; however, standard telecommunications fibers used today have a very low photosensitivity. Solutions to this problem have been designed special photosensitive fibers and/or methods to make non-photosensitive fibers more sensitive to UV radiation. Recently, the most used technique is the standard telecommunication fiber (SMF-28 silica fiber with 3% GeO_2) loaded with hydrogen. This loaded fiber is called hydrogen-loaded fiber. Because it has extremely high photosensitive for the 248 nm wavelength, nearly all the fiber Bragg gratings are produced in manufactory using the hydrogen loaded fiber.

This technique that Bragg gratings are made by hydrogen loaded fiber has fatal limitation. It was found that when increasing the ambient temperature the grating reflectivity started to decay and did not completely stabilize even for long treatment times. Additional increased temperature results in an even larger decrease in reflectivity. Although the gratings appeared to be stable at room temperature, this behavior placed significant limitations on deployment, considering the required lifetime of some components in the telecommunications industry exceed several decades. The problems facing sensor applications are even more stringent, as the temperature sensor may be used in harsh environment comparing with the typical –40 to +80 °C temperature requirements for telecommunications.

1.3. Thesis layout

Chapter 1 Fiber Bragg grating sensors, especially the temperature sensors based on the hydrogen loaded fiber Bragg grating was introduced in this prologue.

Chapter 2 In this chapter, we will give the reader a general understanding of different areas in the fiber Bragg grating's field, such as fiber Bragg gratings and photosensitivity of grating. This chapter deals with definitions of Bragg gratings, their applications, manufactory technique and a short summary of the color center mode theory of the mechanisms responsible for the change in refractive index.

Chapter 3 This chapter is an overview of hydrogen loaded fiber grating and the issues regarding the thermal stability of fiber Bragg gratings. The thermal treatment of Bragg gratings will be discussed in this chapter. As well as being a building block, hydrogen has played a central role in the hydrogen-loaded fiber Bragg grating.

Chapter 4 The goal of this chapter is to present three hypotheses of high temperature sensor design based on the hydrogen loaded fiber Bragg grating. This three hypotheses are summarized in my studies of the thermal decay of fiber Bragg grating's reflectivity. Meanwhile, the relationship between Bragg wavelength and temperature is also discussed in this chapter.

Chapter 5 The process of the three-designed hydrogen loaded fiber Bragg grating being tested is described in this chapter. My experimental results during the testing and evaluations in a temperature range from room temperature to 936 °C are presented. The hydrogen-loaded fiber Bragg grating working at high temperature range as well as the setting of the experiment ensures the theoretical and practical accomplishment.

Chapter 6 In this chapter, the conclusions base on the fountainhead from the results presented in the previous chapter and future direction are delivered.

Chapter 2
Fiber Bragg gratings and photosensitivity

Bragg gratings are refractive index structures manufactured by exposing the core of a germanium doped silica fiber to intense periodic ultraviolet radiation. The ability to a permanent change in the refractive index of the fiber core with radiation is referred to as photosensitivity. This chapter is an introduction to fiber Bragg gratings and photosensitivity and gives a basic understanding of different areas in the field. This chapter deals with definitions of Bragg gratings and their applications, how they are made and a short summary of the different theories of the mechanisms responsible for the change in refractive index. Finally, a brief introduction to the fabrication of Bragg grating will be given.

2.1. Fiber Bragg gratings

A fiber Bragg grating is an optical fiber for which the refractive index in the core is forming a periodic or quasi-periodic index modulation profile. One of the most important properties of fiber Bragg gratings is wavelength-selective reflection. Assume that a broadband light is coupled into a fiber with fiber Bragg grating inside. The light whose wavelength matches the Bragg condition will be reflected back. The light whose wavelength does not match the Bragg condition will be transmitted through the fiber, as shown in Figure 2.1.

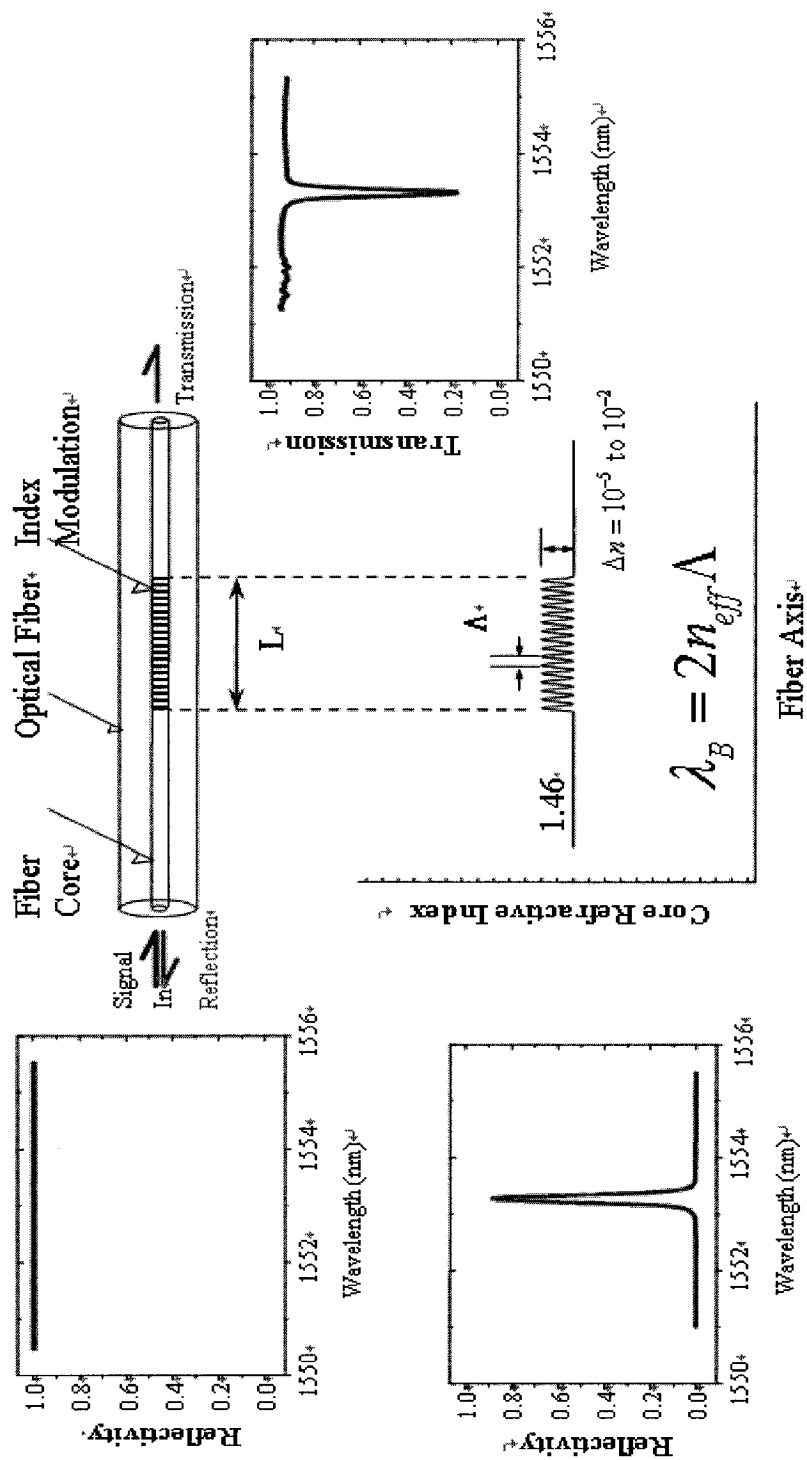

Figure 2.1 *Illustration of uniform fiber Bragg grating and its wavelength selective reflection property.*

The Bragg grating condition is simply the requirement that satisfies both energy and momentum conservation. Energy conservation ($\hbar\omega_f = \hbar\omega_i$) requires that the

frequency of the incident radiation and the reflected radiation is the same. Momentum conservation requires that the incident wave-vector, κ_i, plus the grating wave-vector, K, equal the wave-vector of the scatted radiation κ_f. This simply stated as

$$\kappa_i + \mathrm{K} = \kappa_f \tag{2.1}$$

Where the grating wave-vector, K, has a direction normal to the grating planes with a magnitude $2\pi/\Lambda$ (Λ is the grating spacing shown in Figure 2.1). The diffracted wave-vector is equal in magnitude, but opposite in direction, to the incident wave-vector. Hence, the momentum conservation condition becomes

$$2\left(\frac{2\pi n_{eff}}{\lambda_B}\right) = \frac{2\pi}{\Lambda} \tag{2.2}$$

Mathematically, the first order Bragg condition is give by:

$$\lambda_B = 2n_{eff}\Lambda \tag{2.3}$$

where λ_B is the Bragg wavelength, n_{eff} is the effective modal index and Λ is the perturbation period. By modulating the quasi-periodic index perturbation in amplitude and (or) phase, we may obtain different optical filter characteristics.

The simplest uniform fiber Bragg grating structure in optical fibers is an axial (z) and periodic change of the refractive index of the core, as shown schematically in Figure 2.2, with a refractive index modulation given by [9]:

$$n(z) = n_0 + \Delta n \cos(\frac{2\pi z}{\Lambda}) \tag{2.4}$$

where Δn is the amplitude of the induced refractive index perturbation (typical values 10^{-5}~10^{-2}); n_0 is the average refractive index; z is the distance along the fiber's longitudinal axis; and Λ is the geometrical grating period.

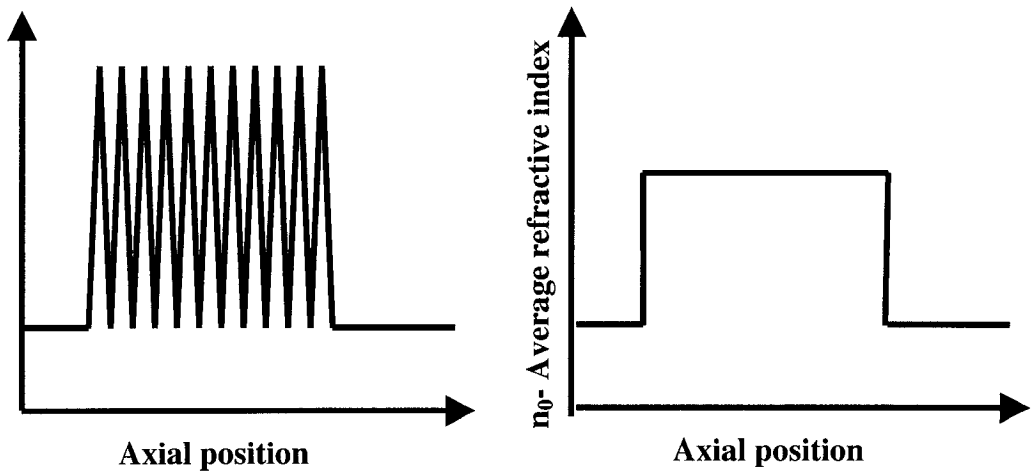

Figure 2.2 *Schematic of refractive index modulation and effective refractive index of the grating structure.*

The spectral reflectivity of the grating, solved using coupled-mode theory, is given by: [10]

$$R(L,\lambda) = \begin{cases} \dfrac{\Omega^2 \sinh^2(SL)}{\Delta\beta^2 \sinh^2(SL) + S^2 \cosh^2(SL)} & \text{for } \Omega^2 > \Delta\beta^2 \\ \dfrac{\Omega^2 \sinh^2(QL)}{\Delta\beta^2 - \Omega^2 \cosh^2(QL)} & \text{for } \Omega^2 < \Delta\beta^2 \end{cases} \tag{2.5}$$

where R(L,λ) is the reflectance as a function of wavelength λ, and fiber Bragg grating length L; Ω is the coupling coefficient; $\Delta\beta = \beta - \pi/\Lambda$ is the detuning wave-vector; $\beta = 2\pi n_0/\lambda$ is the propagation constant; Λ is the Bragg grating period; and $S = \sqrt{\Omega^2 - \Delta\beta^2}$, Q = iS For the single-mode sinusoidal modulated grating as described by Eq. (2.2), the coupling constant Ω is given by[11]:

$$\Omega = \frac{\pi\Delta n}{\lambda}\eta \tag{2.6}$$

where η is the fraction of the fiber mode power contained by the fiber core , which can be approximately expressed as

$$\eta = 1 - V^2 \tag{2.7}$$

where V is the normalized frequency of the fiber and it given by $V = (2\pi a/\lambda)\sqrt{n_{co}^2 - n_{cl}^2}$, where a is the core radius and n_{co} and n_{cl} are the core and cladding refractive indices, respectively.

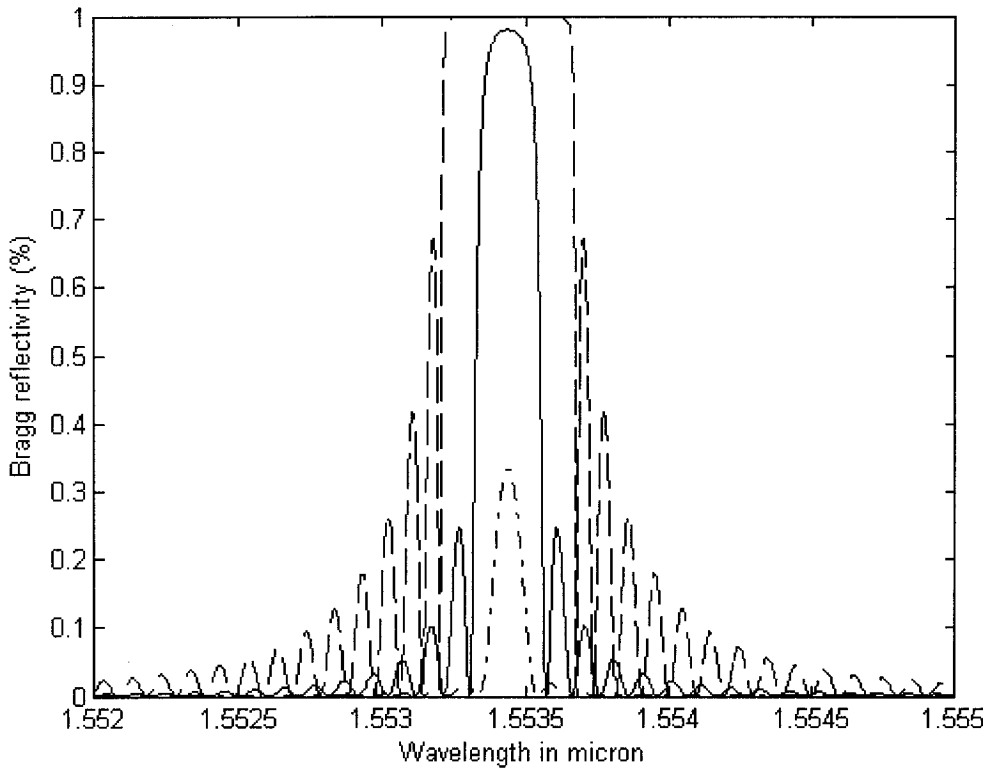

Figure 2.3 *Simulation of the reflection spectra of an 8 mm long uniform Bragg grating as a function of wavelength with different coupling constant. Dashed line:* $\Delta n = 5\times10^{-4}$*; solid line:* $\Delta n = 2\times10^{-4}$*; and dash-dot line:* $\Delta n = 0.5\times10^{-4}$.

As an example, a calculated refraction spectrum as a function of the wavelength is shown in Figure 2.3. The following parameters are used during calculation: $NA = 0.14$, $a = 4.2\ \mu$m, $\Delta n = 5\times10^{-4}$ $\Lambda = 0.532\ \mu$m, and the grating length $L = 8$ mm. The dashed line corresponds to the strong coupling case, with $\Delta n = 5\times10^{-4}$. The solid line corresponds to the strong coupling case, with $\Delta n = 2\times10^{-4}$. The dash-dot line corresponds

to the weak coupling case, with $\Delta n = 0.5\times10^{-4}$. From this figure, it can be seen that a higher reflectivity is achieved for the stronger coupling case.

At the Bragg grating center wavelength, the detuning factor $\Delta\beta = 0$. Thus, the peak reflectivity of the Bragg grating is [11]

$$R(L,\lambda) = \tanh^2(\Omega L) \tag{2.8}$$

From Eq. (2.8), it can be seen that the peak reflectivity increases as the refractive index modulation depth Δn and/or grating length L increases. A general expression for the approximate full-width-half-maximum (FWHM) bandwidth of the grating is give by [12]

$$\Delta\lambda = \lambda_B \cdot q\sqrt{\left(\frac{\Delta n}{2n_0}\right)^2 + \left(\frac{\Lambda}{L}\right)^2} \tag{2.9}$$

where q is a parameter that approximately equals 1 for strong gratings (with near 100% reflection), whereas q ~ 0.5 for weak grating. Λ/L is the number of fringes (typically Λ/L~20 000 for a 10 mm long grating).

2.2. History

In 1978, Hill and coworkers [13] reported the first observation of photosensitivity in optical fibers when exposing a germanium doped silica core fiber with coherent counter propagating light from an argon-ion laser at 488 nm wavelength. The result was a periodic change in the refractive index corresponding to the period of the interference pattern generated by the two beams. As the light reflected from the gratings has the same wavelength as that used to write the grating, this technique is limited to applications using wavelengths at or near the writing wavelength. Almost a decade later, in 1989, Meltz *et al.* [11] presented the transverse holographic method using a writing wavelength

of 244 nm (5 eV), which made it possible to write gratings at wavelengths other than the writing wavelength. Previous studies of the growth dynamics of the grating strength, when using counter propagating waves, showed that the photosensitivity using 488 nm wavelength was a two-photon process . The writing wavelength of 244 nm used by Meltz et al. coincided with a germanium oxygen-vacancy defect band and the second harmonic of the wavelength used by Hill. Since the discovery of photosensitivity in optical fiber by Hill and the developments of the transverse holographic writing method by Meltz, thousands of articles have been published concerning photosensitivity and Bragg gratings. Today, fiber Bragg gratings have become almost synonymous with the field itself. Most fiber-optics sensor system makes use of Bragg grating technology [6, 7].

2.3. Classification of fiber Bragg gratings

Several different types of fiber Bragg gratings have been reported. The following sections briefly describe two different classification schemes based on the coupling characteristics and the growth behavior of the grating during manufacturing [5, 6].

2.3.1. Classification by coupling characteristics

There are three different types of basic gratings depending on the coupling function. The Bragg gratings described previously are usually referred to as ***short period gratings***. The grating period is typically 0.22-0.54 μm with the light coupled into the backward propagating direction, reflection. By tilting the fringes of short period gratings, it is possible to couple light out from the core into backward propagating radiation modes. These loss gratings are usually referred to as ***slanted*** or ***tilted gratings*** [14]. Such gratings have been used for gain equalization in erbium-doped fiber amplifiers.

The third type of gratings is referred to as ***long-period gratings*** [15]. These gratings have a period that is typically 100-500 μm and the light is coupled into forward propagating cladding modes. Acting as loss filters, these gratings are typically used for gain equalization. Due to the long period of the grating, they can be successfully manufactured using point-by-point writing with either UV exposure or heat. For local heating of the fiber, a CO_2-laser or an electric-arc discharge can bee used.

3.3.2. Classification by growth characteristics

There is also a classification scheme used depending on the growth behavior of the grating during inscription. This scheme is mainly used to describe short-period gratings. Prior the discovery of photosensitivity in fibers, ***surface relief gratings*** was used for some applications. Here a surface corrugation/modification of cladding near the core results in interacting with the evanescent field causing strong reflection. These gratings were typically manufactured through etching or polishing [16].

Type 0 gratings or *Hill gratings,* are the self-organized gratings, discovered by Hill *et al.* [13], formed by launching light in the fiber from which partial reflection at the cleaved fiber end-face creates the periodic interference pattern. As the grating is formed more light will be reflected within the fiber and hence increase the growth rate of the grating. These gratings have limited use, as the writing wavelength is also the Bragg wavelength of the grating.

Type I gratings refers to the most common gratings characterized by a monotonous growth. It is commonly observed in most photosensitive fibers under either continuous wave (CW) or pulsed UV irradiation. More specifically, this classification refers to a grating produced with 100mJ/cm^2/pulse. It is interesting to note that the reflection

spectrum of the guiding mode is complementary to the transmission signal, implying that there is negligible loss due to absorption or reflection into the cladding. This is a fundamental characteristic of a Type I Bragg grating. Furthermore, due to the photosensitivity type of the Bragg grating, the grating itself has a characteristic behavior with respect to temperature erasure. Type I gratings can be erased at relatively low temperatures (approximately 200 ^{O}C). Nevertheless, Type I gratings are the most utilized Bragg gratings and operate effectively from -40 ^{O}C to +80 ^{O}C, a temperature range that satisfactorily covers most telecommunications and sensor applications [7].

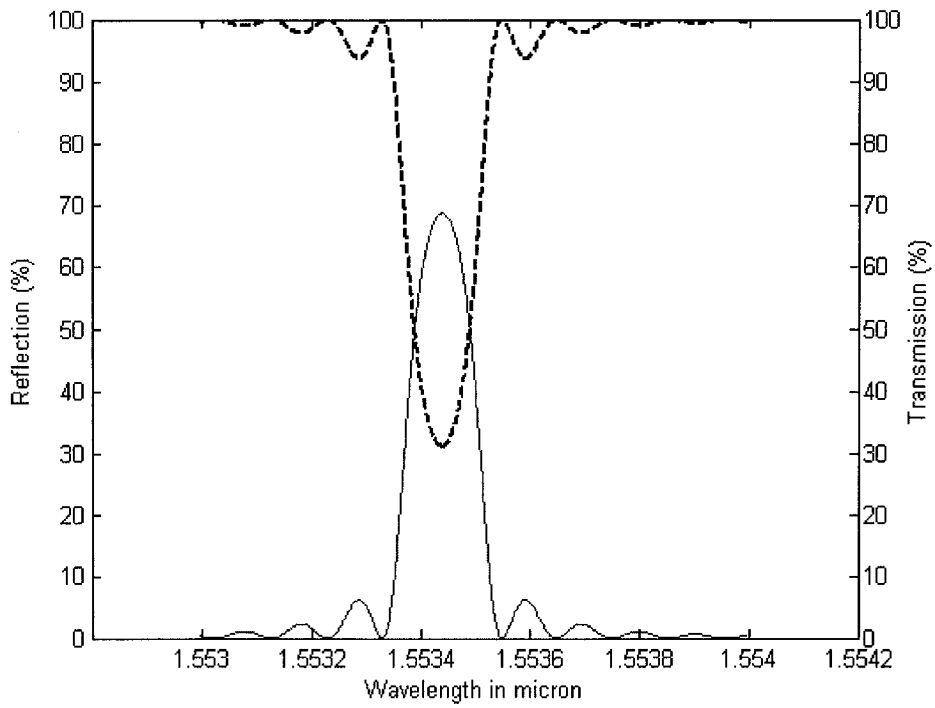

Figure 2.4 *A typical spectral response of a uniform period, Type I grating. Transmission and reflection spectral of a broadband light source in the region of the Bragg condition is satisfied.*

Type II gratings are high power single-pulse (>0.5J/cm^2) "damage" gratings characterized by large losses on the short wavelength side of the Bragg wavelength [17]. The damage is often localized at the core-cladding interface. The typical transmission and

reflection spectrum of Type II grating can be described as following: The reflection appears to be broad and several features over the entire spectral profile are believed to be due to non-uniformities in the excimer beam profile that are strongly magnified by highly nonlinear response mechanism of the glass corn. Type II gratings pass wavelengths longer than Bragg wavelength, whereas shorter wavelengths are strongly coupled into the cladding, as is observed for etched or relief fiber grating, permitting their use as effective wavelength selective taps.

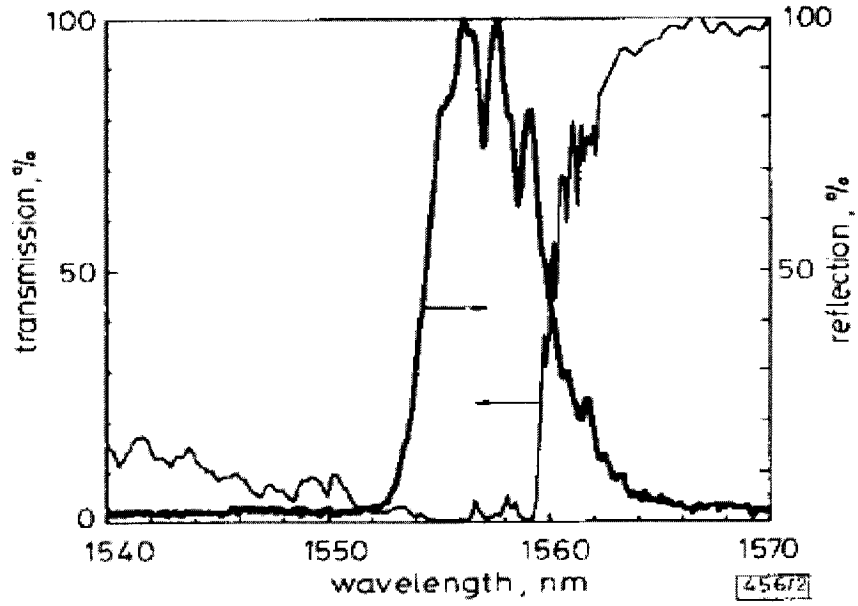

Figure 2.5 *Reflection and transmission spectra of a Type II grating. At wavelengths below the Bragg wavelength of 1556 nm the light is strongly coupled into the cladding* (from [17]).

Results of stability tests have shown Type II gratings to be extremely stable at elevated temperature. At 800 ^{O}C over a period of 24 hours, no degradation in grating reflectivity was evident. At 1000 ^{O}C most of the gratings disappears after 4 hours,

implying that the localized fusion has been thermally "washed out". This superior temperature stability can be utilized for sensing applications in hostile environments [7].

Type IIa gratings are characterized by the fact that the reflection initially grows as for type I gratings then decreases followed by a subsequent growth. Also referred to as negative index gratings, these gratings probably contain two components; one positive index grating (type I) and one negative index grating [18]. Type IIa gratings are most often observed in high GeO_2-doped fiber (>25%, high numerical aperture (NA) fibers). It is almost certain that the mechanisms responsible for Type I and Type IIa are different. It is interesting to point out that the formation and erasure of a Type I spectrum induces a shift in Bragg wavelength toward the red part of spectrum; increase both the mean and modulated index changes. At the time of erasure, the Bragg wavelength either shifts toward the blue part of the spectrum or does not significantly shift in the course of the Type IIa grating inspection [7].

2.4. Mechanisms of photosensitivity

This section is a short summary of the color-center model to clarify different suggested mechanisms for photosensitivity. Here just give references [6], [7], and [19].

Defects are important to optical fibers because their absorption bands cause deleterious transmission losses; these defects are called color-centers. Photosensitivity in germanium doped fibers was an absorption band peaking at ~240 nm [11] which was attributed to germanium-oxygen deficiency [120]. Irradiating the core, using near 240 nm wavelength, results in bleaching of the 240 nm band and growth of absorption bands located near 190 nm [21]. An example from R. M, Atkins *et al.* [22] of changes in the

absorption of germanium doped silica after 248 nm UV irradiation is shown in Figure 2.6. The absorption spectrum in the UV range is as shown in Figure 2.7 [22].

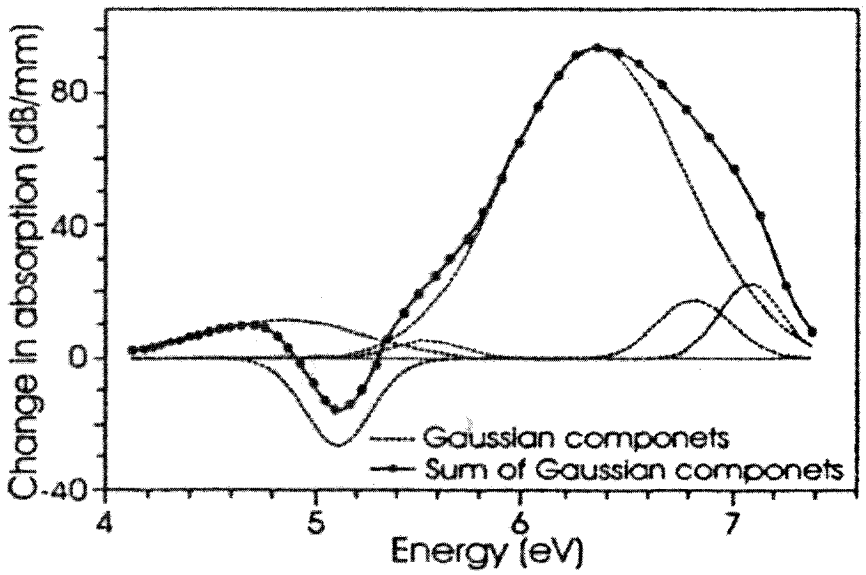

Figure 2.6 *Changes in the UV absorption spectra for 3 mol% germania MCVD fiber perform core: data point (solid circuits), six Gaussian components of fit (dashed line), and sum of Gaussian components (solid line)* (from [21]).

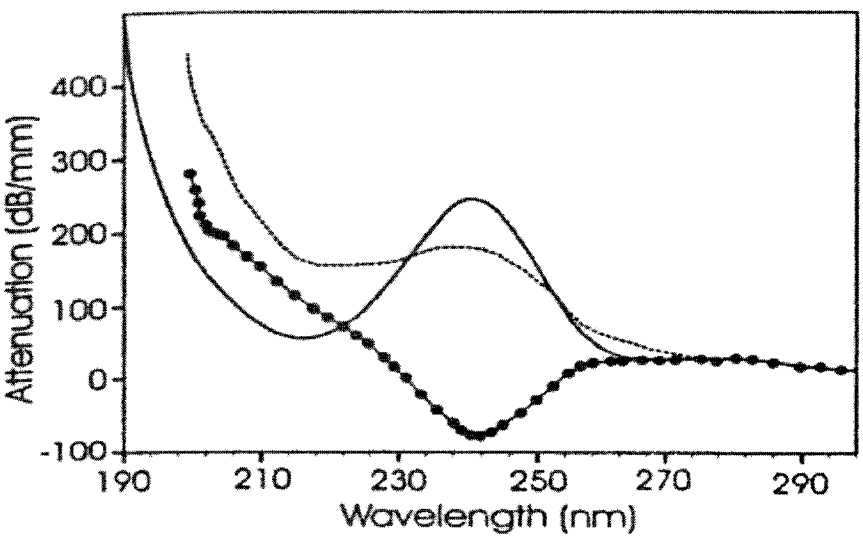

Figure 2.7 *UV absorption spectra before (solid line) and after 248 nm exposure (dashed line) writing an 81% peak reflectivity grating in AT&T Accutether single-mode fiber. The change in attenuation (solid circles) is also shown* (from [22]).

A number of different defects [7] have been observed of which the most commonly discussed are schematically shown in Figure2.8 and Figure2.9. Correlative absorption bands for the main defects are given in Table 2.1.

Table 2.1 Correlative absorption bands for the most common defects related to photosensitivity.

Table 2.1 absorption bands for the defects		
Defect	Absorption peak	Reference
NBOHC	260 nm	[6]
Peroxy radical	160 nm	[7]
SiE'	215 nm	[7]
GODC	240 nm	[7]
Ge(1)	282 nm	[22]
Ge(2)	214 nm	[22]
GeE'	195 nm	[7]

Generally, Germanium oxygen deficient centers (GODC) are precursors [7] and GeE´, Ge(1) and Ge(2) are products of the photochemical processes although there are numerous different photochemical pathways, which have been presented to explain transformation of defects and the glass structure. The results of Atkins *et al.* [22], who measured the UV induced absorption change down to 165 nm, indicated that the main absorption changes in germanium-doped silica are due to bands at 195 nm (6.35 eV) and 242 nm (5.1 eV).

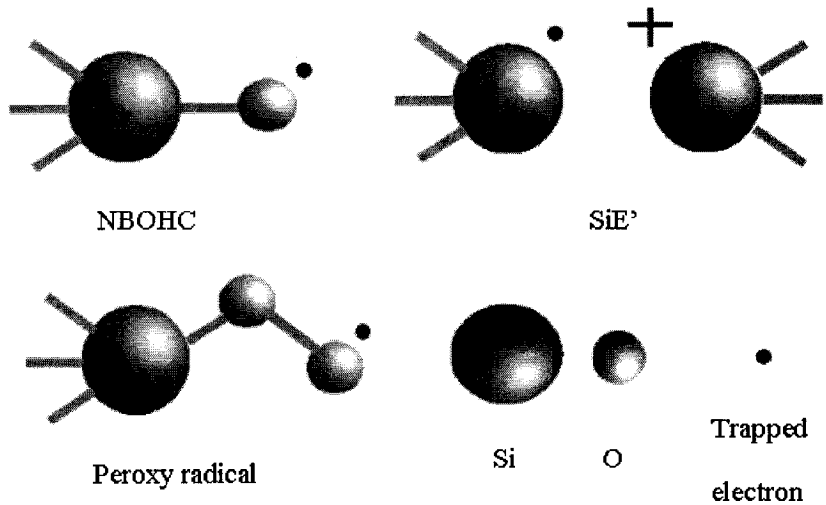

Figure 2.8 *The structure of point defects in silica (NBOHC – Non bonding oxygen hole center).* See e.g. [6, 7]

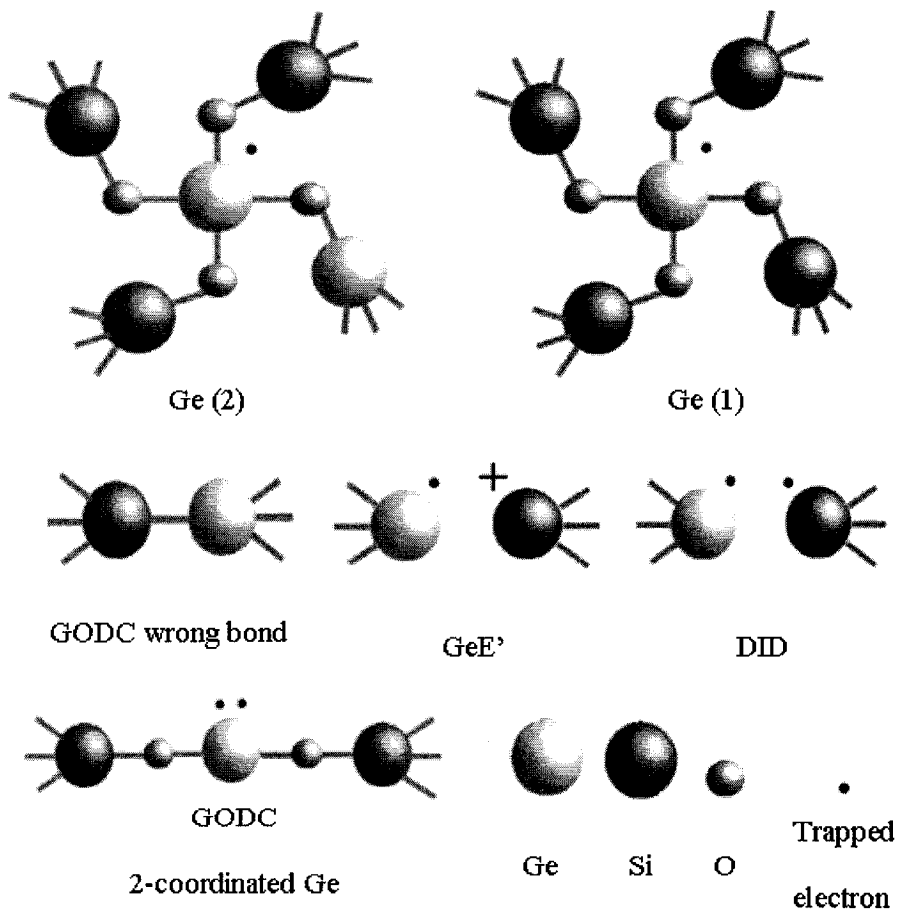

Figure 2.9 *Possible GODC (GODC – Germanium oxygen deficient center) candidates. The GeE' center and the Ge(1) and Ge(2) electron trap centers and DID (DID -- Drawing induced defect).* See e.g. [6, 7]

The photosensitivity of germanosilicate optical fibers has attracted considerable interest because it allows one to imprint index gratings in the fiber core. Such gratings can be written by pulse UV radiation with the excitation of a singlet–singlet (S_0 –S_1) transition band (240 nm) of a germanium–oxygen-deficient center (GODC) [23]. The mechanism of the index change has been actively debated, but this phenomenon has not been completely clarified to date. Nevertheless, the GODC photo-excitation is certainly an initial stage of this process for the Type I and Type IIa gratings. A schematic for the GODC singlet-singlet (S_0-S_1) transition band is shown in figure 2.10 and 2.11.

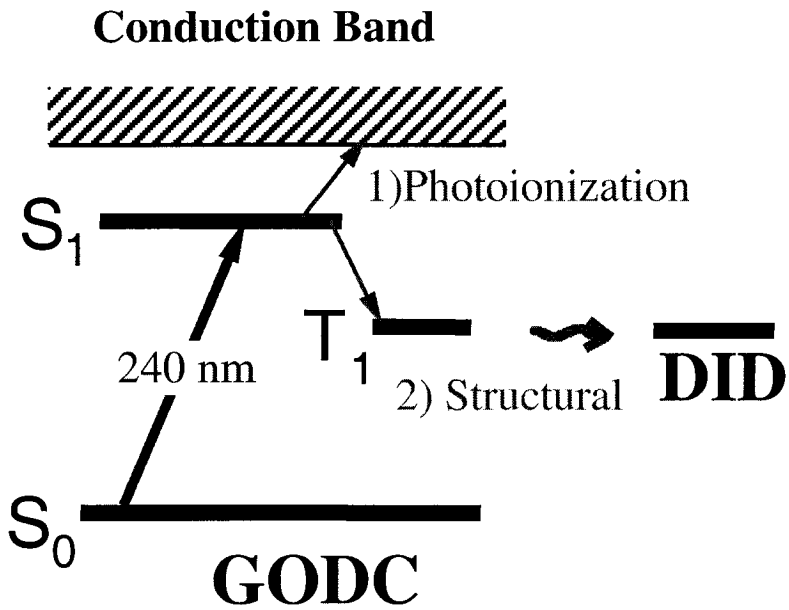

Figure 2.10 *Energy level diagram of a germanium oxygen deficient defect, showing proposed pathway with pulsed UV laser at 240 nm. The excited triple state relaxes into a new defect state, a drawing-induced defect. This relaxation causes the index change that makes the Bragg gratings* [23].

Light at 240 nm excites a GODC from its ground single state S_0 to its excited state S_1 from which it can ionize spontaneously or by absorbing another 240 nm photo-such ionization is thought to be necessary for an index change. However, a GODC excited to S_1 can also relax to the long-lived triplet-stat T_1. From there the defect undergoes a

metamorphosis and changes its structure to a DID (Drawing induced defect). It is proposed that structural rearrangement of GODC into the DID is the principal cause of light induced change of refractive index modulation.

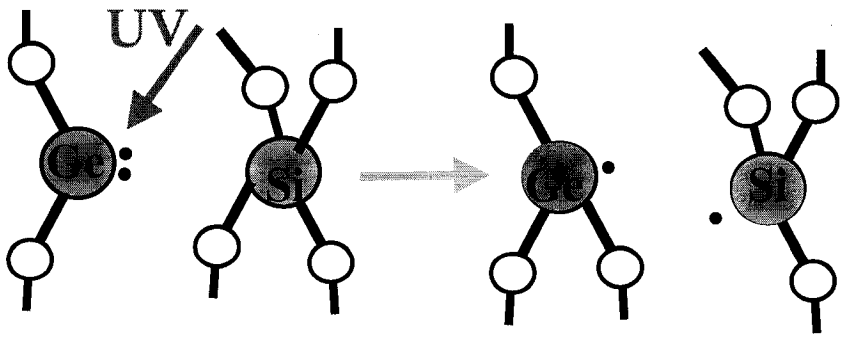

Figure 2.11 *Model of pulsed UV-induced structure change in germanosilicate optical fibers. The structural rearrangement of GODC into the DID is the principal cause of light induced refractive index change.*

2.5 Fiber Bragg grating fabrication using phase mask

The previous section described the absorption and photosensitivity of the optical fiber. Now, we turn to the more challenging task of fabricating Bragg gratings using the phase mask technology. As discussed in section 2.3.1, the periodicity of Bragg gratings ranges from 220 – 540 nm, which places them just beyond the reach of conventional photolithography. The purpose of this section is to introduce phase mask interference lithography and the fabrication of the conventional Bragg gratings using phase mask technology briefly.

2.5.1 Phase Mask Interference Lithography

One of the most effective methods for patterning Bragg gratings in photosensitive fiber is the phase mask technique [11]. This method employs a diffractive optical element to modulate the UV laser writing beam. Generally, phase masks may be formed either

holography or by electron beam lithography. One of the advantages of the electron beam lithography over the holographic technique is that complicated patterns can be written into the mask's structure such as quadratic chirps and patterns.

Phase masks are corrugated circular pieces of silica. Usually, it is a relief grating etched in a silica plate. Each phase mask has a different pitch (periodicity) to the corrugated ridges on its surface. This pitch determines what wavelength of Bragg grating will be manufactured. Figure 2.12 depicts the most common configuration for phase mask photolithography. The phase mask functions to split the incoming UV light into multiple diffracted beams. For the UV radiation at normal incident (the incident angle is equal zero), the diffracted radiation is split into $m = 0$ and ± 1 orders, as shown in Figure 2.12. The phase mask, which is used in fabrication of Bragg gratings, is carefully designed to suppress the 0^{th} diffracted order (the etched depth $d = \lambda_{uv} /(2(n_{uv} - 1))$). The + 1 and −1 diffracted orders interfere, leading to a standing wave pattern. It is relatively easy to verify that the periodicity of the resulting standing wave is half the period of phase grating on the mask [6].

$$\Lambda_g = \frac{N\lambda_{Bragg}}{2n_{eff}} = \frac{\Lambda_{PM}}{2} \tag{2.10}$$

where N≥1 is an integer indicating the order of the grating period.

This result applies regardless of the wavelength of illumination (provided the illuminating wavelength is short enough to produce ± 1 orders.) This means the phase mask lithography does not require narrowband coherent laser to produce a grating.

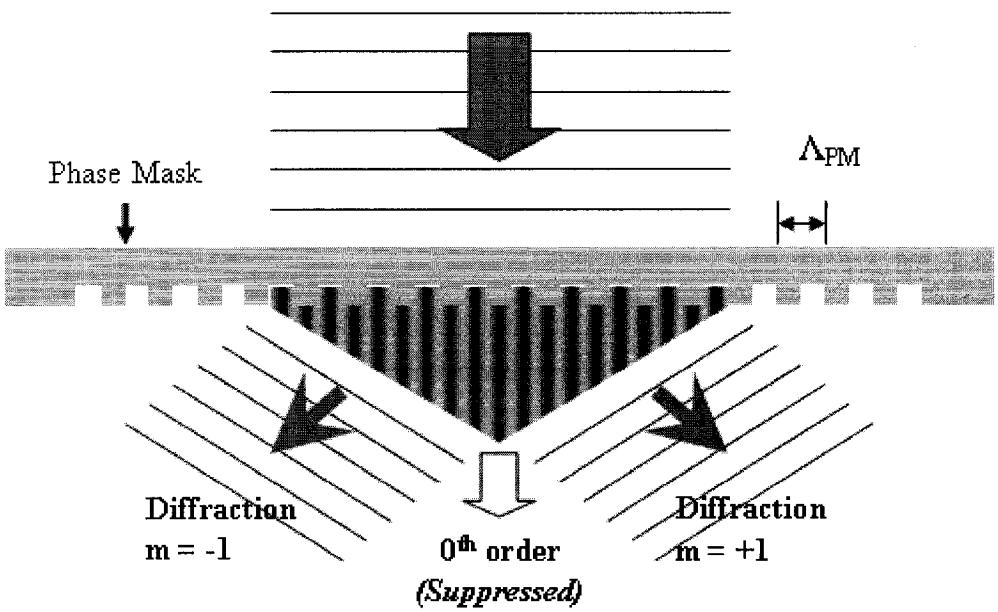

Figure 2.12 *Diagram of a phase mask interference lithography system (sometimes also called near-field holography.) Normally incident UV beam diffracted into ±1 orders. The remnant radiation exits the phase mask in the zero order ($m = 0$).*

Furthermore, phase mask lithography systems are typically more stable than conventional interference lithography systems. In a conventional interference lithography system, the split beams traverse two relatively long paths before interfering on the fiber, whereas in a typical phase mask system the mask is usually held rigidly against the fiber. Provided the phase mask and fiber are rigidly connected, the illuminating source can be scanned over the phase mask to expose the desired area. For these reasons, phase mask lithography is the method of choice for patterning fiber Bragg gratings.

The major disadvantage of phase mask lithography is that the period of the exposed grating cannot be changed without replacing the phase mask. Another limitation is that it is difficult to completely eliminate the 0th order.

2.5.2 The fiber Bragg grating writing system

The fabricate fiber Bragg grating system (in *Bragg Photonics Inc.*) is shown in Figure 2.13. The pulse power of the excimer laser (BraggStar 500 from Tuilaser AG) centered at 248 nm was adjusted to 10 mJ and the repetition rate to 50 Hz. The Plano-cylindrical lens was used to focus the fringe pattern along the fiber core. A stripping photosensitive optical fiber placed in close proximity and immediately behind the phase mask. The distance between the phase mask and the fiber is in micron level. The interference pattern photo-imprints a refractive index modulation in the core of a photosensitive optical fiber. The photosensitive fiber is connected to a broadband light source and an optical spectrum analyzer (OSA). The OSA is used to monitor the effects on the fiber Bragg grating writing process. The position of the slit is front of the phase mask and very close to the phase mask. The function of the slit is to control the width of the focused laser beam and also indirectly control the FWHM of the Bragg grating (See section 2.1 and Equation 2.9).

Alignment process: The first step is to ensure that the two first order-diffracted beams are aligned properly. Use a white business card as the image plane, and adjust the rotational stage until the two diffracted beams lie along the same horizontal line. The second step is place the piece of scrap fiber into the fiber holder to check for vertical alignment and focus distance. If everything is aligned and focused, we can see an interference pattern on the white business card. Now, the station is ready to make Bragg gratings.

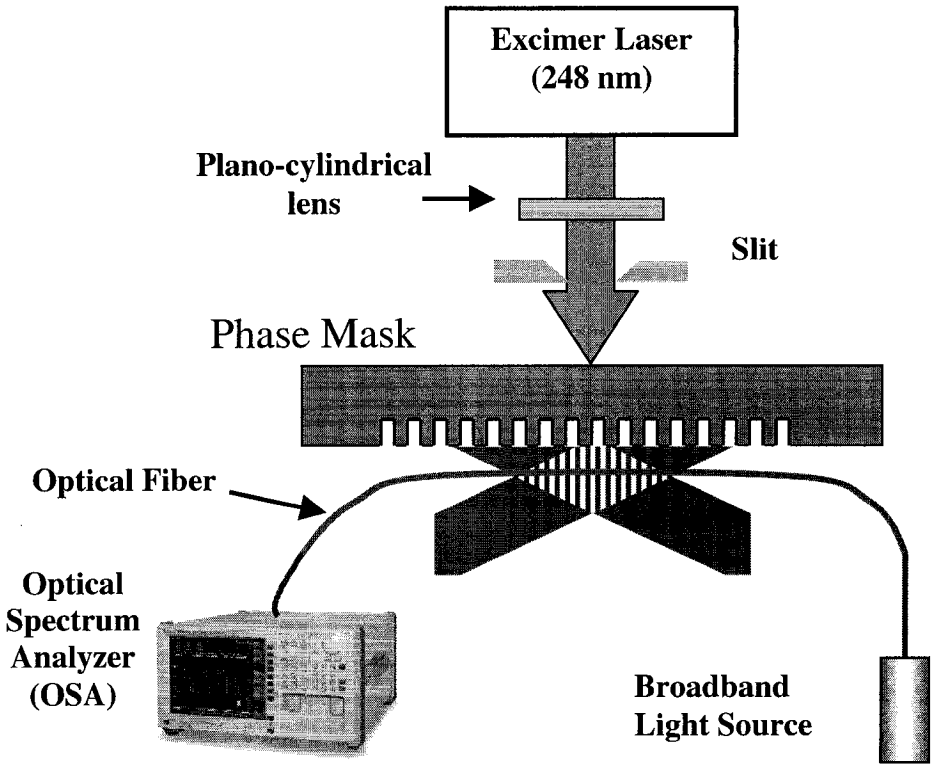

Figure 2.13 *Fiber Bragg grating writing system using an excimer laser.*

Chapter 3
Hydrogen loaded optical fiber and Thermal stability of fiber Bragg gratings

A question might be asked frequently: Which is the best fiber to use for the fabrication of most gratings? Undoubtedly, the preferred answer to this question should be the standard communication fibers. The standard single-mode telecommunication fibers, doped with 3% germania, typically display index change to ~$3x10^{-5}$. In general, increasing the doping level or subjecting the fiber or perform to reduce conditions at high temperature can result in large index change to ~$5x10^{-4}$. This index modulation is more often desirable; however, the photo-induced devices in standard optical fibers are fabricated for compatibility with existent systems. Sensitization techniques have been developed for writing high reflectivity gratings in these fibers. Increased photo-induced index modulations to values of the order of 10-3 or higher have been realized via low temperature hydrogen loading (hydrogenation). Recently, the hydrogen loaded standard communication fiber is the most used fiber for fiber Bragg grating production. The mechanisms of the hydrogenation increased photosensitivity of the standard communication fiber and the hydrogen treatment will be discussed in the first and second section of this chapter.

The values of the Bragg wavelength λ_B and the total grating reflectivity depend directly on the refractive index modulation amplitude. The reflectivity decay of this modulation amplitude is expected from relaxation of some unstable defects created upon UV absorption. In order to guarantee the functionality and reliability of the telecommunication devices and the sensors based fiber Bragg grating, it is necessary to determine the grating stability under the operating conditions. Among them, thermal

activation of unstable defects is the most important source of grating degradation. The thermal stability of the fiber gratings may be also affected by the fiber doping characteristics. The decay model of the reflectivity of fiber Bragg grating will be introduced in third section of this chapter.

3.1 Mechanisms of photosensitivity in hydrogen loaded optical fiber

Since the discovery of the photosensitivity and the first demonstration of grating formation in germanium doped silica fibers, there has been considerable effort in understanding and increasing the photosensitivity of the optical fiber. Standard single mode telecommunication fibers, doped with 3% germania (for example the SMF-28 optical fiber from CORNING), typically display index changes to reach approximately $3x10^{-5}$. The main method of increasing photosensitivity in the optical fiber can be summarized as following:

1. Hydrogen treatment [24].
2. Writing at elevated temperatures [25].
3. Mechanical treatment -- Applied strain on photosensitivity [26].
4. Material considerations, especially Co-doping silica fibers with B_2O_3 and GeO_2 [27].

The photosensitivity evaluations of the various fibers are shown in Table 3.1. It clearly demonstrates that the B-Ge co-doped fibers are the most photosensitive among the series (not include the photosensitivity of the hydrogen loaded fibers). An atypical report written by H.G. Limburger *et al.* in 1993 pointed out the index modulation as high as $1.2x10^{-3}$ [28]. To compare with Limburger's result, recently, a technique called hydrogen treatment or hydrogenation [24] is used to increase the photosensitivity of the standard

optical fiber in manufactory. By using this technology, the photo-induced index modulation can arrive to 10^{-3} or higher.

Table 3.1 The photosensitivity evaluations of four different fibers.

Fiber Design	Fiber Δn	Saturated index modulation	Maximum reflectivity of 2mm grating	Time for reflectivity to saturate
Standard low loss fiber ~ 4 mol% germania	0.005	$3.4x10^{-5}$	12%	~ 2 h
High index fiber ~ 20 mol% germania	0.03	$2.5x10^{-4}$	45%	~ 2 h
Reduced fiber ~ 10 mol% germania	0.01	$5x10^{-4}$	78%	~ 1 h
Boron co-doped fiber ~ 15 mol% germania	0.003	$7x10^{-4}$	95%	~ 10 min

Lemaire *et al.* [29] showed a simple, alternative, but highly effective approach for achieving very high UV photosensitivity in optical fibers using high-pressure H_2 loading at room temperature (hydrogen treatment hydrogenation), before these fibers were written using UV laser. Fiber are drenched at temperature ranging from 20 °C - 75 °C and pressure from around 20 atm to more than 750 atm (the process of hydrogenation in Bragg photonics Inc. is 60 °C and pressure is less 115 atm, or 1700 psi, for 96 hours), which makes for diffusion of hydrogen molecules into the fiber core. After irradiating H_2-loaded fibers with pulsed 241-nm light, Lemaire and his colleague observed a large refractive-index change ($\Delta n \sim 3x10^{-3}$) and a large concentration (~ 8 mol %) of induced

OH, which was roughly twice the initial concentration of H2. Lemaire suggested that the index modulation was caused by a reaction of hydrogen at normal Ge sites to produce OH groups and oxygen-deficient centers. The photosensitivity evaluations of the various fibers are shown in Table 3.2. Undoubtedly, the hydrogen-loaded optical fibers (SMF-28) are the most photosensitive among the tested series. One of the advantages of hydrogen loading is the Bragg gratings can be fabricated in any germanosilicat optical fiber and germanium free optical fibers.

Table 3.2 The photosensitivity evaluations of three different fibers.

Fiber Design	UV Wavelength (writing)	Pulse Energy (Laser)	Pulse frequency	Maximum reflectivity of grating	Time for reflectivity	Ref.
B-Ge codoped silica fiber (Fibercore Ltd.)	248 nm	12 mJ	200 Hz	saturated	< 10 min	[30]
Ge doped silica fiber (Redfern GF1)	248 nm	12 mJ	200 Hz	saturated	75 min	[30]
Hydrogen loaded fiber (SMF-28)	248 nm	10 mJ	50 Hz	100%	< 5 min	[31]

In Lemaire's experiments [29], the grating, which are standard AT&T MCVD (Modified Chemical Vapour Deposition from AT&T Bell labs) single-mod optical fibre with 3-mol% germania and loaded with 3.3 % hydrogen, was formed by using UV side-writing technique using 241 nm radiation with a influence of ~300 mJ/cm^2 at 30 Hz for 10 minutes. This grating has bandwidths of 4 nm and the average core index has increased by $\sim 3.4 \times 10^{-3}$. A comparison of the refractive index profile at midpoint of a grating with unsettled fibre is shown in figure 3.1. Similar bandwidths and index changes were obtained using other MCVD and VAD fibres containing ~3% germania.

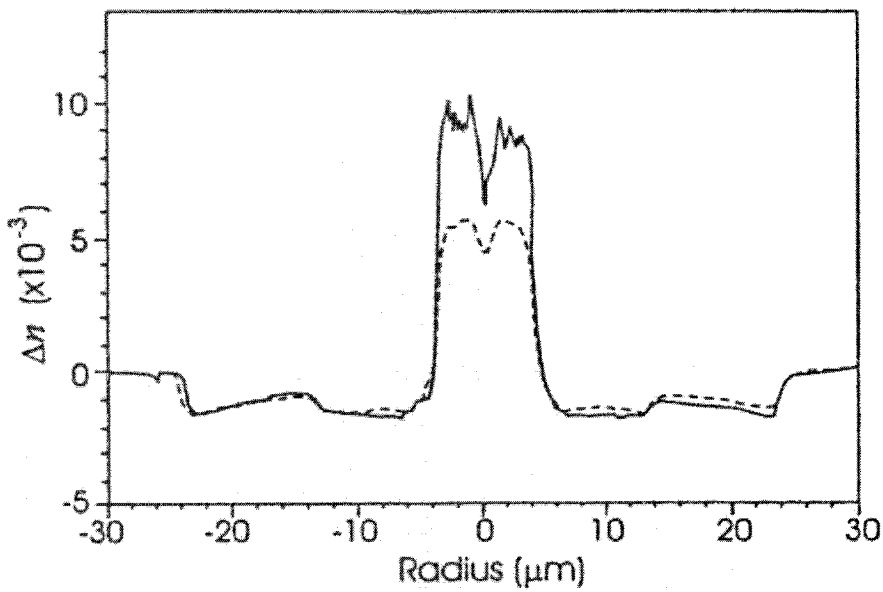

Figure 3.1 *Refractive index profiles for a standard AT&T single-mode fiber with 3% GeO_2, and for a grating which was UV written in the same fiber after loading with 3.3% hydrogen (solid curve). Δn refers to index with respect to un-doped silica. The dash curve is the refractive index profiles for a standard AT&T single-mode fiber with 3% GeO_2* [29].

The Lemaire's work has shown the UV induced loss of changes, which occur in response to write a strong grating in a 9% germanium-doped silica fibre that loaded with 4.1% hydrogen in figure 3.2. He described in his article [29]: "The spectrum shows a strong short wavelength edge and a prominent Si-OH absorption at 1.39 μm. The concentration can be estimated to be ~8.4-mol%, quite similar to the GeO_2 content of the fiber. A similar spectrum for a 3% GeO_2 doped fiber containing 1.4% hydrogen showed ~2.9% OH and a proportionally lower wavelength edge." The OH concentration is consistently close to the germanium content of the fiber. By studying his achievement, we can summarize the results above mentioned as following: The mechanism is not depending on the type of fiber or perform processing, but rather on the function of germanium and hydrogen concentration and the UV exposed conditions.

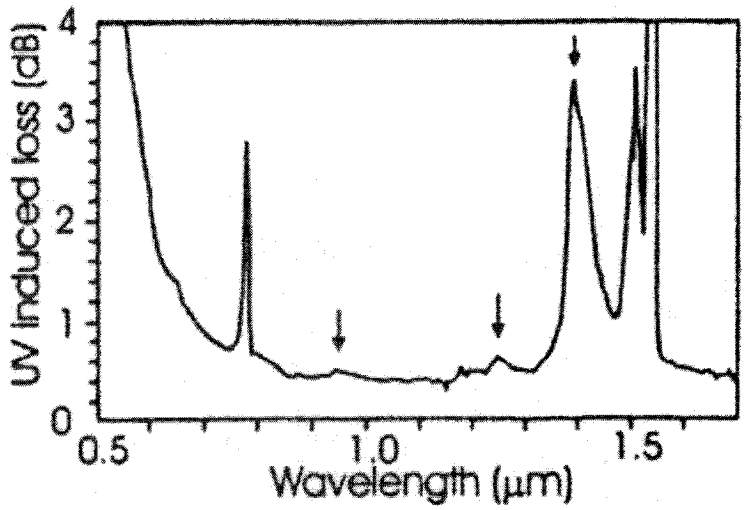

Figure 3.2 *UV induced losses in ~5mm long grating in fiber with 9% GeO_2 and 4.1% hydrogen. Features at 770 nm and 1500 nm are due to the grating. The arrow marked peaks at 0.95, 1.24, and 1.39 μm are due to OH* [29].

Figure 3.3 [32] shows the absorption spectrum changes in the IR for MCVD and VAD fibers exposed to 1 atmospheric pressure of hydrogen gas at 100 °C. During the first 2 hours exposure, the increased absorption, which is due to prominent loss peaks of molecular hydrogen, appears at 1.24, 1.70, and 1.88 μm wavelengths. The absorption increase due to molecular hydrogen is saturated after 10 hours. The absorption band, which is due to OH formation, has two very closely spaced peaks at 1.39 μm (Si-OH) and 1.41μm (Ge-OH) [32].

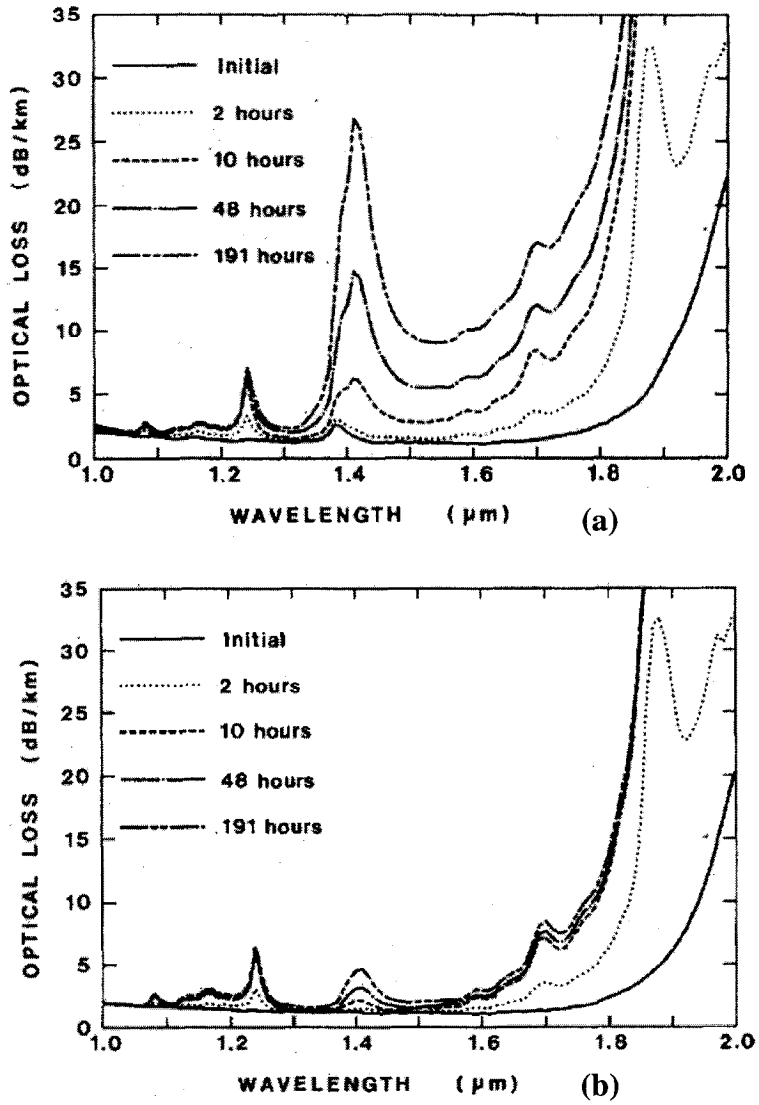

Figure 3.3 *Absorption spectrum changes in the IR for (a) MCVD and (b) VAD fibers exposed to 1 atmospheric pressure of hydrogen gas at 100 °C* [32].

The rate and saturated value of the loss-increases due to molecular hydrogen for the both MCVD and VAD fibers are very similar; therefore, the loss-increase phenomenon due to molecular hydrogen should be considered to be independent on the fiber doping material or fabrication method. The rate for the absorption increase due to OH formation of the MCVD fiber is extremely larger than that of the VAD fiber. This

fact shows that the rate of the OH-formation reaction greatly depends on the fiber doping material or fabrication method.

Optical absorption spectra of a germanosilicate (VAD) perform rods heated in H_2 atmosphere at 500 °C at different times are shown in Figure 3.4 [33]. The increased intensity of broad absorption band peaking at 240 nm (5.14 eV) is clearly setting out in this figure. This absorption band at 240 nm was assigned to a germanium oxygen deficient center (GODC; see chapter 2). This phenomenon denotes that the reaction of hydrogen molecules at germanium (Ge) sites produces GODCs.

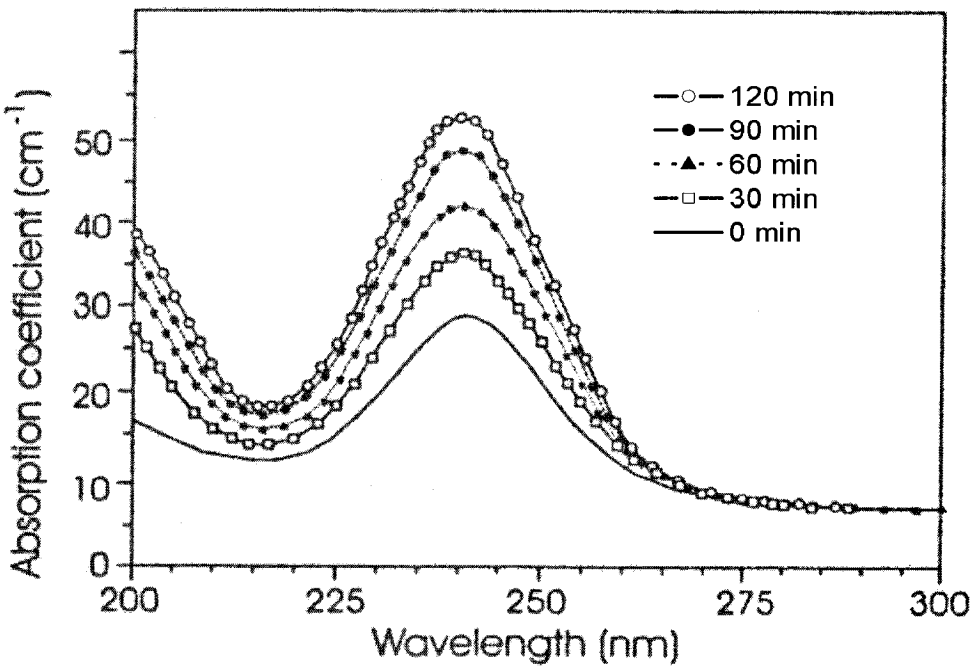

Figure 3.4 *Optical absorption spectra of a germanosilicate (VAD) perform rods heated in H_2 atmosphere at 500 °C for different times* [33].

Figures 3.2, 3.3, and 3.4 imply that the result of the GODC's formation and OH species is reaction between hydrogen molecules and Si-O-Ge sites of germanium doped fiber. Obviously, the role of Bragg gratings in hydrogen loaded fibre includes undoubtedly both thermal and photolysis mechanisms.

$$\equiv Si-O-Ge-O-Si\equiv \; + \; H-H \; \rightarrow \; = Ge^{\bullet}_{\bullet} + 2(H-O-Si\equiv)$$

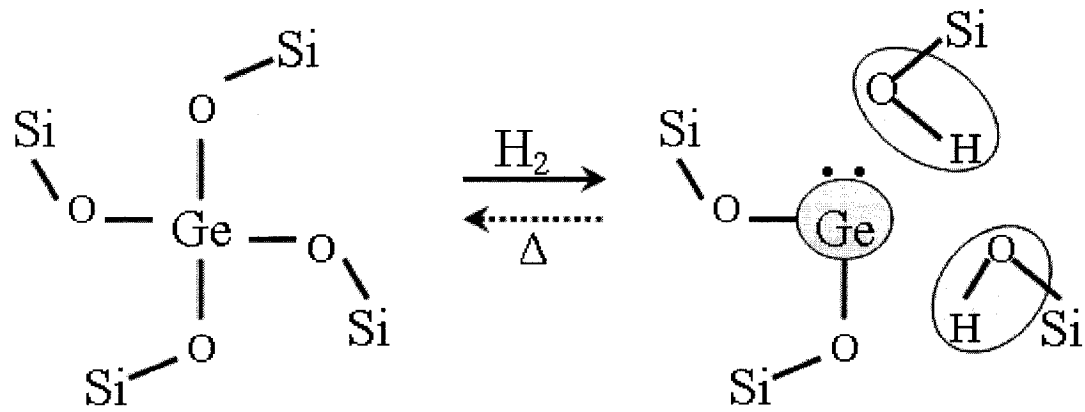

Figure 3.5 *Model of H2 loading introduced a large amount of GODC and Si-OH (Ge-OH) groups*

Up to now, it has been always believed that the photosensitivity of the germanium-doped fiber depends on the concentration of GODC. The mechanism of H_2 loading is deduced as follows: The H_2 molecules infiltrating the glass matrix by H_2 loading will break the Si(Ge)-O-Si(Ge) bonds in the SiO_4 (GeO_4) tetrahedral network, resulting in the formation of Si-OH (Ge-OH) groups, and introduce a large amount of GODC. According to this theory, a suggested structure model of germanium doped fiber loaded with H_2 molecule is shown in Figure 3.5. The OH group adjacent to the Ge^{2+} center lowers the dimension of the glass network and increases the degree of freedom of the structure around the Ge^{2+} center. Such a germanium atom can then moves freely along a long distance between the equilibrium bond lengths in the ground state and arrives at the excited state.

3.2 Hydrogen treatment -- Low-temperature hydrogen loading

The following section is a short description of the hydrogen treatment, loading hydrogen molecules into the conventional telecommunication fiber in low temperature range, used for increasing the photosensitive response of optical fibers.

When placing a fiber in a high-pressure hydrogen atmosphere at room temperature, hydrogen molecules will diffuse into the glass network. Loading the fiber with hydrogen prior to UV exposure significantly increases the photosensitivity [29]. Refractive index changing to as high as ($\Delta n \sim 3x10^{-3}$) [34] were reported for standard hydrogen sensitized telecommunications fiber.

Low temperature high-pressure hydrogen loading or only simple hydrogen loading is the most common method used for increasing the photosensitivity. In vector analytic terms, the diffusion equations can be expressed for any coordinate system as:

$$\frac{\partial C}{\partial t} = \nabla \bullet (D \times C) \tag{3.1}$$

In cylindrical coordinates where the parameters are r, θ, and z defined in the usual manner, equation (3.1) reduces to

$$\frac{\partial C}{\partial t} = \frac{1}{r}\left\{\frac{\partial}{\partial r}\left(rD\frac{\partial C}{\partial t}\right)+\frac{\partial}{\partial \theta}\left(\frac{D}{r}\frac{\partial C}{\partial \theta}\right)+\frac{\partial}{\partial z}\left(rD\frac{\partial C}{\partial z}\right)\right\} \tag{3.2}$$

where D is the diffusion coefficient having the dimensions L^2T^1, and C is the concentration of the substance undergoing diffusion, defined in any standard way.

As the steady-state diffusion of hydrogen through silica is relatively simple to describe, the diffusion process is quite well characterized by the diffusion equation with a diffusivity given by

$$D = D_0 e^{-E/RT} \tag{3.3}$$

where D_0 is a constant independent of ambient gas pressure and temperature; E is the activation energy for the diffusion process; R = 1.99 cal/K-mol is the gas constant, and T is the absolute temperature. The value of diffusion coefficient that the hydrogen diffuses into the silica is [35]:

$$D = 5.65\times10^{-4} e^{-(10.14\ \text{Kcal/mole})/RT}\ \text{cm}^2 s^{-1} \tag{3.4}$$

Here, the problem of diffusion is considered as in a cylinder from first principles, by concern the issue of diffusion in one dimension, for a constant value of D. A fundamental assumption is that the value of D remains a constant for a fixed temperature. Equation (3.1) reduces to [36]

$$\frac{\partial C}{\partial t} = D\frac{\partial^2 C}{\partial x^2} \tag{3.5}$$

Equation 3.5 is the simplest mathematic model of the hydrogen molecular diffusion inside the optical fiber; however, it's an extremely complex process in real hydrogenation of optical fiber. For the conventional optical fiber, the core is doped with germanium to get the light-guiding difference of refractive indices between the fiber core and the cladding. The radii of the core and cladding are 4.1 μm and 62.5 μm, respectively. The polymer layers (two polymers) are 62.5 μm thick and warps around the cladding of the fiber. The structure of the single-mode fiber is depicted in Figure 3.6.

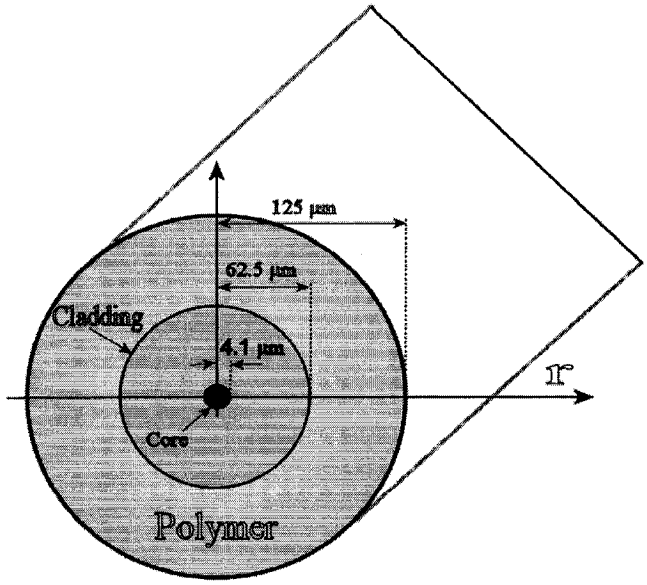

Figure 3.6 *Schematic cross-section of a single-mode fiber: Core (Ge doped silica), Cladding (silica), Polymer (acrylate).*

The concentration of hydrogen molecules and rate of which these molecules diffuse into the core of the optical fiber depend on the pressure and temperature of the hydrogen gas. The pressure of hydrogen gas can increase the saturated hydrogen concentration in the fiber core. Temperature is a significant parameter for the lower temperature hydrogenation. These exhibitions of temperature are: The diffusivity of hydrogen molecules in silica increases with increased temperature. Meanwhile, decreased temperature can result in an increase in the hydrogen concentration saturation level and a significant decrease in the diffusion rate of hydrogen into the core of the optical fiber [7].

The hydrogen concentration in the corn of the fiber is related to the pressure of hydrogen in the chamber, diffusion temperature, the type of fibers, and the characteristic of the fiber Bragg gratings. In general, the grating producers will choose different kind of parameter according to their own database.

For the design of a hydrogen loading system, safety is of the primary concern given that one is dealing with an explosive gas under high pressure. The fiber chambers

are made from copper tubing of small diameter (i.e.1/4 inch). The 1/4 inch copper tubing is capable to hold approximately 20 optical fibers in a small volume, which minimizes the amount of hydrogen required to fill the chamber. The fiber chambers are pumped out with the vacuum pump each time before being filled with high-pressure hydrogen. Heating elements can be placed at various positions along the fiber chamber heating up the hydrogen gas and accelerating the diffusion of hydrogen molecules into the core of optical fiber.

3.3 Thermal stability of the fiber Bragg grating

Although fiber Bragg gratings are often referring to permanent refractive index structures, exposure to increase temperatures usually results the decay of the refractive index modulation. The reflectivity will be erased completely at sufficiently high temperatures. This section gives a general overview of the topic regarding thermal stability of fiber Bragg gratings and also provide background to chapter 4.

Some Bragg grating devices require extremely small tolerance on the optical properties over a long time scale to assemble reliable wavelength division multiplexing (WDM) components. Other applications, such as sensors, are required to survive at high temperatures. In the experimental observations of the decay of the gratings' reflectivity, the thermal stability of gratings depends on several factors such as the type of fiber [37], hydrogenation [38, 39] and the writing wavelength [23]. In 1994, Erdogan *et al.* [40] provided the first detail of grating stability and processed a model to explain the thermal degradation characteristics of fiber Bragg gratings written in germanium and erbium-germanium-co-doped silica fibers. The model demonstrated that the decay of the UV-induced index modulation could be described by a "power law" function of time with a

small exponent (<<1). As the experimental results, the UV-induced index modulation initially decays very rapidly, but the rate of decay decreases as time advances, and the decay of reflectivity of Bragg grating is also a strong function of temperature. In the power-law approach decay measurements are fitted to the following equation:

$$\eta = \frac{1}{1 + A(t/t_1)^{\alpha}} \tag{3.6}$$

where η is the normalized index change (which be described as $\Delta n(t)/\Delta n_0$), t is time, the fitting parameters A and exponent α are proportional to $exp(\alpha T)$ and T respectively. In this equation both A and α are dimensionless, and $t_1 \equiv 1$ minute is induced to keep dimension consistent. Once the parameters (A and α) have been determined, the decay at any temperature and time phase can be calculated using Equation 3.6. The difficulty with this approach is to determine reliable fitting parameters for different types of fibers [40, 41]. As shown in figure 3.7, the data of Erdogan's experimental observations appear to fit Equation 3.6 equally well. The fitting parameter, exponent α, was chosen to be $\alpha = T/T_0$ with $T_0 = 5250$ K. The factor A can be written in form

$$A = A_0 \exp(aT) \tag{3.7}$$

with the temperature T measured in Kelvin $A_0 = (1.86 \pm 0.22) \times 10^{-3}$ and $a = (7.64 \pm 0.19) \times 10^{-3}$ K^{-1}. Figure 3.8 shows the dependence of the power-law factor A on temperature, with plotted on a logarithmic scale. In this plot the error bars represent the values for an obtained directly from nonlinear curve fits using Equation 3.6 in which both A and α were allowed to vary freely.

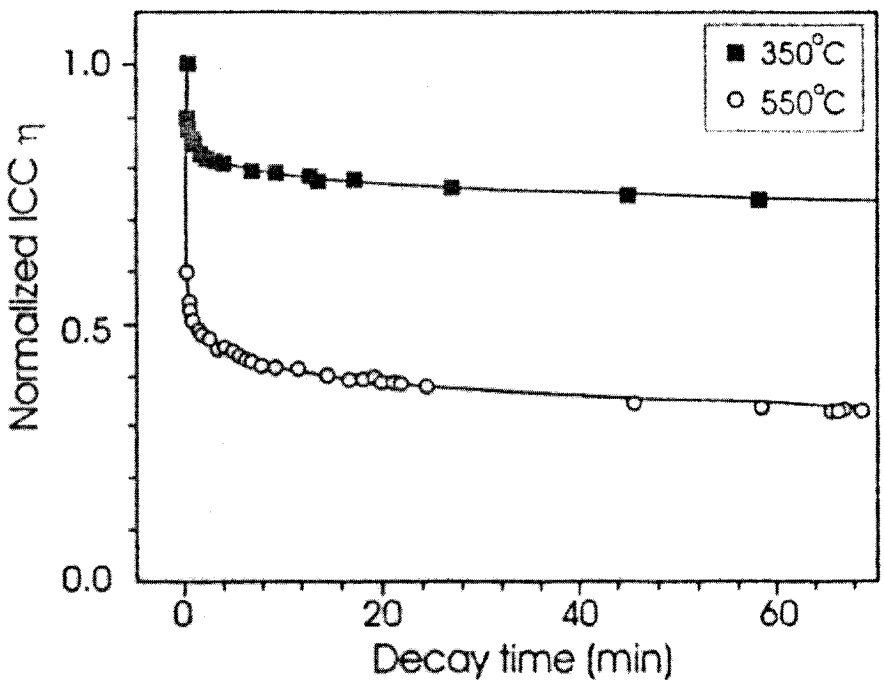

Figure 3.7 *Measured integrated coupling constant normalized to starting value for two gratings heated to 350 and 550°C as a function of decay time. Solid lines are fits to equation 3.6* [40].

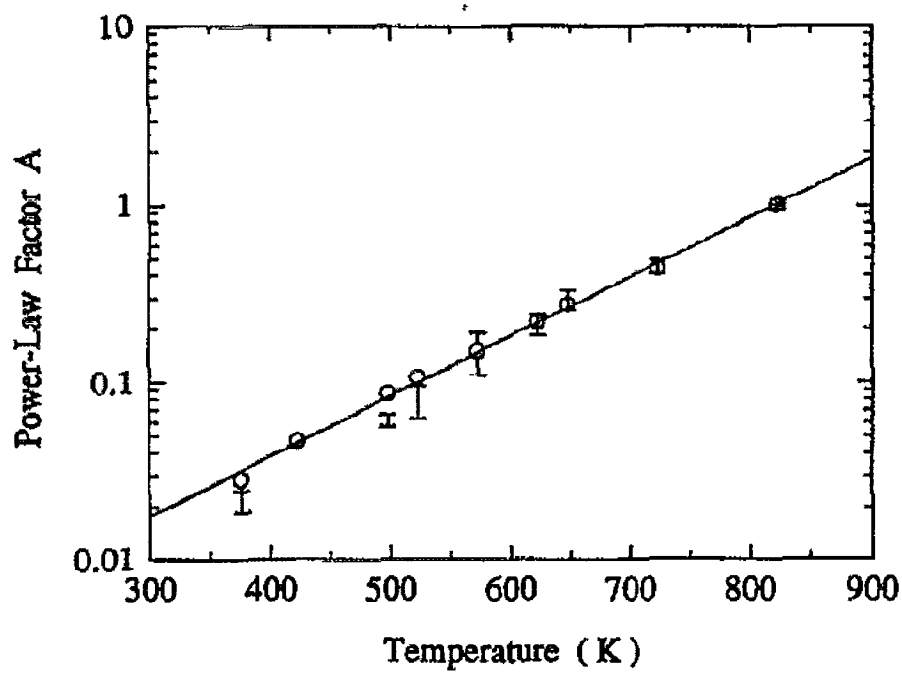

Figure 3.8 *Plot of the power law factor A obtained from curve to equation 3.6 with α allowed to vary freely (error bars), and α fixed by α=T/5250 K (open circles)* [40].

A model might be modified to predict the measured behavior [40]. Carriers are excited by the UV irradiation from the single homogeneously broadened absorption spectrum by GODCs at 5 eV. The carriers are then assumed trapped in a continuous distribution of the energy states, rather than at a single trap level. If we consider that it is the breakage of the wrong bonds that creates defects and free electrons, than it is plausible to assume the thermal excitation of these electrons from traps can lead to the reformation of the wrong bond, simultaneously removing the UV-induced index change. The dissociation energy E_a of the trap follows a simple Arrhenius law of the form

$$\frac{\Delta n(t)}{\Delta n_0} = \exp(-\nu t) \tag{3.8}$$

where ν is a frequency factor related to E_a, temperature T, and Boltzmann's constant K_B via $\nu(T) = \nu_0 \exp(-E_a / K_B T)$. Clearly, this is not the case for standard or hydrogenated fibers, as the Arrhenius law predicts that at a constant temperature the trap depopulation as well as the index modulation should decay exponentially to zero, rather than reaching a plateau [40]; therefore, the correct description is the one in which almost all electrons up to a given trap depth, instead of a fraction of electrons at a single trap, are wrap out by the decay process; by this token, the decay history is important in determining the subsequent behavior. Figure 3.9 shows a simplified diagram for this mechanism. $E = 0$ is the point where electrons are free (the conduction band minimum). The thermal releasing of electrons induces the reoccupation of original deep level occupied prior to UV excitation. The essence of the diagram is the separation of the distribution of trapped carriers into energies above and below demarcation energy E_d that depends on time phase and temperature. It is consequently convenient to interpret the experimental data in term

of E_d, where $E_d = K_B T \ln(\nu t)$, where ν is obtained by acquiring multiple data sets as a function of temperature and fitting them together.

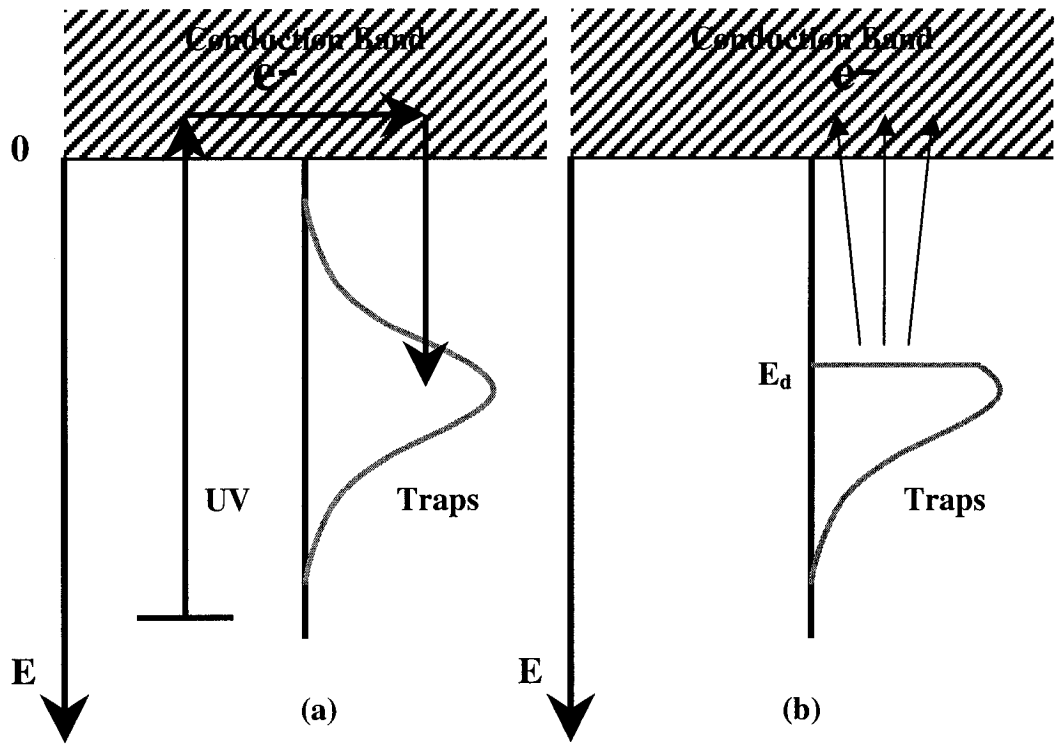

Figure 3.9 *Diagram of the physical model in which (a) electrons excited by UV excitation are trapped in a continuous distribution of traps; and (b) thermal depopulation of the traps at a given time and temperature approximately corresponds to shallower traps ($E<E_d$) being emptied and deeper traps ($E>E_d$) remaining full.*

In Figure 3.10 the experimentally determined values for η (assumed proportional to N, the total number of trapped electrons remaining at a given time phase) are plotted versus the demarcation energy E_d. The different symbols correspond to the different decay experiments performed at various temperatures. Plotting the change in reflective index modulation as a function of the demarcation energy gives the aging curve. The parameter η may also be written as

$$\eta = \frac{1}{1+\exp\left[\left(E_d - \Delta E\right)/K_B T_0\right]} \tag{3.9}$$

This form represents a simple analytical form for the dependence of the normalized UV induced index change on the demarcation energy E_d; hence, the aging of the grating should be predicted. From the experimental data of Figure 3.10 and the corresponding fit, the energy distribution of the traps (ΔE) is ~2.8 eV deep, with a width of 1.6 eV. Figure 3.10 immediately suggests which combinations of time and temperature are capable for erasing a given fraction $1-\eta$ of the initial UV induced index change.

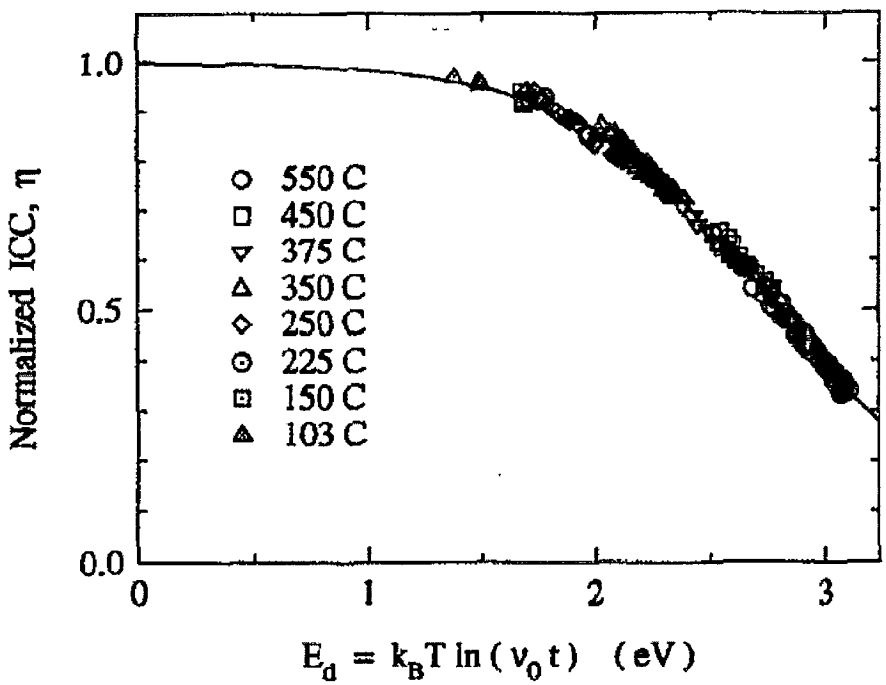

Figure 3.10 *Plot of the normalized integrated coupling constant as a function of the demarcation energy E_d. The solid line is a fit using equation 3.9* [40].

Chapter 4
High temperature fiber Bragg grating sensors

4.1 Fiber Bragg grating temperature sensors and system configuration

Bragg gratings have widespread applications in the rapidly growing field of optical sensors. The principle of the dielectric Bragg grating temperature sensor is based on the measurement of the reflected Bragg wavelength. Recently, the most popular design for this kind of sensor is to use the fiber Bragg grating. Fiber gratings are compacting intrinsic to the sensing elements, which are relatively inexpensive to produce, easy to multiplex, and applicable to a range of physical measurands [42]. A fiber Bragg grating is formed by a periodic change in the refractive index caused of a fiber core by exposure to an UV laser beam [13].

The fiber Bragg grating temperature sensor reflects one particular wavelength and transmits all others and, moreover, the reflected wavelength can vary with the modifying of the sensor's temperature; thus, fiber Bragg grating temperature sensors have been widely used in applications in monitoring temperature. One of the advantages of the fiber Bragg grating temperature sensors is that several of these sensors can be multiplexed in series along with a single optical fiber, so, a single instrument can simultaneously monitor many individual sensors [42]. Additionally, the fiber Bragg grating temperature sensor also has some other advantages such as resistant to electromagnetic interference, tiny in size, and light in weight.

A fiber Bragg grating is an optical fiber in which the refractive index in the core has a periodic or quasi-periodic profile. One of the most important properties of fiber Bragg gratings is wavelength-selective reflection. Assume that a broadband light is

coupled into a fiber with fiber Bragg grating inside. The light that its wavelength matches the Bragg condition will be reflected back. The light that its wavelength does not match the Bragg condition will be transmitted through the fiber.

Mathematically, the Bragg condition is given by [12, 43]:

$$\lambda_B = 2n_{eff}\Lambda \tag{4.1}$$

where λ_B is the Bragg wavelength, n_{eff} is the effective modal index and Λ is the perturbation period.

Most of the work on fiber Bragg grating temperature sensors has focused in the use of these devices providing quasi-distributed point temperature sensing. The thermal response arises due to the inherent thermal expansion of the fiber material as well as the temperature dependence of the refractive index. To explain this phenomenon, we use the following form. The wavelength shift ($\Delta\lambda_B$) as a function of a temperature change (ΔT), for a certain wavelength peak of the mode (λ_B) is given by [42],

$$\frac{\Delta\lambda_B}{\lambda_B} = \left[\frac{1}{n_{eff}}\frac{\partial n_{eff}}{\partial T} + \frac{1}{\Lambda}\frac{\partial\Lambda}{\partial T}\right]\Delta T = (\alpha_{n_{eff}} + \alpha_\Lambda)\Delta T \tag{4.2}$$

where α_Λ is the thermal expansion coefficient and α_n represents the thermo-optical coefficient. Practical values of these constants for typical FBG are $\alpha_\Lambda = 0.55\text{x}10^{-6}\ ^\circ\text{C}^{-1}$ and $\alpha_{neff} = 8.6\text{x}10^{-6}\ ^\circ\text{C}^{-1}$ [42]. The accuracy of this type temperature sensor can be achieved to 0.7°C (at $\lambda_{Bragg} \sim 1.55\ \mu\text{m}$) with a wavelength resolution of 10 pm (0.01 nm), which is the typical wavelength resolution of the optical spectrum analyzer (OSA).

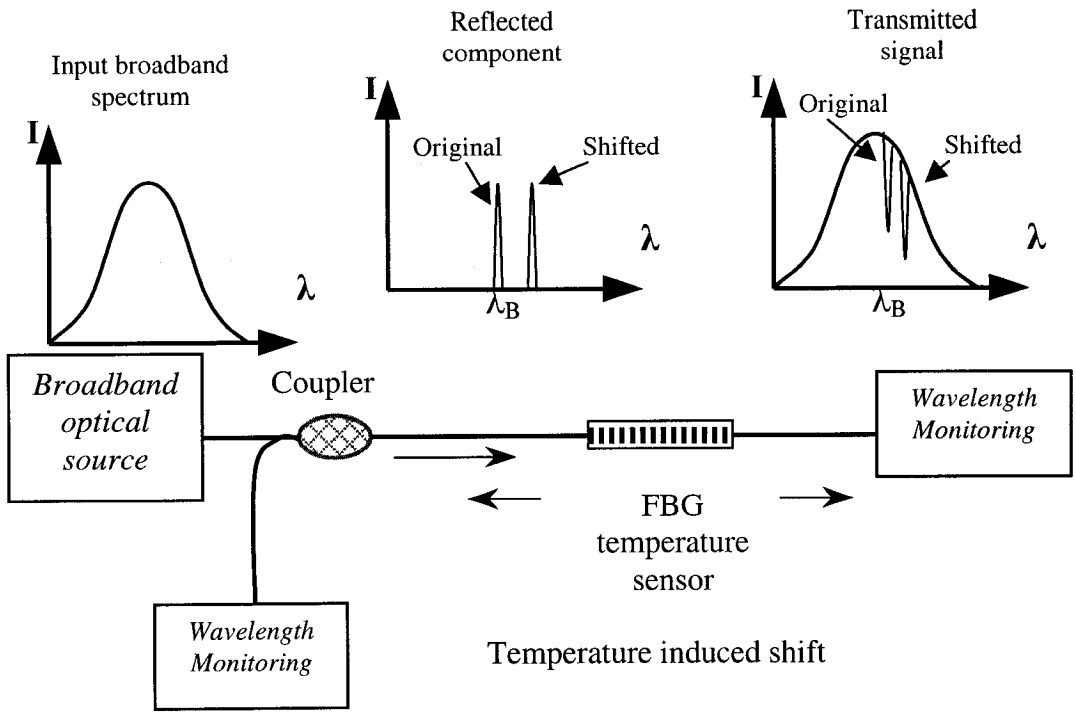

Figure 4.1 *An illustration of fiber Bragg grating-based point sensor* [42].

Figure 4.1 shows the conceptual configuration of the fiber Bragg grating point temperature sensor. The broadband light source, such as coming from an edge-emitting LED, or a super-luminescent LED or an erbium-doped fiber amplifier, is coupled into a single-mode optical fiber with a fiber Bragg grating inside the fiber. Due to the existence of the grating, the wavelength that match the Bragg condition will be reflected back and the other wavelengths will pass through. Then the wavelength monitoring devices, such as an optical spectrum analyzer (OSA), can be used to monitor the wavelength spectra for both the reflected signal and the transmitted signal, as shown in Figure 4.1.

Fiber gratings are compact intrinsic sensing elements. The nature of the output of Bragg gratings provides the Bragg grating temperature sensors with a built-in self-referencing capability. As the sensed information is encoded directly into wavelength of

which it is an absolute parameter, the output does not depend directly on the injected light power, and losses in the connecting fibers as well as couples. Because this kind of theory is widely acknowledged as one of the important advantages of the fiber Bragg grating temperature sensor, these sensors can be used to measure the temperature precisely in execrable circumstance, and to build the temperature sensor array using wavelength division multiplexing (WDM) and time division multiplexing (TDM) technique.

To sum up, the accuracy of the fiber Bragg grating temperature sensor depends on the wavelength resolution, which is attainable using laboratory instrumentation such as optical spectrum analyzers (OSA) and tunable lasers. Generally, for the conventional fiber Bragg grating temperature sensor, the thermal expansion coefficient (α_Λ) is 0.55×10^{-6} $^{\circ}C^{-1}$ and the thermo-optical coefficient (α_{neff}) is 8.6×10^{-6} $^{\circ}C^{-1}$; thus, a wavelength resolution of 10 pm (0.01 nm), which is the maximum wavelength resolution of optical spectrum analyzer AQ6319 in our research laboratory, is required (at $\lambda_B \sim 1.55$ μm) to resolve a temperature change of 0.7 °C.

To increase the accuracy or sensitivity of the fiber Bragg grating temperature sensor, using the technique of an unbalanced Mach-Zehnder interferometer was proposed and implemented [44, 45]. The typical wavelength resolution of this wavelength detection technique is smaller then 1 pm; thus, the sensitivity of the fiber Bragg grating temperature sensor is 0.07 °C. Figure 4.2 shows the basic configuration of applying an unbalanced interferometer to detect the wavelength shift of the Bragg grating induced by external perturbation.

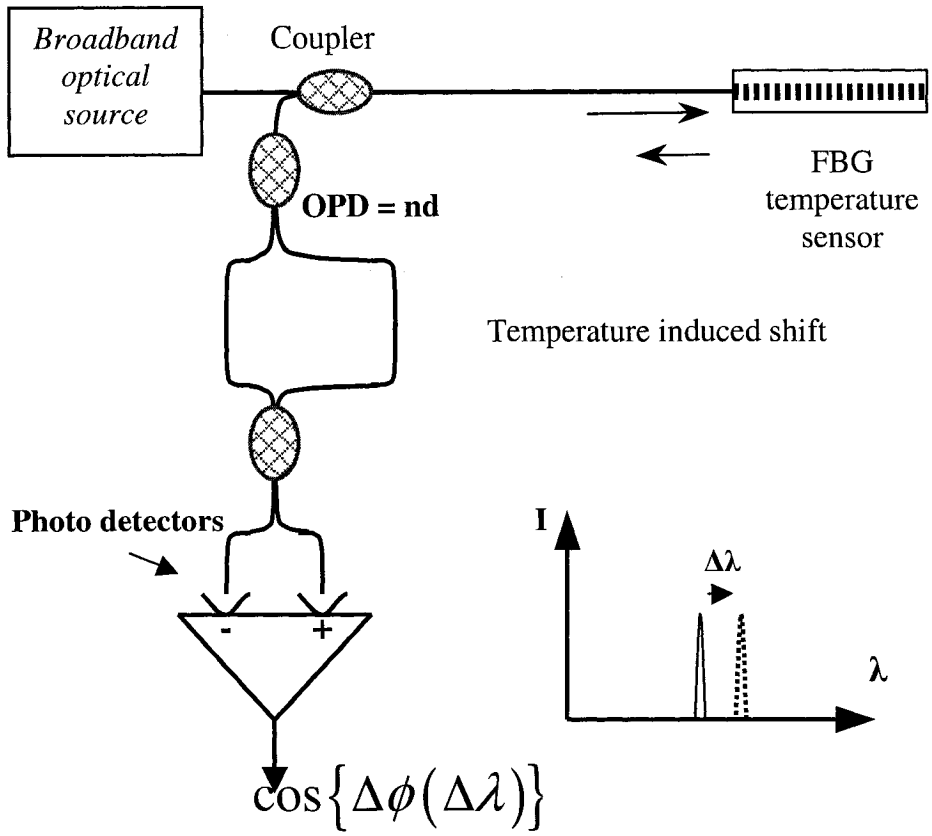

Figure 4.2 *Detection of wavelength shift of fiber Bragg grating temperature sensor is using an unbalanced fiber Mach-Zehnder interferometer* [42].

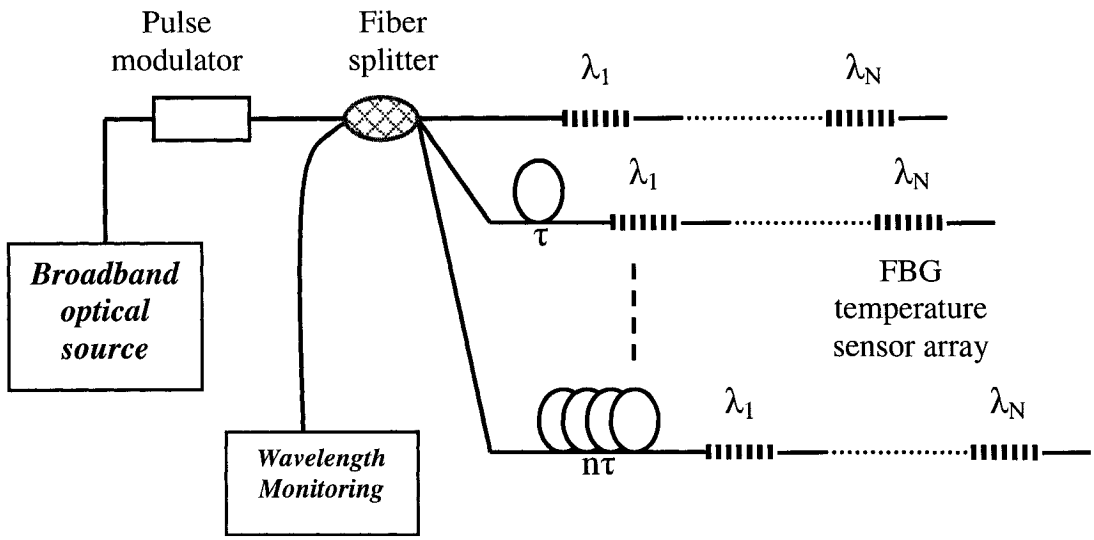

Figure 4.3 *A parallel configuration of combined WDM/TDM multiplexing topology* [42].

The information capacity is one of the important advantages of the fiber Bragg grating temperature sensors. The benefit of using fiber Bragg grating temperature sensors for distributed sensing is that a large numbers of sensors can be integrated along with a single fiber. Currently, with the rapid advent of optical communication networks, more than 100 wavelength channels can be put in a single fiber by using the wavelength division multiplexing (WDM) technique; hence, if we assign one center wavelength for each grating, more than 100 sensors can be integrated into a single fiber. Furthermore, time division multiplexing (TDM) can multiply above-mention number several times by re-using of the spectrum source. With mixed WDM/TDM in the parallel configuration as in Figure 4.3, several wavelength stepped temperature sensor arrays are concatenated using a fiber splitter. To explain Figure 4.3, the input pulse is split into the fiber Bragg grating temperature sensor arrays. A certain length of fiber delay line separates the time window for each WDM set. By launching a short pulse of light from the source, the reflections from fiber Bragg grating temperature sensors, at longer distant sensor array, will return to the detector at later times. The detection instrumentation is configured to respond to the reflected signals only during a selected window of time after pulse is lunched, because of this reason a WDM/TDM set of sensors is selected for detection.

4.2 Hypotheses of fiber Bragg grating thermal decay

The fiber Bragg grating temperature sensor still has some serious disadvantages. Because the fiber Bragg grating exhibit poor stability within the high temperature environment; moreover, the conventional grating can be completely erased at temperature around 500 °C [46], such gratings are unsuitable for sensors intended for using at high temperatures environment. Due to the reflectivity decay of the fiber Bragg gratings,

especially the reflectivity decay of hydrogen loaded fiber Bragg gratings [47], the grating based temperature sensors are usually used in an environment of under 200 °C. For example, the operating temperature range of fiber Bragg grating temperature sensor "Temperature Sense™" from Bragg Photonics is between -40 °C and 100 °C.

In the past ten years, there are many reports have related that the thermal annealing (treatment) can increase the thermal stability of the fiber Bragg grating in higher temperature range [48]. To test and verify this method, a reflectivity decay model has been proposed in chapter 3 to describe the thermal decay of germanosilicate fiber Bragg gratings, leading to very good fit in the case of fibers. The model assumes that thermal decay follows a power law of the type $1/(1+At^{\alpha})$, where t is the time and A and α are two fitting constants. The mechanisms underlying this model postulate that carriers excited during writing the fiber are trapped in a broad distribution of trap states and the rate of thermal depopulation is a function of the trap depth.

For further study of the high temperature fiber Bragg grating temperature sensor and the decay of fiber Bragg grating, we proposed three hypotheses in this thesis. These hypotheses are extended and perfect for the "power law", which is the decay model of fiber Bragg grating from Erdogan *et al.* in 1994. These hypotheses can be describing as following:

1. The quarantine electron, which is trapped electron excited by UV excitation and trapped in a continuous distribution of traps, is not able to move spontaneously. If the heat energy exceeds more than the quarantine energy (trapped energy) of the electron, then the electron will move from its initial place in the traps to the conduction band and disappear in the conduction band.

2. The depth of the traps is limited and stops at the saturation level. The DID (see chapter 2) in gratings is a Gaussian distribution with flattop.

3. The trapped electron excited by UV excitation will fill in the shallower traps (lower activation energies) at first. Then fill in the deeper traps (high activation energies), after the depth of shallower traps (lower activation energies) is saturated.

4.2.1 First hypothesis

"Power law" fits and experimental data points for the thermal decay at four different temperatures are shown in Figure 4.4 (three gratings per temperature) [1]. Obviously, the model (power law) provides a good fit to the data over the full 7000 h.

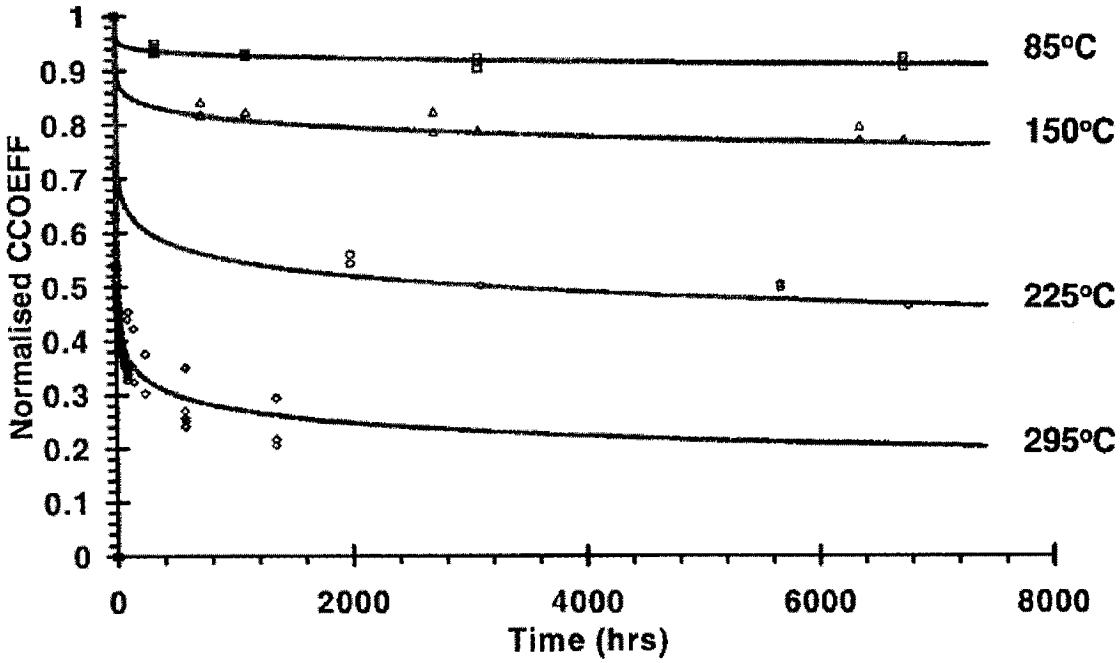

Figure 4.4 *Comparison of "Power law" fits and experimental data points for the thermal decay at four temperatures* [1].

As the experimental results, the UV-induced index modulation the initial decays very sharply, but the rate of decay decreases as time advances, in the meantime the reflectivity decay of Bragg grating has also strong relationship with temperature. As the reflectivity of the fiber Bragg grating of which is annealed at a fixed temperature for a sufficiently long time is nearly unchangeable, there are two of possibilities in this matter. One of them is the thermal depopulation of the traps at a given time and temperature approximately corresponds to shallower traps (which is the trapped energy smaller than the thermal energy) being emptied. Another one is that the trapped electron in deeper traps is not able to move to the shallower traps spontaneously. In this case, if the trapped electron can move spontaneously from one trap to another, (for example, the trapped electron can move from deeper trap to the shallower trap), the reflectivity decay will continue until the reflectivity goes to zero.

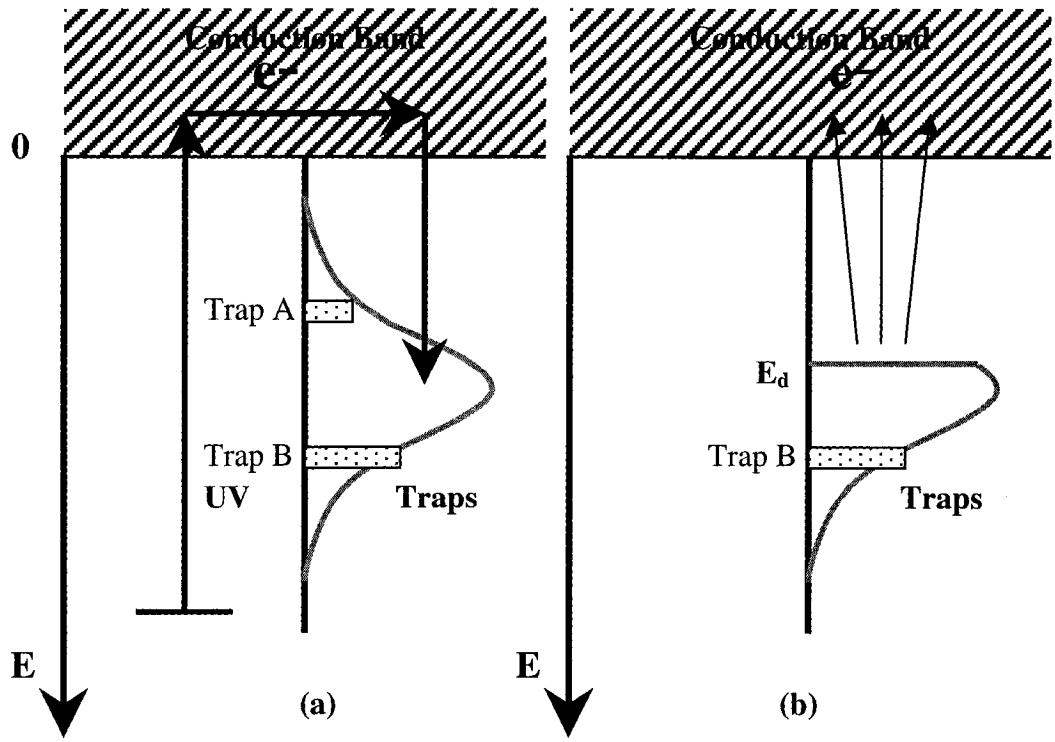

Figure 4.5 *Diagram of the physical model for the first hypotheses.*

Figure 4.5 shows the diagram of the physical model for the first hypotheses. Electrons excited by UV excitation are trapped in a continuous distribution of traps. Some of these electrons are trapped in the trap A and trap B respectively. The position of trapped electron is not changeable and the electrons in at B position will be not able to move to position A spontaneously. In the annealing process, the thermal depopulation of the traps at a given time and temperature approximately corresponds to shallower traps ($E<E_d$) being emptied and deeper traps ($E>E_d$) remaining full, for example, the trap B. If this hypothesis is tenable, the reflectivity decay will not happen unless the temperature is higher than annealing temperature ($E>E_d$). In another word: we can use thermal treatment to increase the non-decay temperature range for fiber Bragg grating temperature sensor.

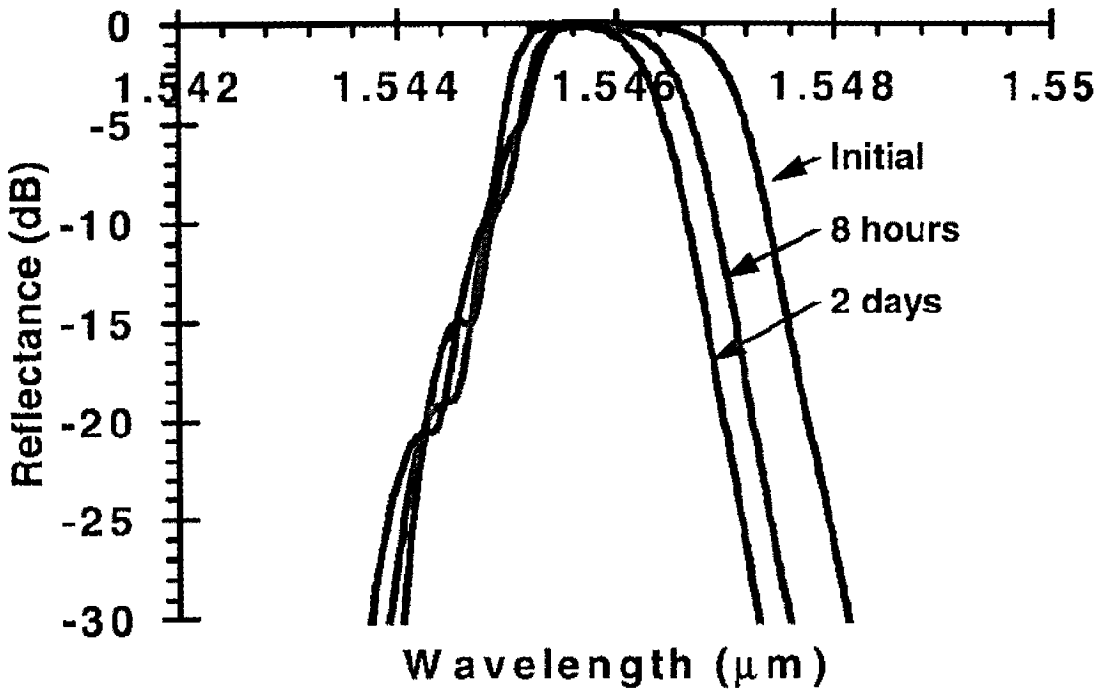

Figure 4.6 *Saturated fiber Bragg grating degradation at 225 °C* [1].

Nowadays, the hydrogen loaded fiber Bragg gratings are the most popular grating product using in the optical communication domain. Hydrogen loading increases the

photosensitivity of the standard optical fiber (See chapter 3), allowing the index modulation (Δn) much greater than in non-hydrogen loaded fiber to be achieved. In Baker's works [8], the boron-germanium-co-doped silica fibers are loaded with hydrogen 140 atm at room temperature for a period of ten days. The hydrogen loaded and unloaded fiber Bragg gratings have been written under the same condition with a continuous-wave (CW) 244 nm laser and 90 mW output. The index modulation respectively for the hydrogen-loaded fiber Bragg grating is $4x10^{-3}$ and for the non-loaded fiber Bragg grating is $0.4x10^{-3}$. The decay of hydrogen-loaded grating is shown in Figure 4.6.

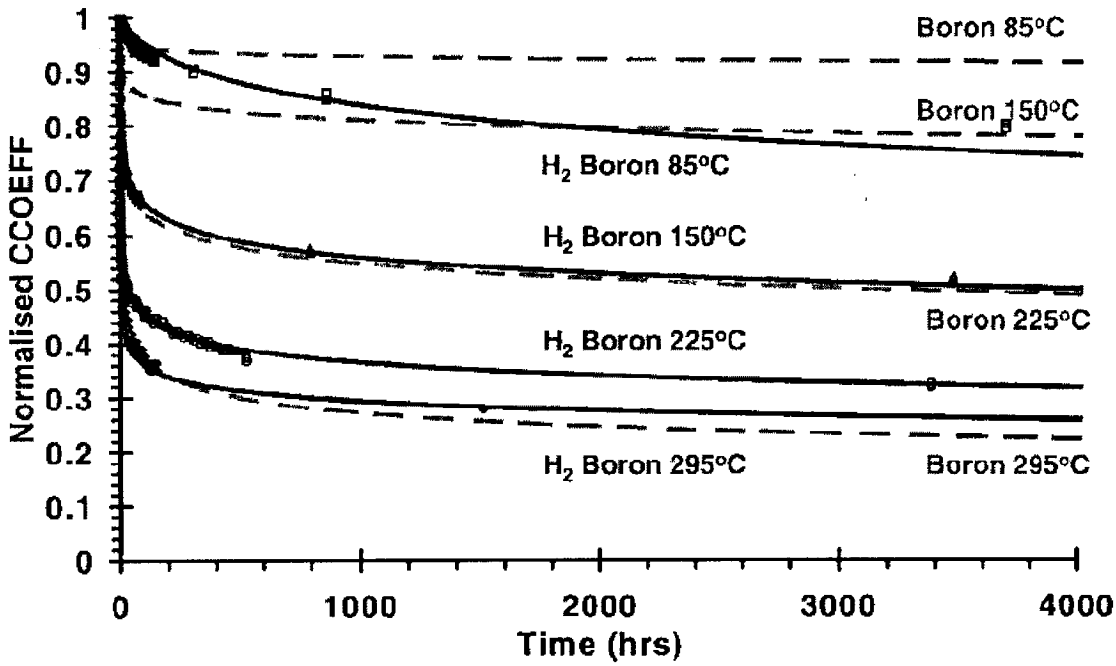

Figure 4.7 *Thermal degradation of hydrogen loaded fiber Bragg gratings (solid line). The dash-lines are the thermal degradation of hydrogen loaded fiber Bragg gratings* [1].

Figure 4.7 shows the normalized index modulation plotted against time for the hydrogen-loaded fiber Bragg gratings. Time zero starts the gratings are placed in the preheated oven at particular test temperature at 85 °C for two days. The decay is sharply

at first followed by a substantially decreasing rate of decay. Comparing with the decay of the non-hydrogen loaded fiber Bragg grating, the decay through follows a different path.

Figure 4.7 gives us a comprehensive view of the thermal decay at the different temperature. At temperature of 85 °C and 150 °C the decay of hydrogen loaded fiber Bragg grating is significantly greater than those non-hydrogen loaded case. In pace of the increased temperature, the disparity of decay with hydrogen loaded and non-hydrogen loaded fiber Bragg grating both tend to equal. The reference data shows, as the temperature approaches 295 °C, the different between these two kinds of fibers becomes less. At temperature of 295 °C, the decay rates are proximately equal; hence, the decay of hydrogen loaded fiber Bragg grating can fit the "power law" in the higher temperature range. The diagram of the physical model of the traps energies (activation energies) can illustrate in Figure 4.8.

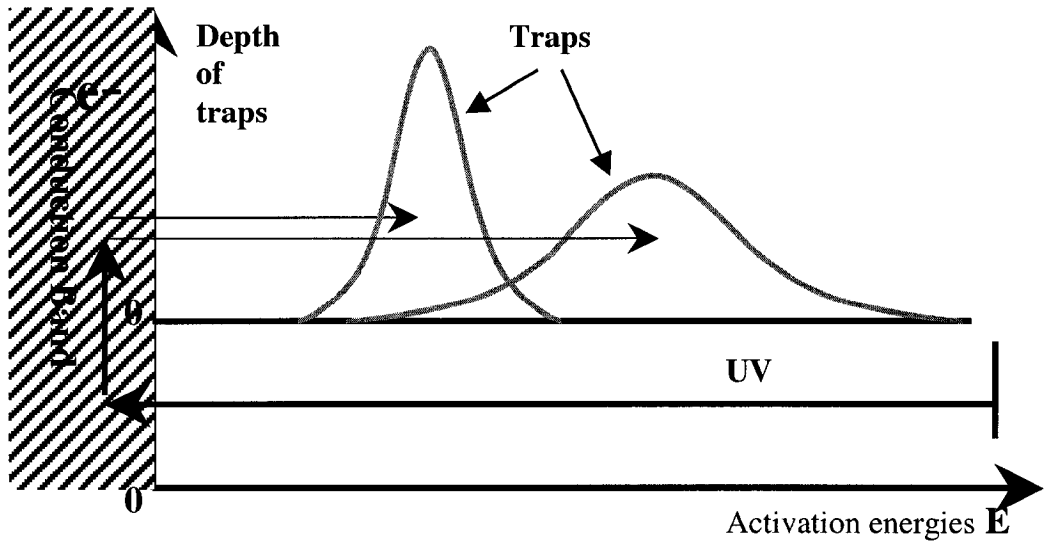

Figure 4.8 *Diagram of the physical model for the hydrogen-loaded fiber Bragg grating.*

Conclusions of the first hypothesis of hydrogen loaded fiber Bragg gratings:

1. In higher temperature range, hydrogen loaded fiber Bragg gratings have the same decay characteristic with non-hydrogen loaded fiber Bragg gratings.
2. Thermal treatment can increase the non-decay temperature range of the fiber Bragg grating.

4.2.2 Second hypothesis

In 1994 Erdogan *et al.* [40] detailed firstly about the grating stability and processed a model to explain the thermal degradation characteristics of fiber Bragg gratings written in germanium and erbium-germanium-co-doped silica fibers. To test and verify his method, a grating was firstly heated to 350 °C, then cooled down and then reheated up to 550 °C again. Figure 4.9 shows this process. The grating decayed to ~33% of its initial value, regardless of whether the grating started this (heating, cooling, and reheating) cycle with its initial strength (Figure 4.10), or with 75% of its initial strength (Figure 4.9), with the first 25% erased at temperature of 350 °C cycle.

Tasi *et al.* did the similar works in 1997 [38]. The fiber Bragg gratings were fabricated in boron-germanium-co-doped silica fibers, using a phase-mask (the period Λ is equal 1.0896 μm). A multi-gas KrF excimer laser (Lambda Physik EMG-103) operated at 30 mJ /pulse and a repetition rate of 20 Hz was used to expose the fibers. The experimental results show in Figure 4.11, in which display the decay of the grating starting at around 300 °C and the decay rate (the change of the index modulation versus the change of temperature) looks like constant. The curve of the change of index modulation is continuous and without any interrupt.

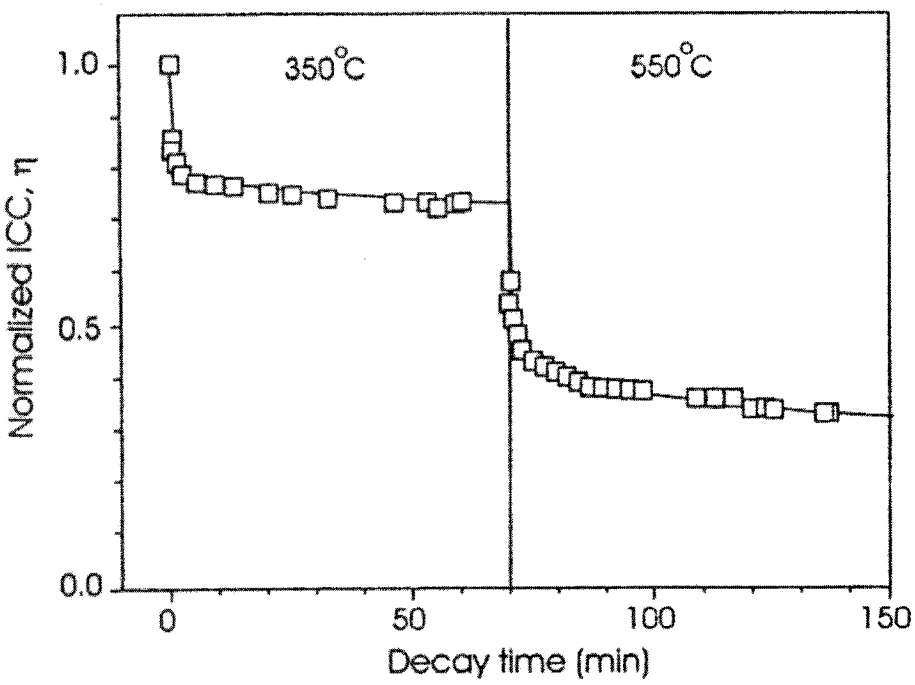

Figure 4.9 *Decay of a single grating heated first to 350 °C and then to 550 °C. The data are consistent with the treatment of the 350 °C segment as decelerated aging of the 550 °C decay, as shown by the solid curve prediction* [40].

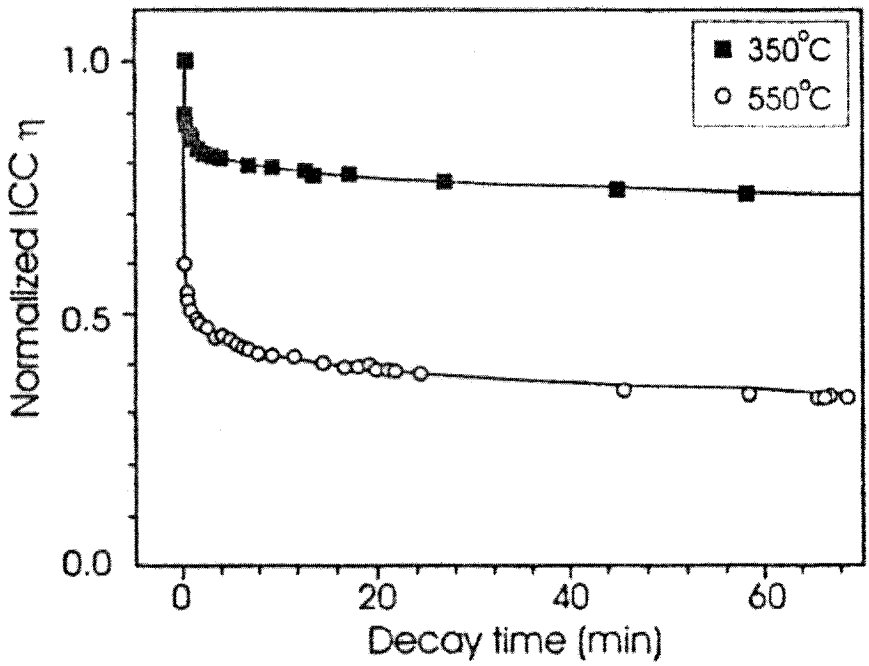

Figure 4.10 *Measured integrated coupling constant normalized to starting value for two gratings heated to 350 and 550°C as a function of decay time. Solid lines are fits to equation 3.6* [40].

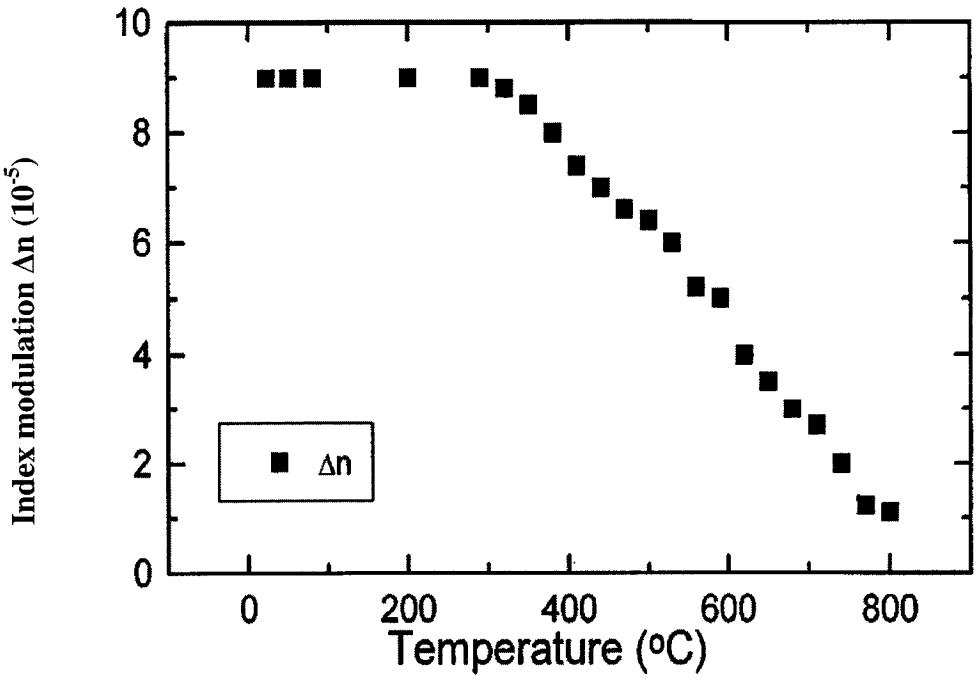

Figure 4.11 *The index modulation Δn in the isochronal annealing process versus temperature and fit to linear relationship* [38].

Conclusions of the second hypothesis of fiber Bragg gratings:

1. The depth of the traps (activation energies) is limited.
2. The rate of the decay of index modulation versus temperature fits the linear relationship.
3. The shape of the electron traps conforms to Gaussian distribution, being continual and having a flat top.

The extended diagram of the physical model for fiber Bragg grating can redraw as Figure 4.12.

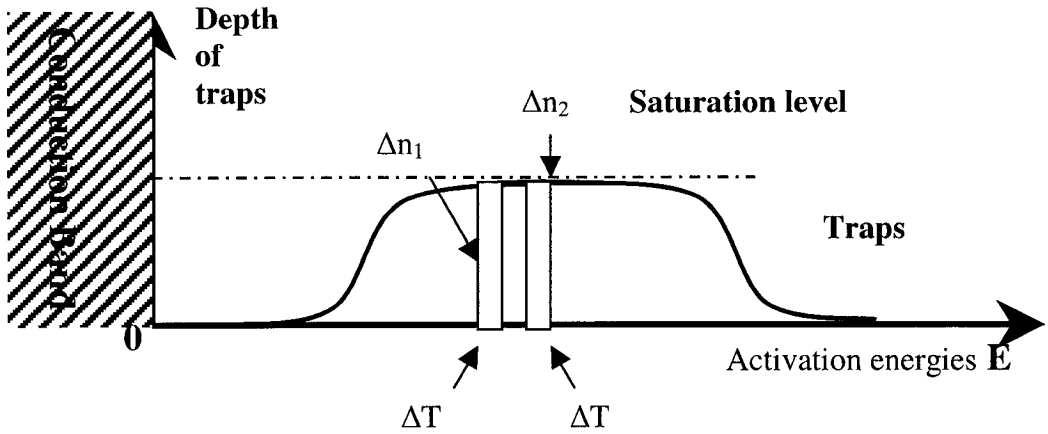

Figure 4.12 *Extend diagram of the physical model for fiber Bragg grating.*

4.2.3 Third hypothesis

Thermal reflectivity decay of fiber Bragg grating is always a major topic in optical communication domain and concerning about optical sensor. The thermal stability of gratings depends on several factors such as:

1. The type of fibers [49, 50].
2. The writing wavelength [51, 52].
3. The treatment process [53, 54].
4. The writing time [55].
5. The writing energy [55].

Dong and Liu [55] have examined the thermal induce decay of fiber Bragg grating with different writing time phase. Two gratings were written at 193 nm in Boron-co-doped germanosilicate fiber, with same UV laser writing energy, but in different writing time phase. The experimental results are shown in Figure 4.13 and Figure 4.14.

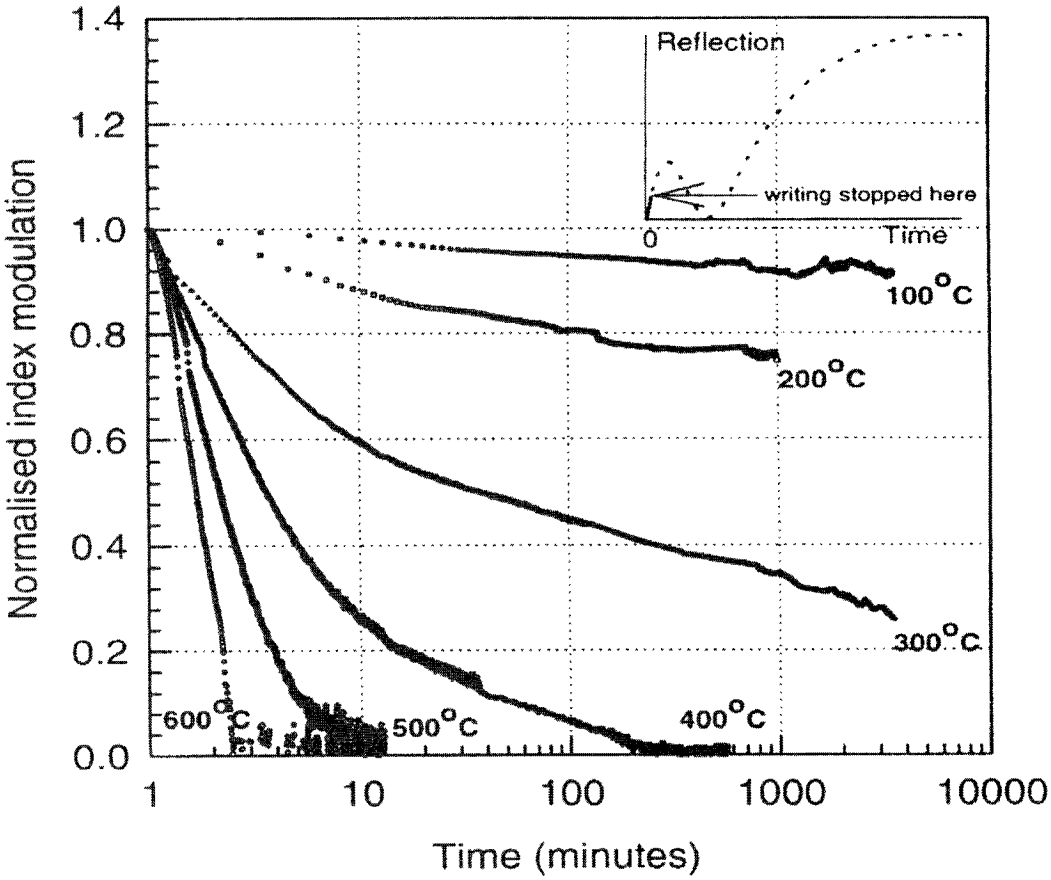

Figure 4.13 *Decay of grating formed with a short writing time (30 seconds) at different temperature and power law fittings to the data* [54].

In Figure 4.13, the Bragg grating, which possess a lower reflectivity (30 seconds writing time), can not stabilize at all measured temperatures, even the thermal annealing temperature was as low as 100 °C and was erased after two minutes at temperature of 600 °C. Oppositely, the Bragg grating has higher reflectivity as shown in Figure 4.14 (30 minutes writing time), can survive at temperature of 600 °C for nearly 10 minutes and also keep for long time non-decay with annealing at temperature of 400 °C.

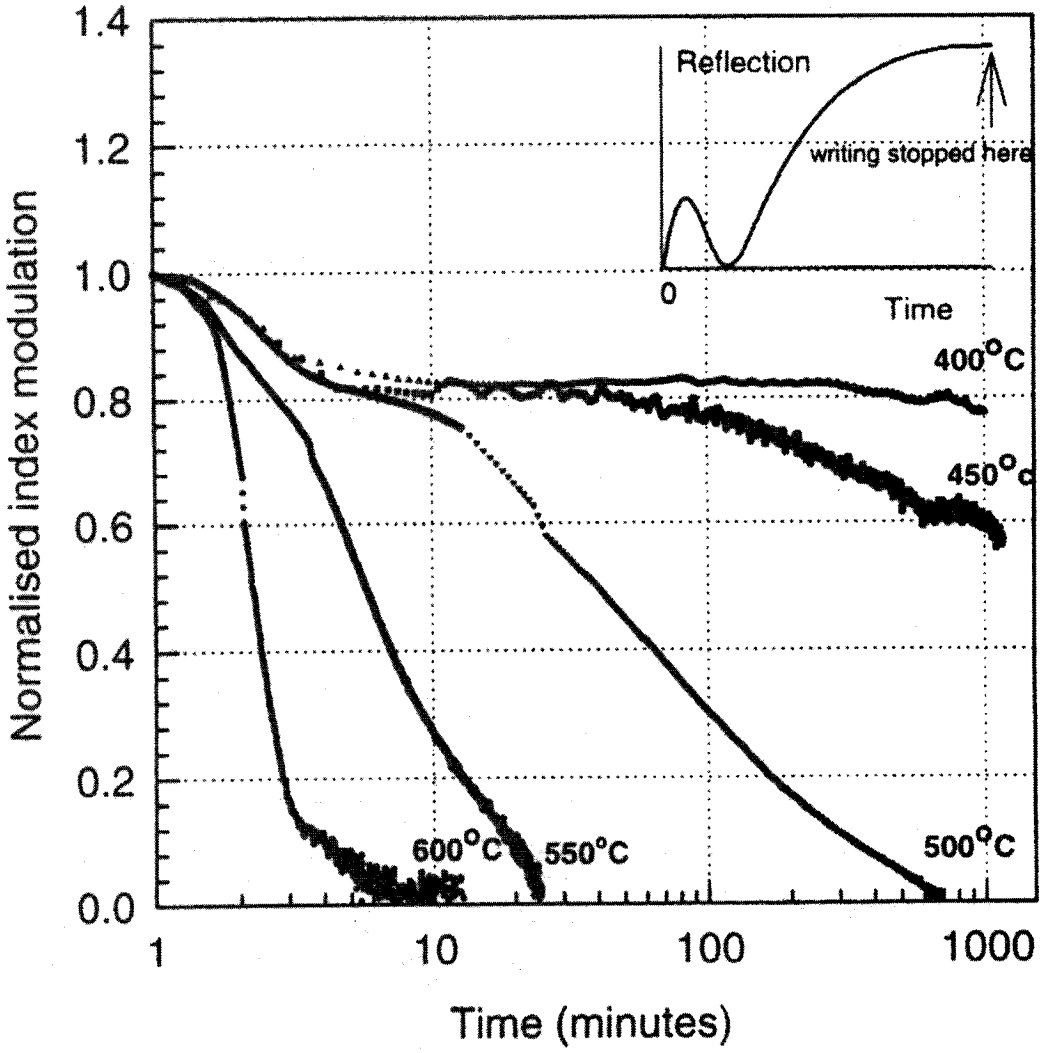

Figure 4.14 *Decay of grating formed with a long writing time (30 minutes) at different temperature and power law fittings to the data* [54].

Conclusions of the third hypothesis of fiber Bragg gratings:

1. Increased writing time phase may cause more effective thermal stability of fiber Bragg gratings.
2. Increased index modulation (Δn) can rise the non-decay temperature of annealed grating for the sensing using.
3. Based on the "power law", the trapped electron excited by UV excitation will fill

in the shallower traps (lower activation energies and activate at lower temperature) firstly and then fill in the deeper traps (high activation energies).

4.2.4 Summary of the hypotheses

These three hypotheses give the descriptions of the simple physical model of the trapped electron in the fiber Bragg grating. The first hypothesis is about the thermal annealing model of the trapped electron of fiber Bragg grating. It is extended and perfect for the "power law" and expatiates the moving ability and moving direction of the trapped electron in the fiber Bragg grating of the thermal annealing. The second hypothesis is concerning the structure model of the distribution of the trapped electron in the fiber Bragg grating. The third hypothesis describes the "filling" process, in which the excited electrons by UV laser fills into the traps in the fiber Bragg grating writing process.

4.3 Design of hydrogen loaded fiber Bragg gratings for high temperature sensor applications

Fiber Bragg gratings are compact intrinsic temperature sensing elements. The fiber Bragg grating temperature sensor reflects one particular wavelength and transmits all others. The reflected wavelength can vary with the changing of sensor's temperature. So, fiber Bragg grating temperature sensors have been widely used in applications in monitoring temperature.

The ability of being stubborn of the fiber Bragg grating is based on the effective "filtering" of the inject light. The thermal decay of reflectivity may cause invalidation of fiber Bragg grating at high temperature circumstance. The motivation of the design for high temperature fiber Bragg gratings are to increase the non-decay temperature range of

fiber Bragg grating or pull up the erasing temperature of sensors. Nowadays, researchers are attempting variant methods to get their common goal, which is to let the fiber Bragg grating temperature sensors work in high temperature range. To improve the stability of gratings has generally involved experimenting with various dopants, include Tin (Sn) [57]. Fiber Bragg gratings written into such fibers appear stable at about 575 °C; however, the grating temperature sensors, which are written into the Tin (Sn) co-doped fiber, can not replace the conventional temperature sensors widely, because the price of these sensors are too expensive to acceptable.

Nowadays, most gratings are fabricated using hydrogen loaded germanosilicate optical fibers in optical component industry. Due to the large-scale production, the price of these gratings is reasonable. No matte how bad the thermal stability of the hydrogen loaded fiber Bragg grating is, we are still unremitting effort, notwithstanding.

Present-day, the most promising method for improving the stability of fiber gratings is thermal annealing. As we all know, the physical diagram of the electron traps (activation energies) was described as Gaussian distribution, being continually, and having a flat top. The annealing temperature, which is called as E_d (in Figure 4.5) or activation energies from the heating, is limited by the position of highest trap or activation energy of gratings. That means the range of annealing temperature is proportion to the bandwidth of the traps. This relationship between heating temperature and FWHM of the traps is related in Figure 4.15.

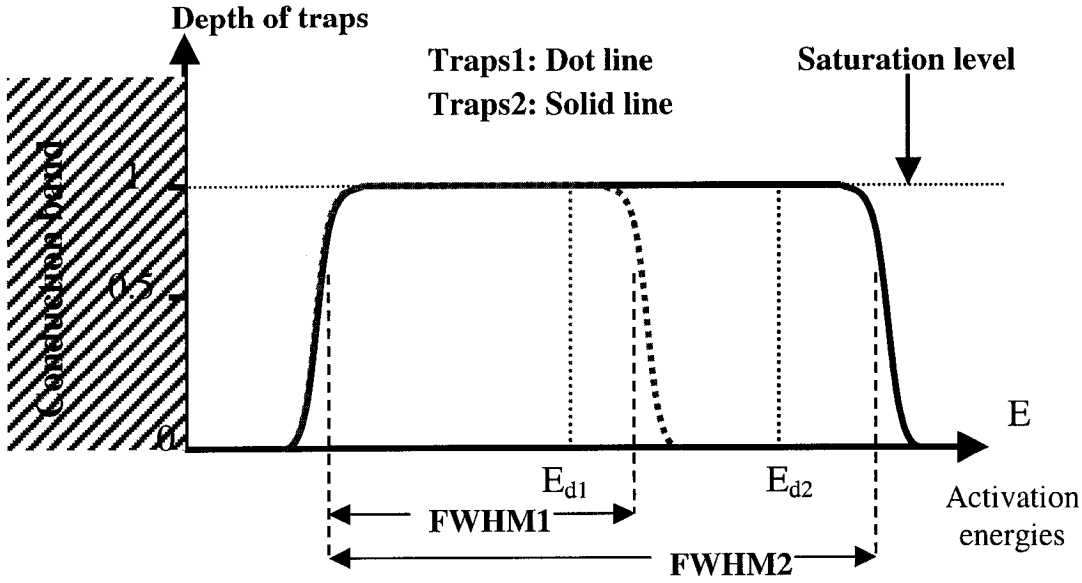

Figure 4.15 *Diagram of the physical model for the increased FWHM of traps.*

In the diagram of Figure 4.15, the number of trapped electrons excited by UV laser is the number of DIDs. The total area of the shape or the number of the traps is related to the index modulation (Δn). Two fibers, which are written under the same conditions with different writing time t_1 and t_2, have different index modulations Δn_1 and Δn_2 for the first fiber and second fiber. If t_1 (non-saturation) is smaller than t_2 ($t_1 < t_2$), we have index modulation of fiber 1 less than fiber 2 ($\Delta n_1 < \Delta n_2$), or the $FWHM_1$ less than $FWHM_2$, which is shown in Figure 4.15. When we heat the first fiber to reach the temperature of T_1, which is related to the point of E_{d1}in Figure 4.15, the normalized reflectivity R_1 can be written as $\Delta n_1' / \Delta n_1$, hereinto $\Delta n_1'$ is the remain area or traps beyond E_{d1}line. We assume the second fiber has the same remained reflectivity of the first fiber ($R_2 = \Delta n_1' / \Delta n_1 = \Delta n_2' / \Delta n_2$). During the increased index modulation, the activation energies are moved from point $E_{d1}$to E_{d2}. That means using this method, which

increases the index modulation of hydrogen-loaded fiber Bragg gratings, the thermal stability of gratings can be increased.

In this deduction, we used:

First hypothesis:

1. In higher temperature range, hydrogen loaded fiber Bragg gratings have the same decay characteristic with non-hydrogen loaded fiber Bragg gratings.
2. Thermal treatment can increase the non-decay temperature range.

Second hypothesis:

Due to the depth of traps is limited at the saturation level, the increased trapped electrons excited by UV laser must move to higher traps or higher activation energies.

Third hypothesis:

This hypothesis is the basic point of our design; only the different is this hypothesis talked about non-hydrogen loaded fiber Bragg gratings.

The deduction, which is discussed above, shows the thermal stability of gratings can be increased by the raising of the index modulation of fiber Bragg grating. If two fibers have the same reflectivity, the strong thermal stability of hydrogen loaded fiber Bragg grating could be provided by the wider bandwidth (larger FWHM) of grating, or the less effective grating length of grating (See chapter 2).

Chapter 5
Performance evaluation of designed high temperature sensors

This chapter gives the overall evaluation of the designed hydrogen loaded fiber Bragg grating temperature sensors in high and ultra temperature range.

5.1 Temperature sensors

Three hydrogen-loaded fiber Bragg gratings from different companies were used in the research of high temperature sensor based on the hydrogen-loaded fiber Bragg gratings. The gratings were fabricated using Conning (SM-28) and contain 3mol% of germanium.

The characters of fiber Bragg gratings show as following:

Fiber Bragg grating sample #1:

Table 5.1 Characteristics of fiber Bragg grating sample #1.

Produce Number: 080235720027 from Bragg photonics in Montreal	
TCWL: 1550.16 nm	Reflectivity: 99.62%
FWHM: 0.33 nm	Grating length: 8 mm
Fiber type: Hydrogen loaded SM-28 fiber	
Calculated index modulation: 3.6×10^{-4}	

Spectrum and Bragg wavelength at 24.4°C show in Figure 5.1.

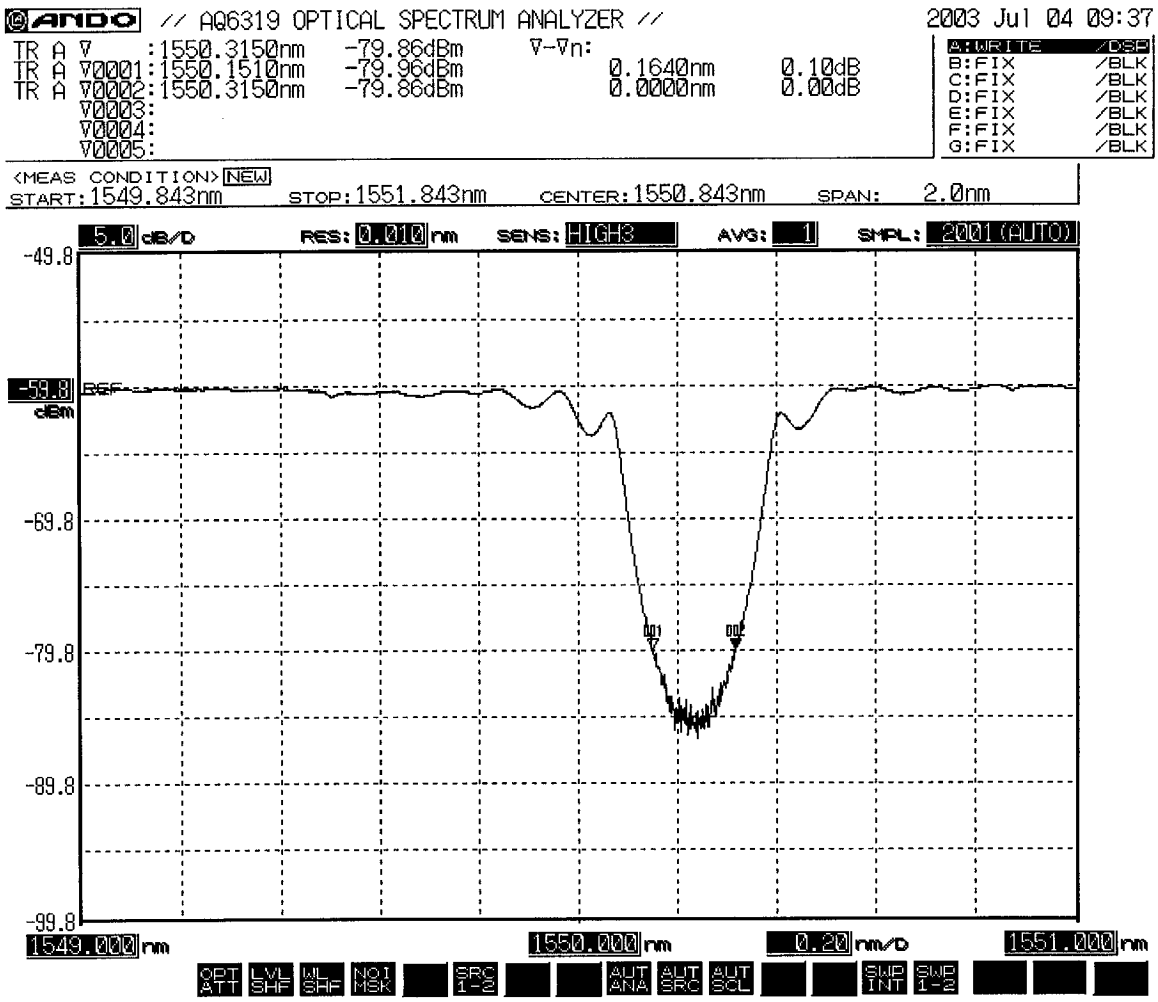

Figure 5.1 *Transmitted spectrum of fiber Bragg grating sample one* at *24.4°C.*

Fiber Bragg grating sample number #2:

Table 5.2 Characteristics of fiber Bragg grating sample #2.

Produce Number: OEFBG 14-033-2-7051 from O/E land in Montreal	
TCWL: 1484.138 nm	Reflectivity: 99.98%
FWHM: 0.45 nm	Grating length: 5 mm
Fiber type: Hydrogen loaded SM-28 fiber	
Calculated index modulation: 5.5×10^{-4}	

Spectrum and Bragg wavelength at 52.2°C show in Figure 5.2.

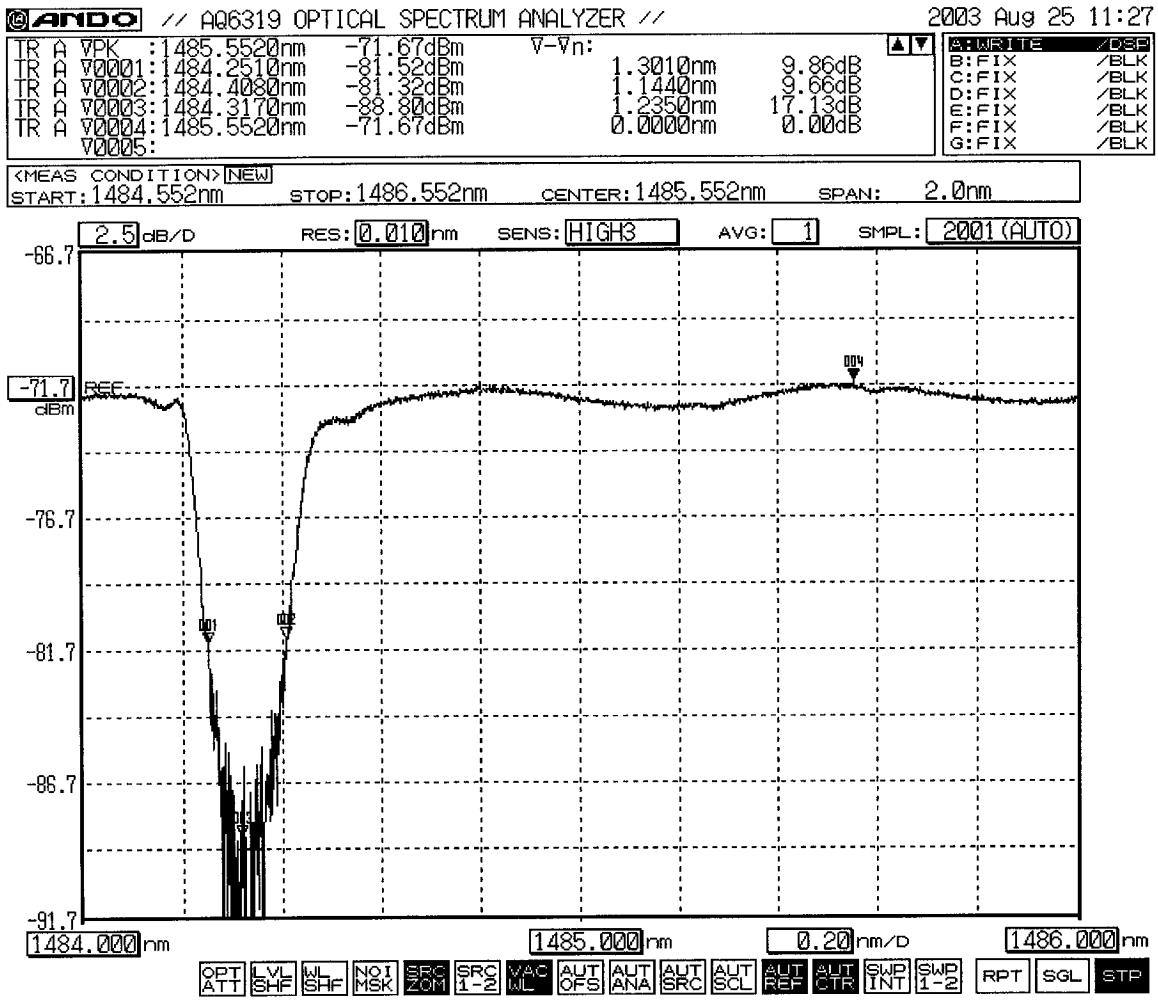

Figure 5.2 *Transmitted spectrum of fiber Bragg grating sample two at 52.2°C.*

Fiber Bragg grating sample #3:

Table 5.3 Characteristics of fiber Bragg grating sample #3.

Produce Number: OEFBG 14-033-2-7056 from O/E land in Montreal	
TCWL: 1484.981 nm	Reflectivity: 99.97%
FWHM: 0.48 nm	Grating length: 5 mm
Fiber type: Hydrogen loaded SM-28 fiber	
Calculated index modulation: 5.4×10^{-4}	

Spectrum and Bragg wavelength at 21.7°C show in Figure 5.3.

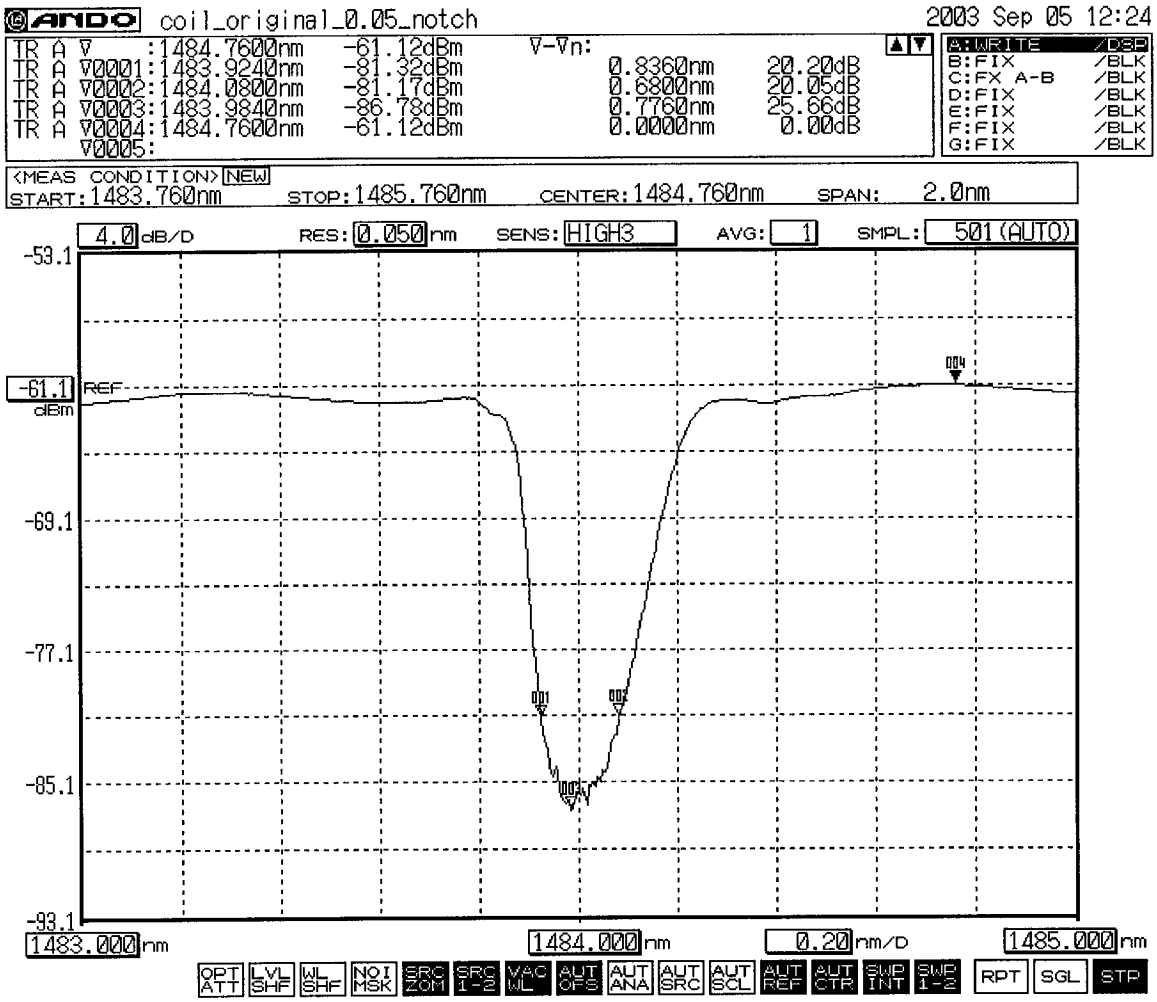

Figure 5.3 *Transmitted spectrum of fiber Bragg grating sample three at 21.7°C.*

5.2 Experimental setup and apparatus

Figure 5.4 shows the schematic performance evaluation system [58] of fiber Bragg grating temperature sensors. Following description explains the setup for examination of the FBG temperature sensor. The grating sample and the reference sensor thermometer were both placed in the middle of a small diameter glass tube (PIP of Figure 5.5). This step will prevent any deformation of the grating. The glass tube was laid inside the furnace to anneal. Then the samples have been tested for some important aspects such as the temperature sensitivity, thermal characteristics, and thermal stability at temperature

range from room temperature to above 900°C. A LED, which is the internal light source inside optical spectrum analyzer (OSA) with the central wavelength of ~1530 nm, a bandwidth of ~100 nm, and an output power of -10 dBm, used as the light source. The transmitted spectrum of the FBG was monitored by an optical spectrum analyzer (AQ6319) during the thermal testing.

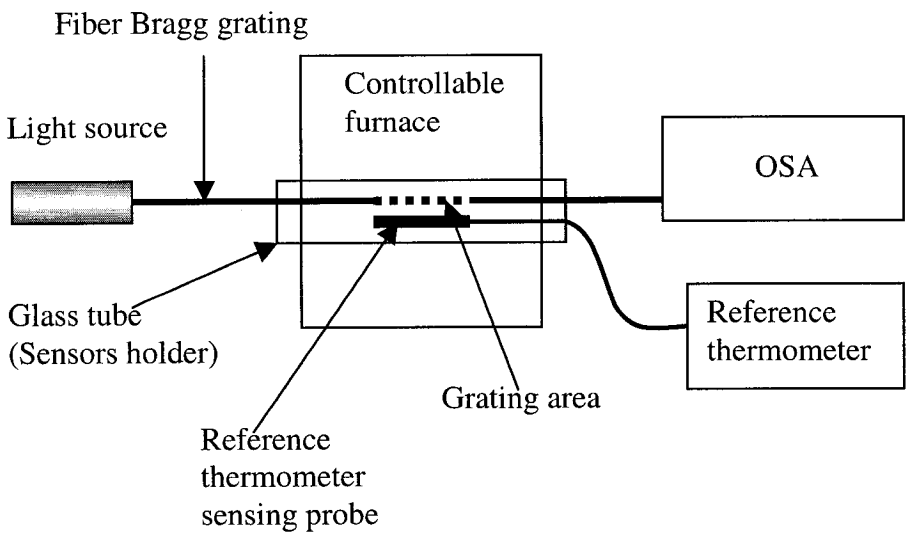

Figure 5.4 *Schematic of fiber Bragg grating temperature sensor's evaluation system.*

Since the variation in the Bragg wavelength caused by temperature fluctuations is quite small (our calculation in chapter 4 shows this change is 14 pm/°C), it is essential to have a high-resolution optical spectrum analyzer. In our evaluation testing, we use an optical spectrum analyzer AQ6319 from Ando as the wavelength detector and the light source. The setting of AQ6319 lists as following:

Resolution: 0.01 nm (depend on the measurement)

Measurement sensitivity: High 3

Number of averaging: 1

Span: 2 nm

SMPL: Auto

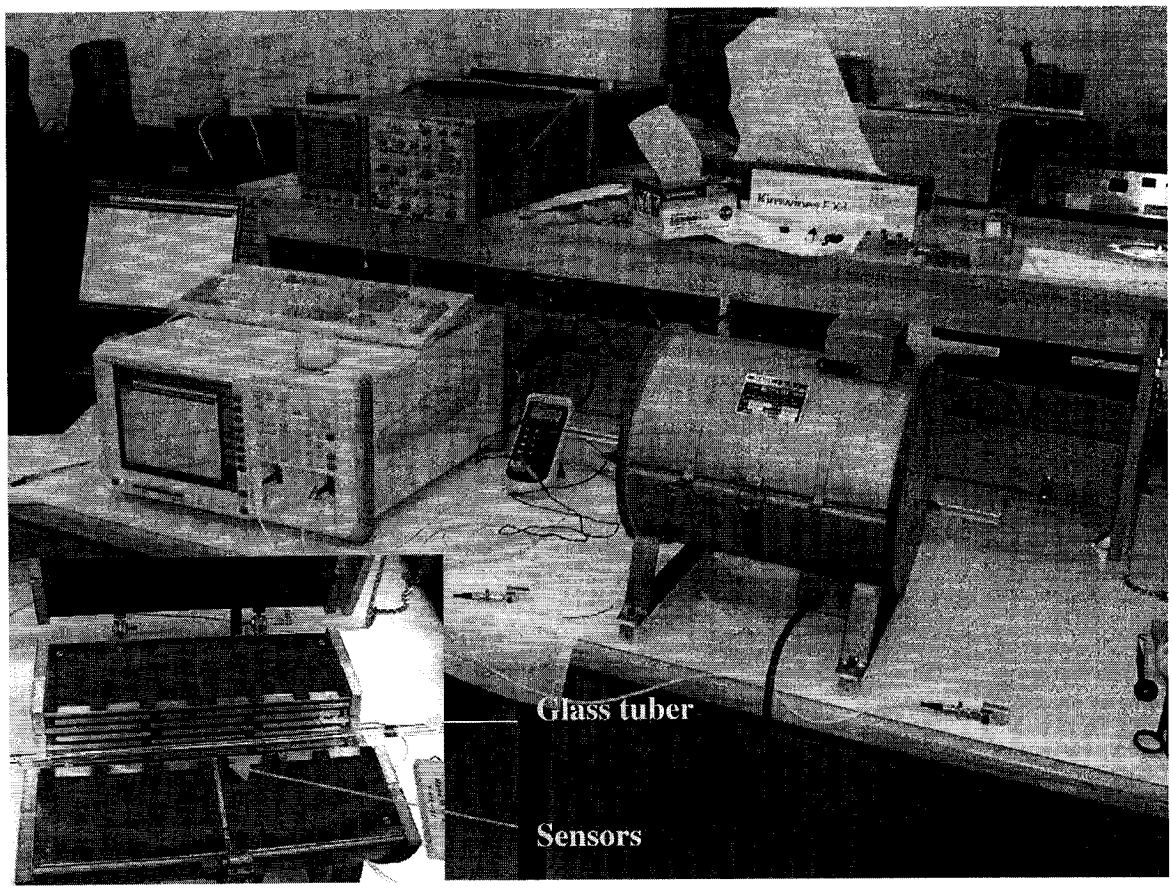

Figure 5.5 *Setup of fiber Bragg grating temperature sensor's evaluation system. The picture in picture shows the glass tuber and sensors inside the furnace.*

The reference thermometer is HH11 produced by Company Omega. The sensing probe of the thermometer is a Type K thermocouple and the resolution of the thermometer is 0.1 °C (below 200 °C) and 1°C (above 200 °C).

5.3 Experimental process

Three hydrogen loaded fiber Bragg gratings were tested in our research for validation of the three hypotheses, which are described in chapter 4, and the characteristics of hydrogen fiber Bragg gratings in high as well as ultra high temperature

range. In order to describe their distinguishing feature, we divided the entire experiment into four parts.

Evaluation processes:

In the first part, experimental #1, the grating sample #1 was tested from room temperature to above 800 °C. In the second part, experimental #2, the characteristics of hydrogen loaded fiber Bragg grating in high and ultra high temperature range were gauged by using grating sample #2 mainly. In the third part, experimental #3, step of experimental #1 was repeated using grating sample #3. The goal in this part is to grope for the different thermal stability between grating sample #1 and #3 because of their different Bragg wavelengths (1550 nm and 1485 nm). In the fourth part, experimental #4, the thermal decay of hydrogen loaded Bragg grating in high and ultra high temperature range was examined using grating sample #3, which had been cooled down for two days after experimental #3. The steps of four experimental testing are shown in follow.

5.3.1 Experimental #1 of evaluation processes

In the first process, step 1, grating sample #1, which has Bragg wavelength around 1550 nm and formatted by using UV laser in the hydrogen loaded SMF-28 fiber, was annealed from room temperature to about 470 °C for an hour, and then was cooled down to room temperature.

In the second process, step 2, the grating sample #1 was subjected to different testing temperatures in the range from room temperature to about 870 °C. The temperature changed of about 20°C in each sub-step and at each sub-step the specimen was left for approximately 2 minutes to achieve thermal equilibrium. The same procedure

was performed for all temperature section except at 700 °C; the sample #1 was left for about 2 hours to test the decay of isothermal annealing.

For both processes, the transmitted waveform was recorded by OSA. Meanwhile, the temperature of the reference thermometer was also noted.

5.3.2 Experimental #2 of evaluation processes

In the first process, step 1, grating sample #2, which has Bragg wavelength around 1480 nm and formatted by using UV laser in the hydrogen loaded SMF-28 fiber, was annealed from room temperature to about 450 °C for an hour, and then was cooled down to room temperature.

In the second process, step 2, the grating sample #2 was subjected to different testing temperatures in the range from room temperature to about 820 °C. The temperature changed of about 20°C in each sub-step and at each sub-step the specimen was left for approximately 2 minutes to achieve thermal equilibrium. The same procedure was performed for all temperature section except at 800 °C, for at this temperature the sample #2 was left for 20 minutes to test the decay of isothermal annealing.

In the third process, step 3, the grating sample #2 was cooled down from the last temperature section of process 2-- around 820 °C to the room temperature.

For last two processes, step 2 and step 3, the transmitted waveform was recorded by using OSA. Meanwhile, the temperature of the reference thermometer was noted also.

5.3.3 Experimental #3 of evaluation processes

The steps of this testing is similar to the experimental #1. In the first process, step 1, grating sample #3, which has Bragg wavelength around 1480 nm and formatted by

using UV laser in the hydrogen loaded SMF-28 fiber, was annealed from room temperature to about 450 °C for an hour, and then was cooled down to room temperature.

In the second process, step 2, the grating sample #3 was subjected to different testing temperatures range from room temperature to about 800 °C. The temperature changed of about 20°C in each sub-step and at each sub-step the specimen was left for approximately 2 minutes to achieve thermal equilibrium. The same procedure was performed for all temperature section except at 700 °C, for at this temperature the sample #3 was left for about one hour to test the decay of isothermal annealing.

For step 2, the transmitted waveform was recorded by using OSA. Meanwhile, the temperature of the reference thermometer was noted also.

5.3.4 Experimental #4 of evaluation processes

The experimental #4 is the continuum of the experimental #3. The grating sample #3 was cooled down after experimental #3 from 700 °C to about room temperature. After two days, the grating sample #3 was reheated by furnace slowly (slowly increased the input voltage of the furnace) until the temperature of furnace was up to 936 °C. The temperature changed of about 20°C in each sub-step and at each sub-step the specimen was left for approximately 2 minutes to achieve thermal equilibrium. The same procedure was performed for all temperature section except at 700 °C, for at this temperature the sample #3 was left for about two hours to test the decay of isothermal annealing.

5.4 Experimental results and discuss

5.4.1 Bragg wavelength shift with temperature

Figure 5.6 shows the dependency of the grating Bragg wavelength shifting on temperature during the whole experiment.

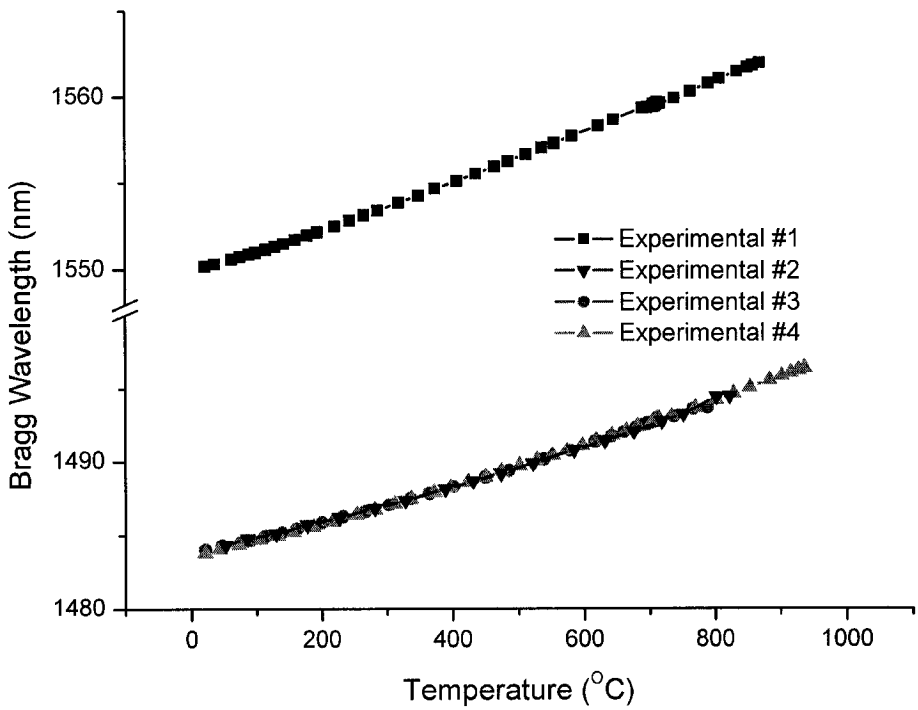

Figure 5.6 *Bragg Wavelength shift on temperature for all experimental testing in a wide temperature range.*

The dependency is approximately linear for all experimental testing (Figure 5.6). In these experiments, the highest operating temperature is 936 °C from experimental #4.

In the Figure 5.7, the square symbols indicate the Bragg wavelength of grating #1 at different temperature section in experimental #1, and the filled circles are the measured

points of Bragg wavelength of grating #3 in experimental #4 at different temperature section.

Figure 5.7 illustrates that trends of the increased Bragg wavelength are slightly different between hydrogen-loaded fiber Bragg grating sample #1 and sample #3 (experimental #4) within the lower temperature range. Within the range of high temperature, which is the operational temperature, even the tested fiber Bragg gratings have their own Bragg wavelength as well as different annealing temperature, the fiber Bragg grating made by hydrogen loaded SM-28 fiber, has the same rate of Bragg wavelength shift corresponding with temperature.

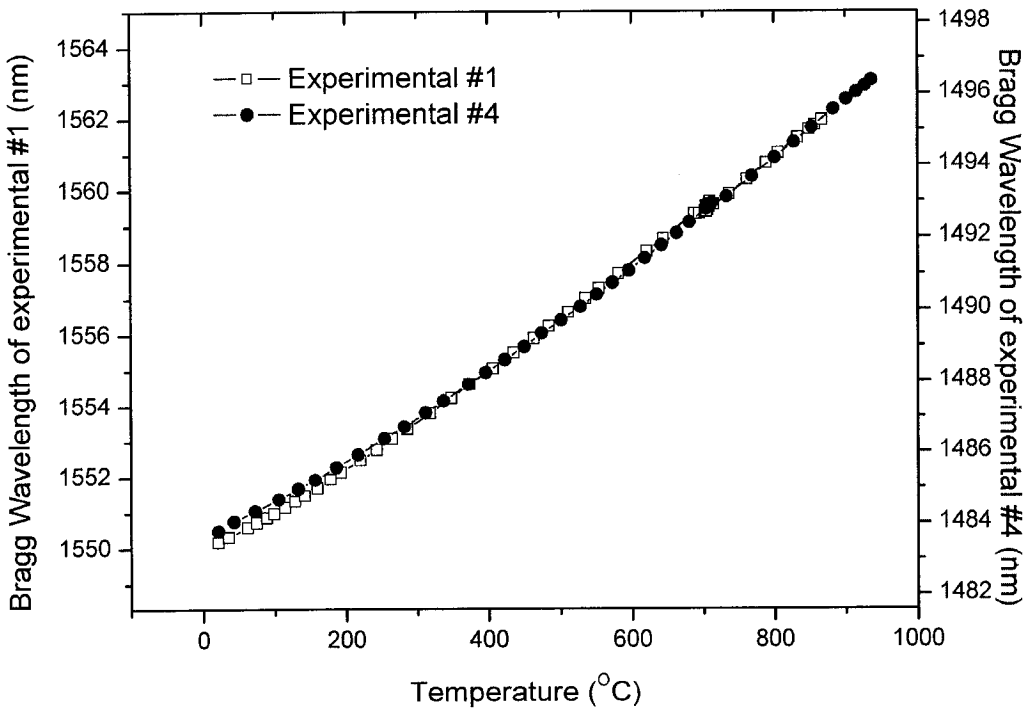

Figure 5.7 *The curves show the different of ascended Bragg Wavelengths of sample #1 and sample #4 from room temperature to above 800 °C.*

The fiber Bragg grating samples of experimental #2 and #3 are fabricated in the same company and with similar Bragg wavelengths. Table 4 shows the characteristics of grating sample #2 and sample #3.

Table 5.4 Characteristics of fiber Bragg grating sample #2 and sample #3.

Parameters / Samples	TCWL (nm)	FWHM (nm)	Annealing temperature (^{O}C)	Annealing time (hour)
Sample 2	1484.138	0.45	450	1
Sample 3	1483.981	0.48	450	1

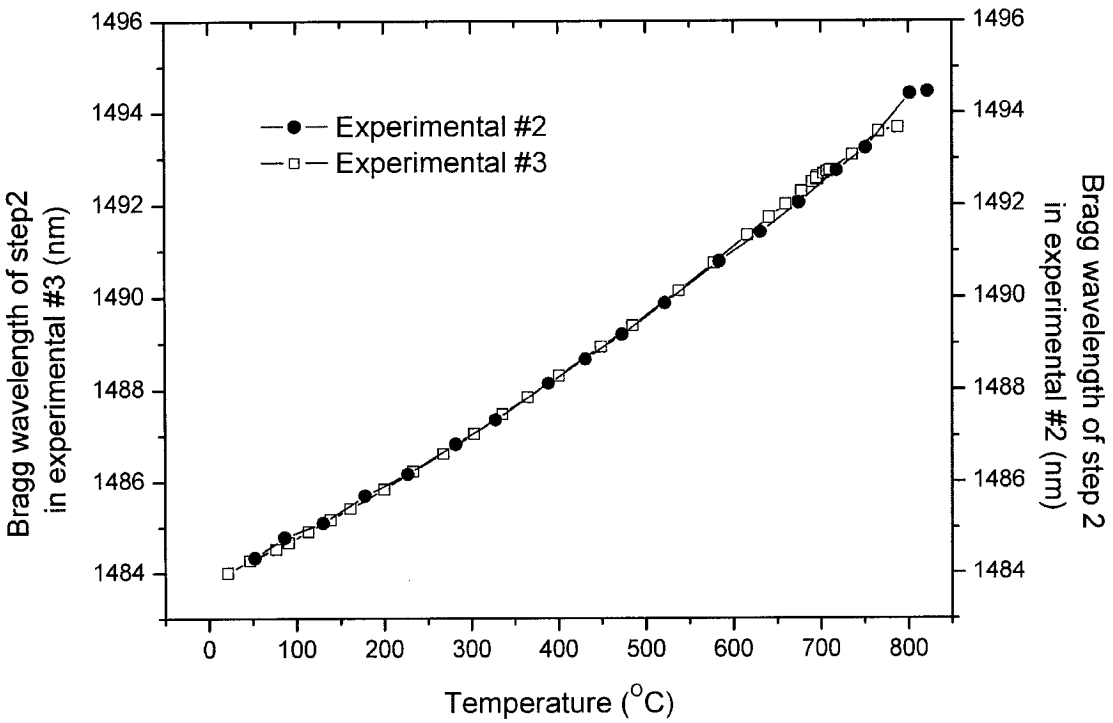

Figure 5.8 *Bragg wavelength of fiber Bragg grating sample #2 and sample #3 at different temperature with zero applied strain.*

In Figure 5.8, the two curves, which are the curve of filled circuits and the curve of square samples, coincide with each other. This means the sensitivity of the Bragg wavelength around 1480 nm is uniquely related to temperature.

The average temperature sensitivity of the hydrogen loaded fiber Bragg grating was 0.013nm/°C. However, as shown in Figure 5.9, it is necessary to note that the Bragg

wavelength temperature dependency is not strictly obey the lineal law (See chapter 4, [58]), the sensitivity at lower temperatures is 0.010nm/°C but changes to 0.017 nm/°C at temperature around 700 °C (Figure 5.7, experimental #4). In contrast, the theoretical parameter [42] of sensitivity of grating temperature sensor provides a coefficient of about 0.0136nm/°C, which calculated using equation 4.22 with $\alpha_\Lambda = 0.55 \times 10^{-6}\ ^\circ C^{-1}$, $\alpha_{neff} = 8.6 \times 10^{-6}\ ^\circ C^{-1}$ and 1485 nm Bragg wavelength of fiber sample #3.

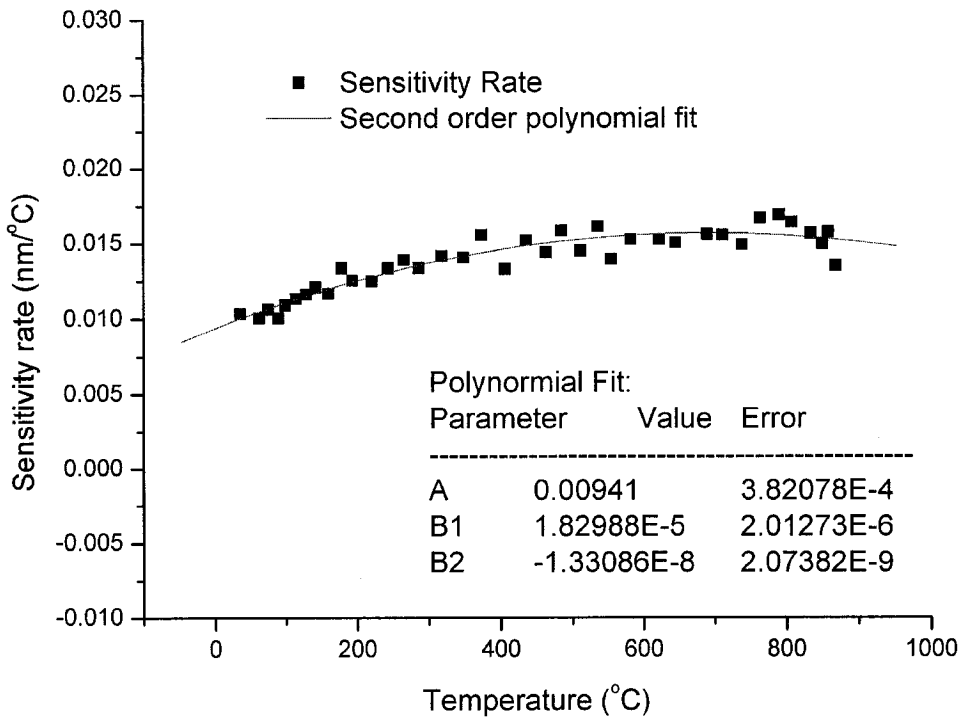

Figure 5.9 *Sensitivity of Bragg Wavelength shift with temperature in experimental #1. The results in this testing are fit to the Second order polynomial (single line).*

The rates of the tested fiber Bragg grating (sample #1) at different temperature are fit to the second order polynomial, which shown as following:

$$R = A + B_1 T + B_2 T^2 \tag{5.1}$$

where R is the sensitivity rate of fiber Bragg grating sample #1 corresponding with temperature, T is the temperature in Celsius, and A, B_1, and B_2 are the parameters, which are shown in Figure 5.9.

As to the fiber Bragg grating temperature sensors, the high temperature circumstance may chemically and physically modify the grating structure. For example, the high temperature may reduce the index modulation and the reflectivity of the grating. The direct outcome is the Bragg wavelength shift to the blue side as shown in Figure 4.6 and Figure 5.10. In optical term the blue shift is the phenomenon that is the wavelength shift from long wavelength to short wavelength. In Figure 5.10, all Bragg wavelengths are forced to move from longer wavelengths (filled circuit curve) to the short wavelengths (filled square curve) in the low temperature rang after annealing.

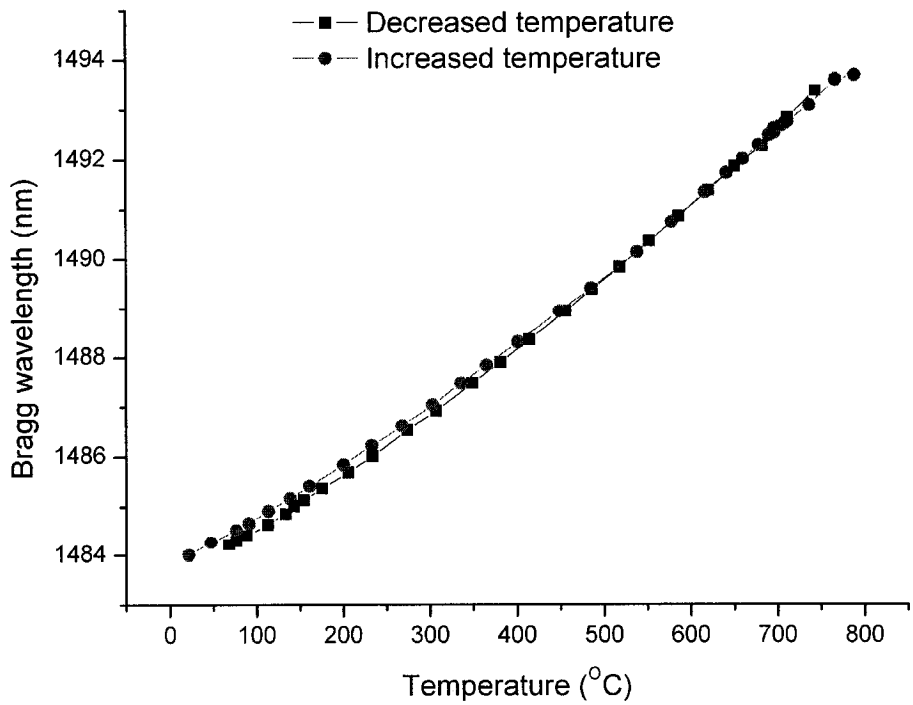

Figure 5.10 *Bragg Wavelength shift with temperature for experimental #3. This figure illustrates the blue shift at low temperature with one hour annealing time at 700 °C.*

This blue shift is concomitance with the thermal decay. If the grating temperature sensors are annealed for a sufficient long time, the decay of the grating structure will be stabilized. Afterwards, if operated temperatures are lower than the annealing temperature, the grating generally does not experience further thermal decay. Then the blue side shift will not occur in this case. In the optical communication system, the annealed Bragg grating of which is annealed at 350 ℃ for 40 second can be used under 80℃ for 25 years without evident Bragg wavelength shift. For this reason, the un-annealed hydrogen loaded fiber Bragg grating cannot be used for the temperature sensor. Because the thermal treatment can increase the thermal stability of grating temperature sensors, the thermal treatment also can restrain the blue shift of Bragg wavelength. It is important that the Bragg wavelength at room temperature remained unchangeable after each heating step. This fact testifies that the Bragg wavelength is uniquely related to temperature and will not be deviated from the calibration value in the course of operation of a grating-based temperature sensor.

Summary of this section:

1. The Hydrogen loaded fiber Bragg grating temperature sensors are the ideal temperature sensor for a wide range of temperature. The maximum operating temperature is 936 °C in experimental #4.
2. The sensitivity of the annealed Bragg wavelength is uniquely related to temperature.

5.4.2 FWHM and Maximum transmitted power with temperature

Figure 5.11 and Figure 5.12 show the transmitted spectrum of fiber Bragg grating sample #1 at temperature of 20.9°C and 867 °C. As shown in Figure 5.11 and Figure 5.12,

the FWHM was changed from 0.26nm to 0.11nm. That means the spectrum widths of the annealed gratings get narrower corresponding with the increased temperature. It is possible that the modulation part of the grating's index formed by the UV induced inner-stress during fabrication was relieved under the high temperature. Another possibility is that the supersaturated state of the index modulation was palliated. However, the most important explanation that we believe is the index modulation was reduced.

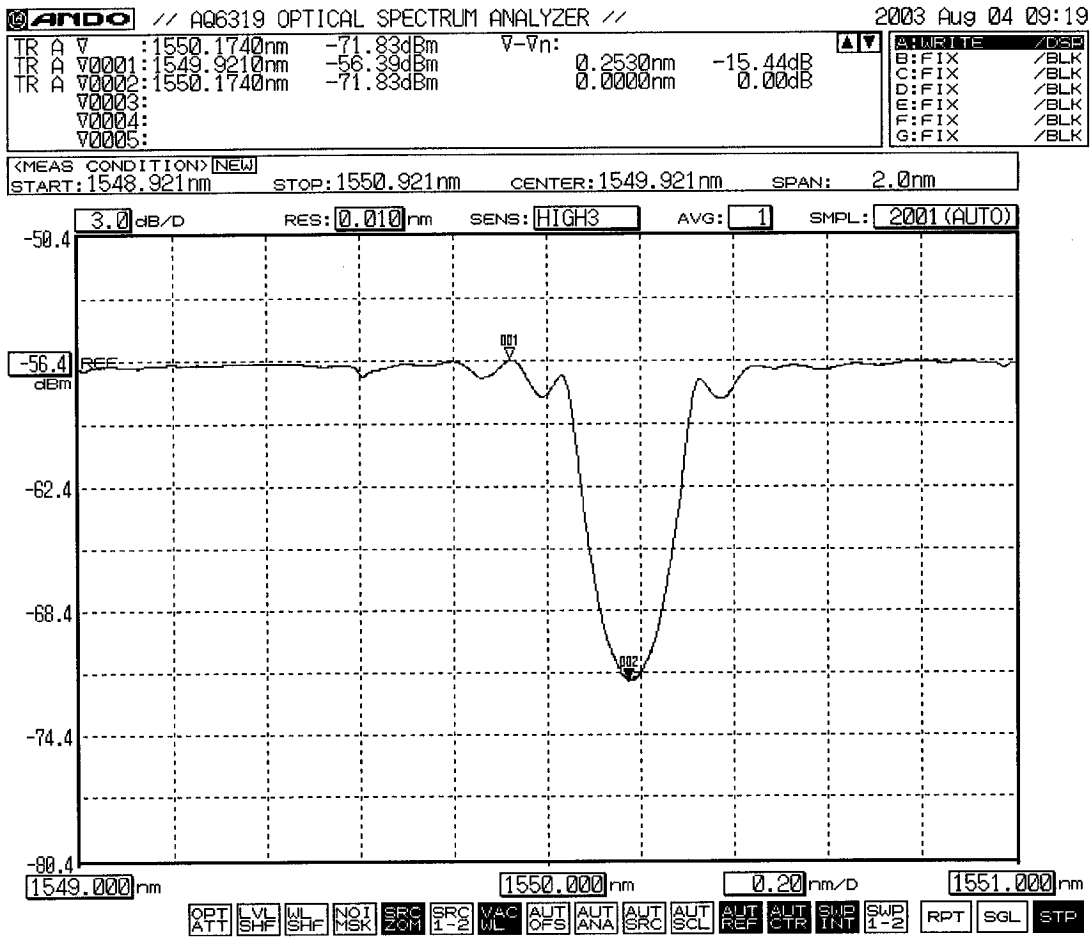

Figure 5.11 *The transmitted spectrum of the fiber Bragg grating sample #1 at 20.9 °C in experimental 1.*

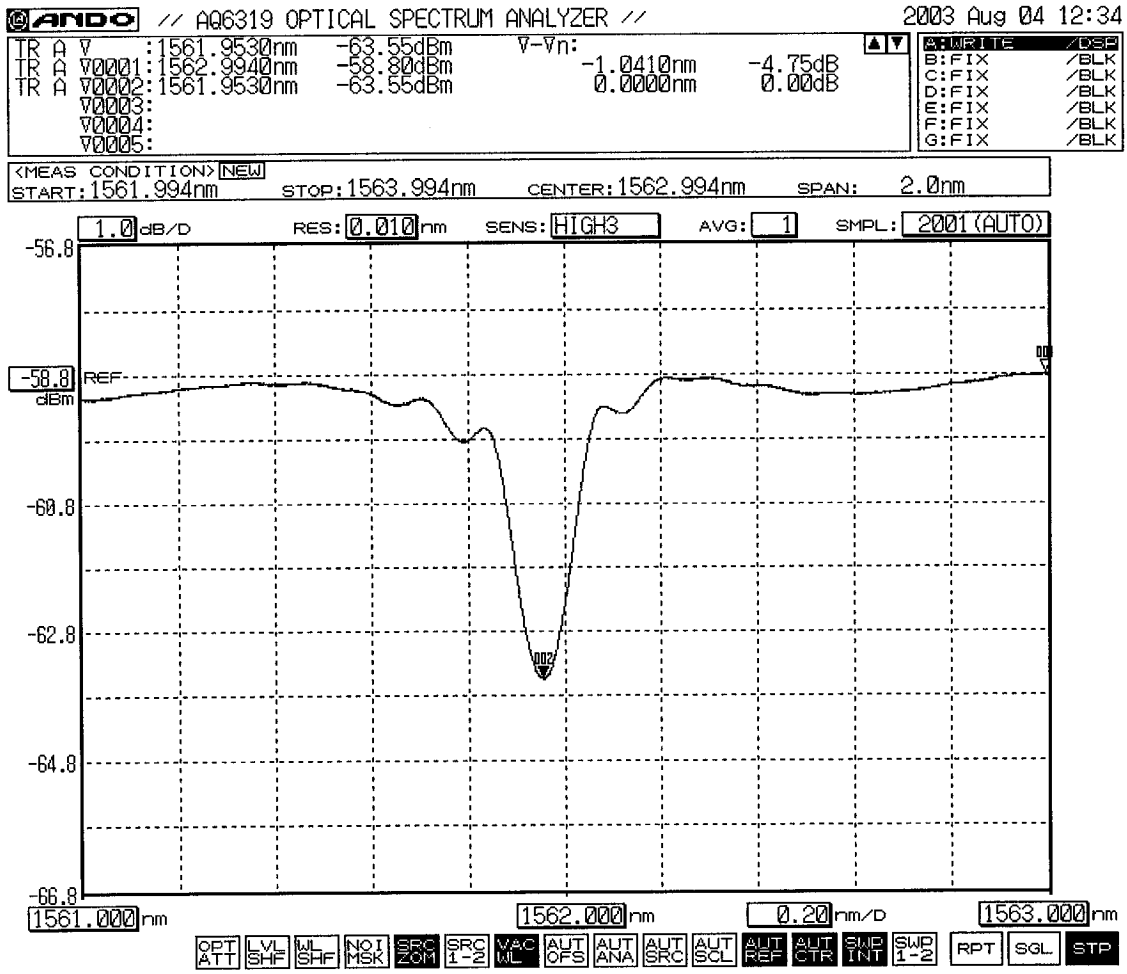

Figure 5.12 *The transmitted spectrum of the fiber Bragg grating sample #1 at 867 °C in experimental 1.*

Figure 5.13 interpret the results of decreased FWHM of grating sample #1 in thermal treatment experimental #1. Most results show the FWHM of grating sample #1 is reduced following the decreased index modulation. The meaning of these results is the thermal treatment can induce the decay of grating index modulation; at the same time, the FWHM of grating can be reduced too. In regard to the wavelength detect apparatuses; the narrow band of Bragg grating can help to increase the sensitivity of the Bragg wavelength.

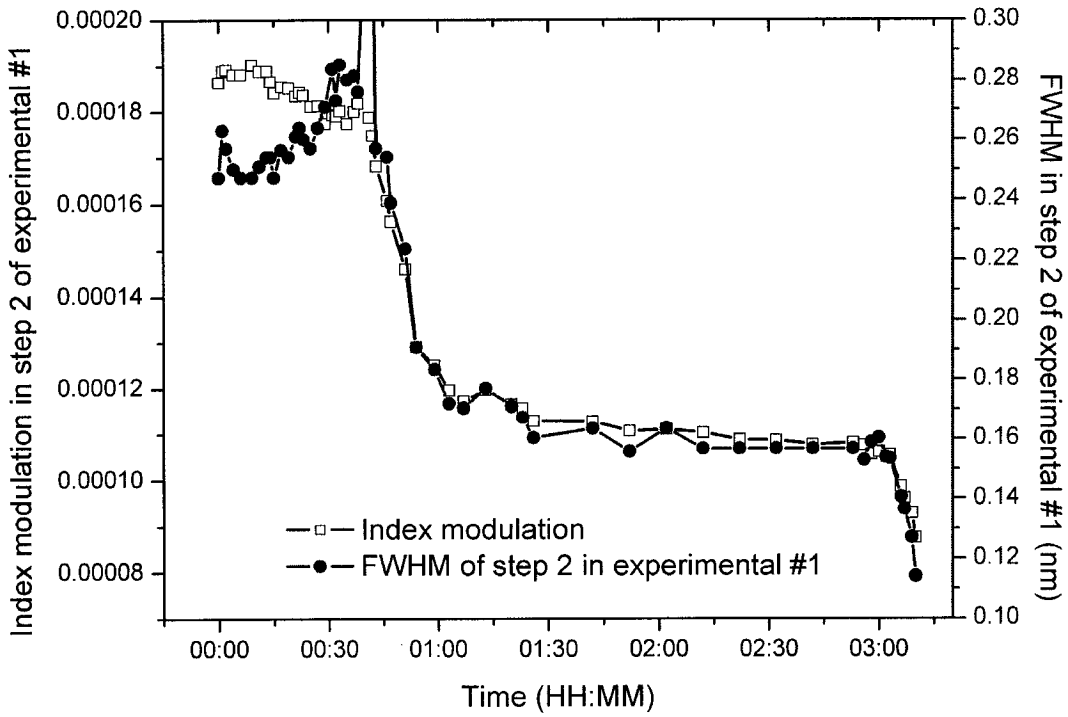

Figure 5.13 *The FWHM of grating sample #1 in experimental 1 is reduced followed by decreased index modulation with increased annealing temperature.*

We also pay a great attention to the maximum transmitted power showing in the Figure 5.11 and Figure 5.12. The spectrum of Figure 5.11 and 5.12 shows the maximum transmitted power are respectively -56.4 dBm and -58.8 dBm. That means the maximum transmitted power of the annealed gratings was decreased with the increased temperature. It is possible that the scattering loss of the grating was increased following the increased temperature.

Figure 5.14 shows part of the maximum transmitted power (grating sample #1) in step 1 of experimental #1. The annealed grating length is 8 cm long in this testing. While the maximum transmitted power was decreased form -59.93 dBm to -60.81 dBm with increased temperature from 304 °C to 463 °C, the reflectivity of grating sample #1 was decreased from 22.68 dB to 15.99 dB in the same temperature range.

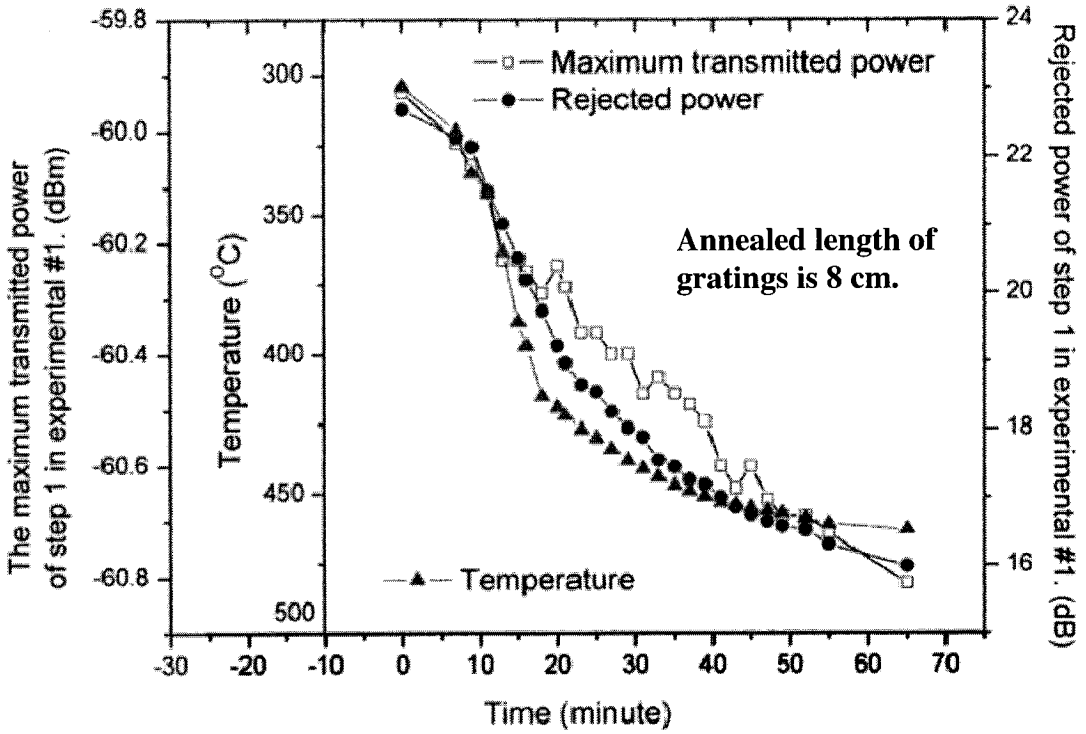

Figure 5.14 *The maximum transmitted power of tested grating sample #1in step1of experimental 1 was decreased follow the increased environment temperature. The annealed length of gratings is 8 cm long.*

As contrast, in the step #2 of experimental #1, the same fiber (grating sample #1) with 40 cm annealed grating length was reheated from room temperature to above 800 °C. The recorded results are enumerated in Figure 5.15. At the same temperature rang, which tested in step 1 of experimental #1, the maximum transmitted power was decreased form -57.32 dBm to -57.69 dBm as temperature increased from 286 °C to 463 °C and the reflectivity of grating sample #1 was reduced from 14.79 dB to 14.31 dB. By analyzing the results, it can be easily noticed that the loss of the maximum transmitted power in step 2 of experimental #1 is less than the loss of the maximum transmitted power in step 1 of experimental #1 (0.37 to 0.88 dB)

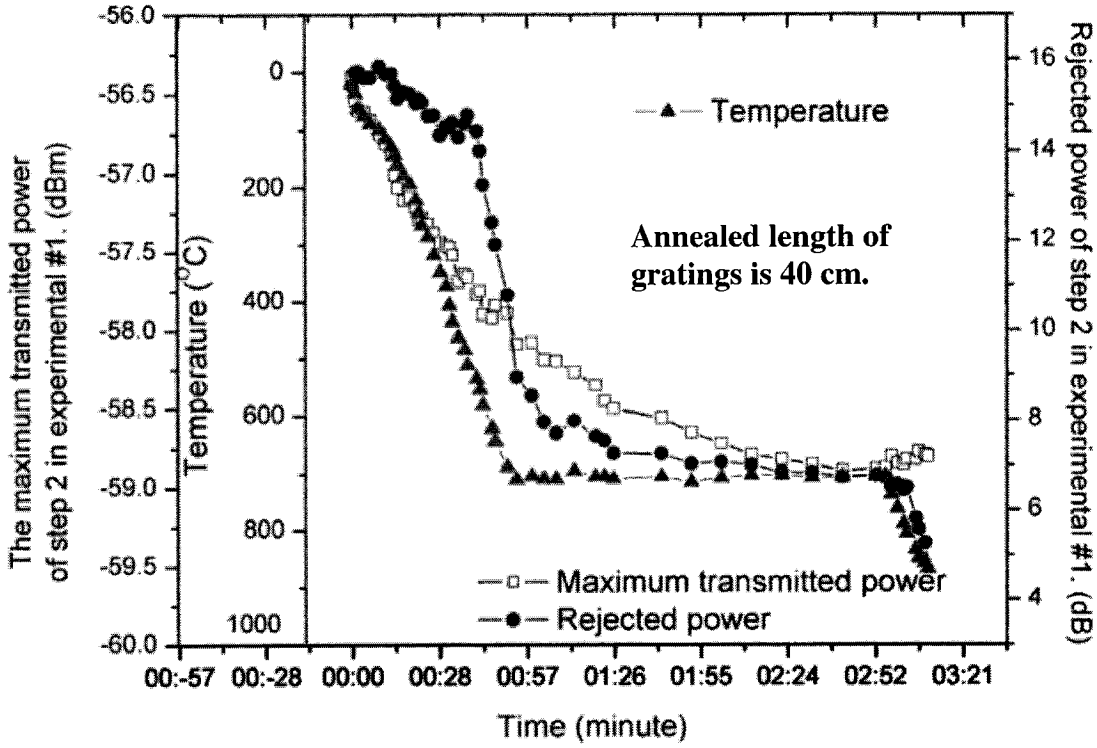

Figure 5.15 *The maximum transmitted power of tested grating sample #1in step 2 of experimental #1 was decreased follow the increased environment temperature. The annealed length of gratings is 30 cm long.*

Comparing the results of Figure 5.14 and 5.15, one can conclude that: The grating area has great scattering loss at high temperature and this scattering loss may be related to the reflectivity of the tested grating and the environment temperature. In the isothermal annealing with annealed temperature about 700 °C in experimental #1 step2, the reflectivity slowly inclines to a constant as shows in Figure 5.16, as the scattering loss in the grating area follows the trend of the change with the grating reflectivity can be clearly seen.

In chapter 4, we refered to the advantages of fiber Bragg grating temperature sensors. One of the advantages is that the grating temperature sensors can multiplexe together to build a WDM temperature sensor array; however, the number of grating

temperature sensor in the WDM temperature sensor array for high temperature applications could be limited by the scattering loss of fiber Bragg grating in high temperature range. To solve this problem, the EDFA need to be installed into the WDM temperature sensor array to amplify the injected light. In experimental #1, we found the thermal annealing is able to reduce the scattering loss of hydrogen-loaded fiber Bragg grating.

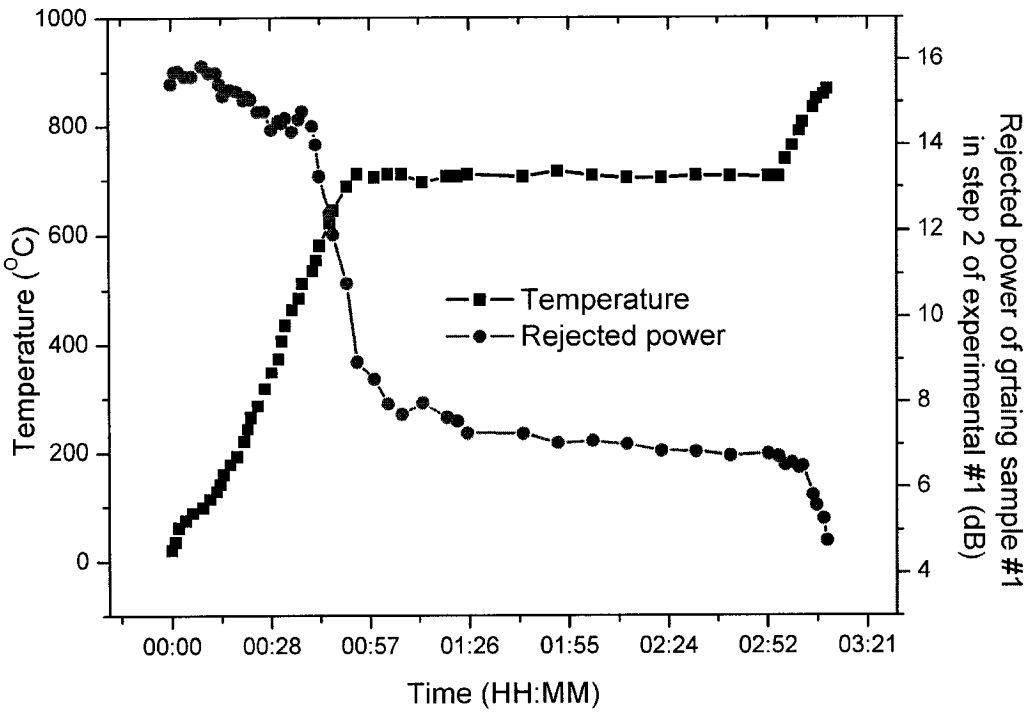

Figure 5.16 *The rejected power (reflectivity) of grating sample #1 in experimental #1 step2 at different temperature.*

Summary of this section:

1. The thermal treatment can reduce the FWHM of the hydrogen-loaded fiber Bragg grating. This speciality can increase the Bragg wavelength resolution of wavelength detect apparatuses.
2. The scattering loss of grating can affect the number of grating in the WDM

temperature sensor array.

3. The scattering loss of grating can be able to reduce by the high temperature thermal annealing. The sensor number of the temperature sensor array with WDM configuration can be increased using annealed hydrogen fiber Bragg grating.

5.4.3 Thermal decay of designed gratings in isothermal annealing

As it was explained in chapter 3, the thermal stability of gratings depends on several factors such as the type of fiber, hydrogenation, and the writing wavelength. Two fiber Bragg gratings, which are the grating sample #1 and sample #3, were tested respectively for isothermal decay in the experimental #1 and #4. The results and the calculated values from Erdogan's "power law" [40] are displayed in Figure 5.17.

Erdogan noted that the growth of the UV-induced index modulation follows the "power law". The decay data fit the functional form of Equation 3.6 ($\eta = 1/\left[1 + A(t/t_1)^{\alpha}\right]$) quite well. The decay of isothermal annealing is apparent from Figure 5.17. The grating decays very sharply at the beginning, but for the long time isothermal annealing the decay rate decreases (solid circuit in Figure 5.17 for the grating sample #1, in experimental #1). In Figure 5.17, the solid square curve is the normalized reflectivity of grating sample #3 in experimental #4, and the filled circuits are the normalized reflectivity of grating sample #1 in experimental #1.

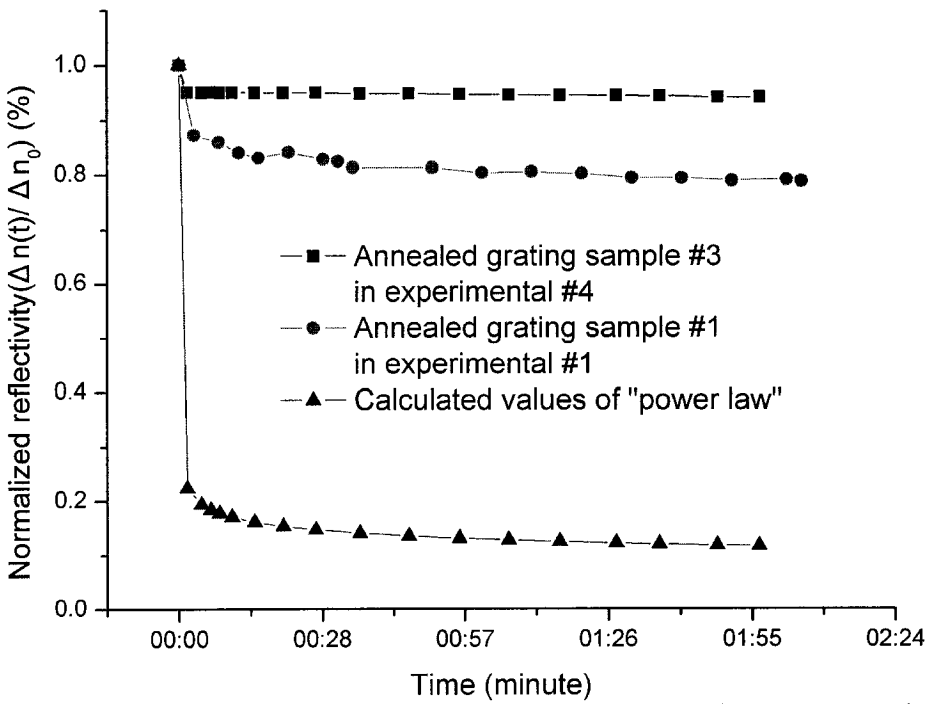

Figure 5.17 *The isothermal decay at 700 °C of annealed grating sample #1 and sample #3 in experimental 1 and 4. The triangle samples display the calculated values using Erdogan's "power law" at 700 °C.*

Figure 5.17 demonstrated that the reflectivity decay of sample #1 is only 20% after it was placed in a temperature around 700°C for 2 hours. This shows that the decay of isothermal annealing of grating sample #1 will be limited (astringently), because of the unchanged reflectivity at longer annealing time (solid circuit curve). This characteristic phenomenon matches to the Erdogan's description of "power law". The characters of the tested fiber Bragg grating samples show in Table 5.5.

Table 5.5 shows that the index modulation of grating sample #3 is much great than the index modulation of grating sample #1. According to our experimental results showing in Figure 5.17, the thermal stability of grating sample #3 is much better than that of grating sample #1 (94% and 79% reflectivity after two hours thermal annealing). This outcome proves the second and the third hypothesis being described in chapter 4. The

second hypothesis detailed the depth of the traps, which is eliminated and forced to stop at the saturation level. The DID in gratings is coincident to the Gaussian distribution with flattop. The third hypothesis shows the trapped electrons, which will fill in the shallower traps (lower activation energies) at first, are excited by UV excitation. Then the excited electrons fill in the deeper traps (high activation energies) after the depth of shallower traps (lower activation energies) is saturated.

Table 5.5 Characteristics of fiber Bragg grating sample #1 and sample #3.

Parameters / Samples	TCWL (nm)	FWHM (nm)	Reflectivity (%)	Length of grating	Index modulation
Sample 1	1550.16	0.33	99.62	8 mm	3.6×10^{-4}
Sample 3	1483.981	0.48	99.97	5 mm	5.4×10^{-4}

Figure 5.17 also shows the Erdogan's "power law" with original fitting parameter (see chapter 3 and section 3.3) can not conform to the thermal decay curve of grating sample #1 and sample #3. In this section, the experimental results verify our hypothesis in chapter 4. It is confirmed that the hydrogen loaded fiber Bragg grating with small bandwidth (FWHM) is less thermal stability than those with wider bandwidth (FWHM).

The index modulation is an important criterion of the fiber Bragg grating. The calculated values of fiber index modulation at different temperatures are presented in Figure 5.18.

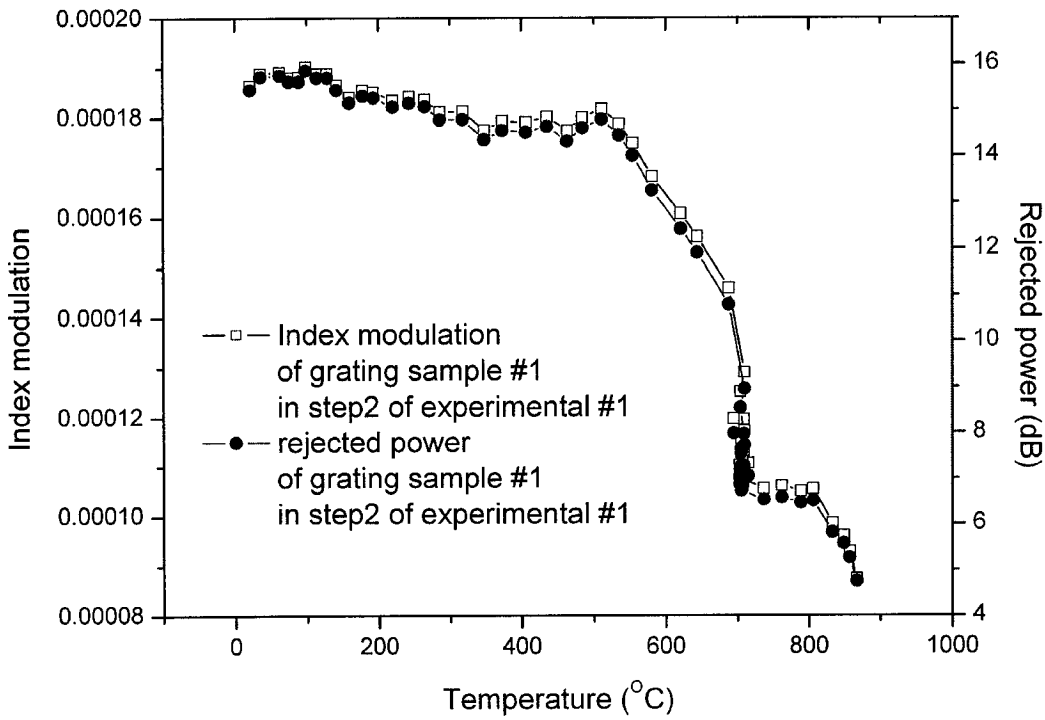

Figure 5.18 *The decay of calculated fiber index modulations in step 2 of experimental 1 obeys the thermal decay of fiber Bragg grating sample #1.*

In Figure 5.18, firstly, the hollow symbols are the calculated index modulation of grating sample #1 in step 2 of experimental #1with measurand reflectivity (%) at different temperatures. Equation 2.8 ($R(L,\lambda) = \tanh^2(\Omega L)$) is used in this calculate. The following parameters are used during the calculation of index modulation (please see chapter 2): $NA = 0.14, a = 4.2\ \mu\text{m}$, and the grating length $L = 8$ mm. Secondly, the filled circles are the reflected ability of fiber Bragg grating sample #1 at different temperature in step2 of experimental #1. Figure 5.18 shows clearly that the grating sample #1 has 4 dB decays of isothermal annealing at 700 °C. During the measurement process, the index modulation of grating sample #1 displayed in figure 5.18 was decreased following the thermal decay of the grating.

5.4.4 Thermal decay of designed gratings in annealing process

Because fiber Bragg gratings are compact intrinsic temperature sensing elements, the fiber Bragg grating temperature sensor reflects one particular wavelength and transmits all others; moreover, the reflected wavelength (Bragg wavelength) can vary with the changing of sensor's temperature. The relationship between Bragg wavelength and the tested environment temperature for different designed fiber Bragg gratings are displayed in Figure 5.6. By summarizing all the results in four different experimental testing, the rate of Bragg wavelength shift corresponding with temperature is very close, even though three designed hydrogen loaded fiber Bragg grating come from different companies with different fabricated parameters. The thermal decay can cause the blue shift of the Bragg wavelength; however, this blue shift will be inconspicuous through the annealing treatment with ultra high temperature.

As to high temperature sensor applications, an important criterion is that the ability of grating is stable at high temperature. Although the fibers Bragg gratings are often referring to permanent refractive index structures, exposure to increased temperature circumstance usually results the decay of the refractive index modulation. The reflectivity will be erased completely at sufficiently high temperature. Since the temperature sensing ability of the fiber Bragg grating is based on the Bragg wavelength of gratings, the stability of fiber Bragg grating reflectivity is more important at high temperature range. In fact, the design of high temperature fiber Bragg grating sensors is to solve the problem, which is the thermal decay of the fiber Bragg grating temperature sensor in the high temperature range.

According to our theory in chapter 4, the increased index modulation of the fiber Bragg grating can have more resistance of the thermal erasing of fiber Bragg grating. The index modulation of gratings depends on several factors such as the doping level of germanium in silica fiber [30], the co-doping level of germanium doped silica fiber [30], the hydrogenation [31], and the writing method. Due to the hydrogen loaded germanium doped fiber Bragg grating has the highest index modulation of gratings [29]; we choose the hydrogen-loaded fiber Bragg grating as our testing samples. Table 5.6 shows the parameters of the designed hydrogen loaded fiber Bragg grating in this work.

Table 5.6 Characteristics of fiber Bragg grating in this work.

Parameters / Samples	TCWL (nm)	FWHM (nm)	Reflectivity (%)	Length of grating	Index modulation
Sample 1	1550.16	0.33	99.62	8 mm	3.6×10^{-4}
Sample 2	1484.138	0.45	99.98	5 mm	5.5×10^{-4}
Sample 3	1483.981	0.48	99.97	5 mm	5.4×10^{-4}

So, the ability of reflectivity of hydrogen-loaded fiber Bragg grating against the thermal annealing can be described as follow based on the three hypotheses in this thesis:

1. The grating sample #1 has the lowest thermal stability among the three fiber Bragg gratings, because it has the lowest index modulation as in Table 5.6.
2. The index modulations of grating sample #2 and sample #3 are very close. Therefore, the characteristics of these two gratings are almost the same in the thermal annealing testing.

The thermal decays of grating sample #1, sample #2, and sample #3 are plotted in Figure 5.19, Figure 5.20, and Figure 5.21 respectively.

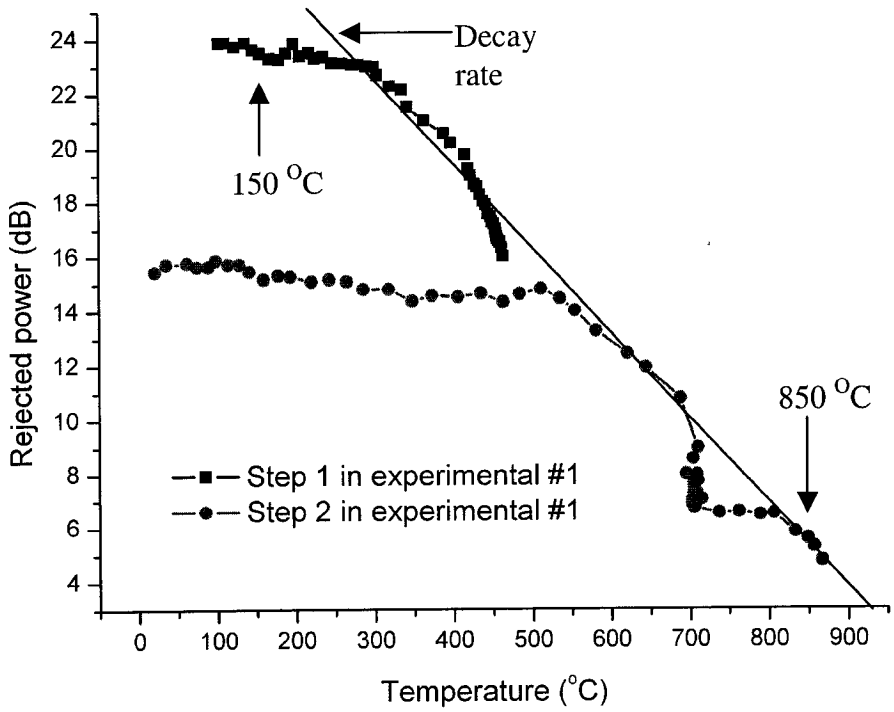

Figure 5.19 *The thermal decay of grating sample #1 of step 1 and step 2 in experimental 1[59]. The reflectivity of grating sample #1 at 867°C is 4.75 dB or 66.5%. The grating has 4 dB thermal decays at 700 ° for two hours isothermal annealing.*

As Figure 5.19 shows, the decay of reflection in grating sample #1 is started around 150°C (filled square curve). No sudden interrupt was observed for temperature up to 850°C (filled circuit curve). Our results of step 1 and step 2 in experimental #1 display the decay rate is nearly constant. In the step 2 of experimental #1, we found the thermal decay of reflectivity, which is the grating sample #1 at temperature range from room temperature to around 470°C, is very small; however, when the temperature increases over 470°C, the decay rate of the sample becomes large and it follows the same pattern as step #1 in experimental #1. This phenomenon can be described as follow: The reflectivity of the sample #1, which is in the step 2 at temperature range from room temperature to 470°C, is provided by reflectivity being the lowest reflectivity in the step 1 of

experimental #1. We name this phenomenon as reflectivity-remembrance of the fiber Bragg grating [58].

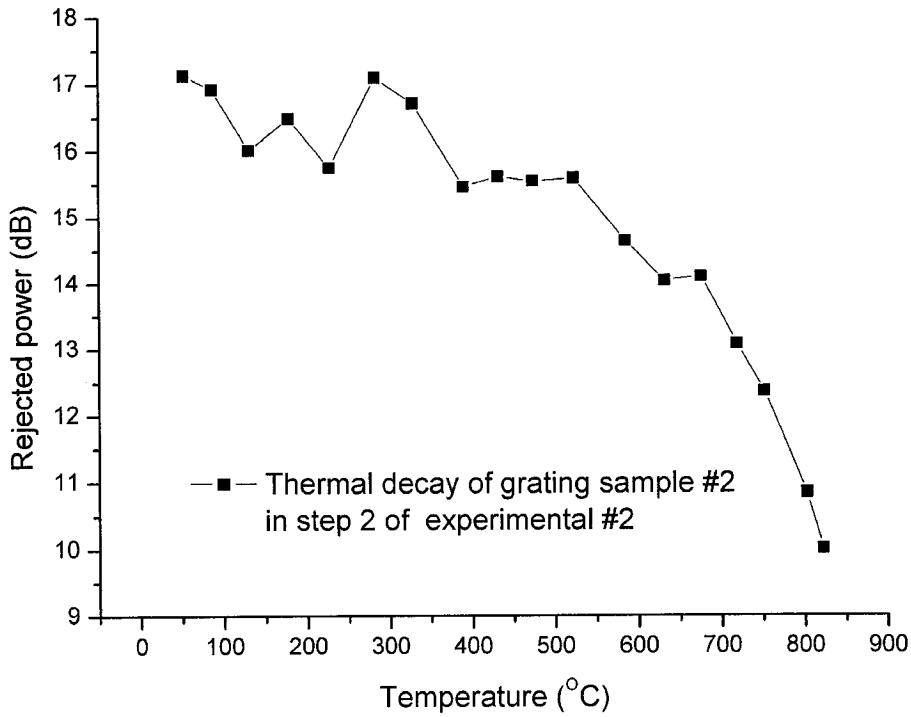

Figure 5.20 *The thermal decay of grating sample #2 in temperature range from room temperature to ultra high temperature for grating sample #2. The reflectivity at temperature around 820 °C is 10 dB or 90%.*

The results of grating sample #2 are plotted in Figure 5.20. This sample was given the same fabricated method as sample #1; however, it has different Bragg wavelength and reflectivity. The thermal decay of reflectivity of grating sample #2 started at temperature of 50°C and this grating survived at temperature in excess of 820°C (with 90% reflectivity).

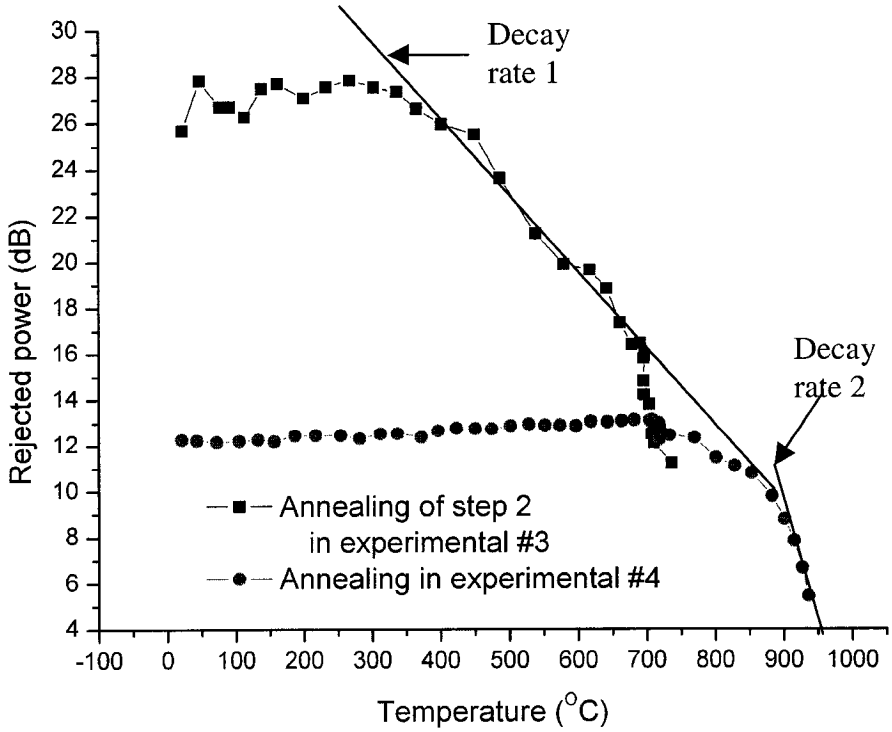

Figure 5.21 *The thermal reflectivity decay of grating sample #3 at temperature range from room temperature to 936°C for step 2 in experimental 3 and experimental 4.The reflectivity of grating sample #3 at 936°C is 5.43 dB or 71.4%. The grating has 3.7 dB thermal decays at 700 ° for about two hours isothermal annealing (black squares).*

The thermal decay in grating sample #3 is started around 200°C, because of the pre annealing of step1 in experimental #3 (filled square curve). No sudden interrupt was observed for temperature up to 936°C (filled circuit curve). The decay rate (decay rate 1 in Figure 5.21) is nearly constant in our measurement from 200 °C to 850 °C; however, at temperature between 850 °C to 935 °C, the thermal decay rate (decay rate 2 in Figure 5.21) changes sharply. In the experimental #4, the thermal decay of the sample #3 at temperature range from room temperature to around 700 °C becomes negative; however, when the temperature was over 700 °C, the decay rate of the sample was alike in the step 2 of experimental #3.

The thermal decay is an important criterion for high temperature fiber Bragg grating design. The decay of the grating's reflectivity may beget some worrying problems, such as loss the sensing ability of grating (erasing problem) and the blue shift of Bragg wavelength. The first hypothesis of "power law" (See chapter 4), which says the thermal ability of fiber Bragg gratings, can be increased by annealing treatment. In experimental #1 (Figure 5.19), the annealing hydrogen loaded fiber Bragg grating confirmed the first hypothesis partly. The annealed grating sample #1 still has a little reflectivity decay at the temperatures below 450 °C (1 dB or 0.8%). According to our theory (first hypothesis), we deemed that the problem concerning the annealing time is not long enough. The trapped electrons with activation energies at the temperature below 450 °C do not move back to the conduction band fully. By this token, if we expect the grating sample #1 with non thermal decay at temperature of 450 °C, we can increase the annealing time until the whole trapped electrons back to conduction band. In the experimental #3 and #4, we repeat the same process as the testing process in experimental #1; however, we increased the annealing temperature from 450 °C to around 700 °C and annealing time from 30 minutes to one hour. The results of grating sample #3 in experimental #3 and #4 were plotted in Figure 5.21. This figure clearly shows the start point of thermal decay of grating sample #3 in experimental #4 (filled circuit curve) is above 700 °C and grating sample #3 in experimental #4 has no thermal decay for temperatures below 700 °C.

The reflectivity of grating sample #3 in experimental #4 is increased from 12.25 dB to 13.08 dB as the temperature increased from room temperature to 704 °C. In terms of optical fiber, this phenomenon is called as "negative index modulation".

The "negative index modulation" is a typical index modulation in Type II fiber Bragg gratings. As described in chapter 2, the fiber Bragg gratings formed at low intensities UV laser are generally referred to Type I gratings. Type II fiber Bragg gratings are formed under very high, single-pulse UV laser (>0.5J/cm^2). It has distinction to all of the grating types. One of the examples will be the thermal stability in high temperature range. The typical Type II Bragg gratings have much higher decay temperature than Type I gratings, being stable up to 800 ^{O}C [7] or higher. This type of grating is a damaged grating, which is caused in the fiber core on the side of the laser beam within a few nanoseconds time period. The sudden growth of the refractive index is accompanied by a large short wavelength loss as shown in Figure 2.5; thus, Type II gratings are not useful in sensor applications.

By using the high temperature annealing treatment, the hydrogen loaded Type I fiber Bragg grating with nearly 100% reflectivity is changed to the Type II grating. As we know, Type II fiber Bragg grating has excellent thermal stability compare with Type I and Type IIA gratings (see chapter 2). Due to the inherence limitation of Type II fiber Bragg grating, it is unuseful for temperature sensor applications. For example, Type II grating needs very strong UV laser as writing source and it can block the blue-side wavelength. Nowadays, we have a new method to produce high thermal stability grating using hydrogen loaded fiber Bragg grating for the temperature sensor applications. The grating sample #3, which tested in experimental #4, works perfectly under 700 °C with reflectivity as high as 13 dB or 95%.

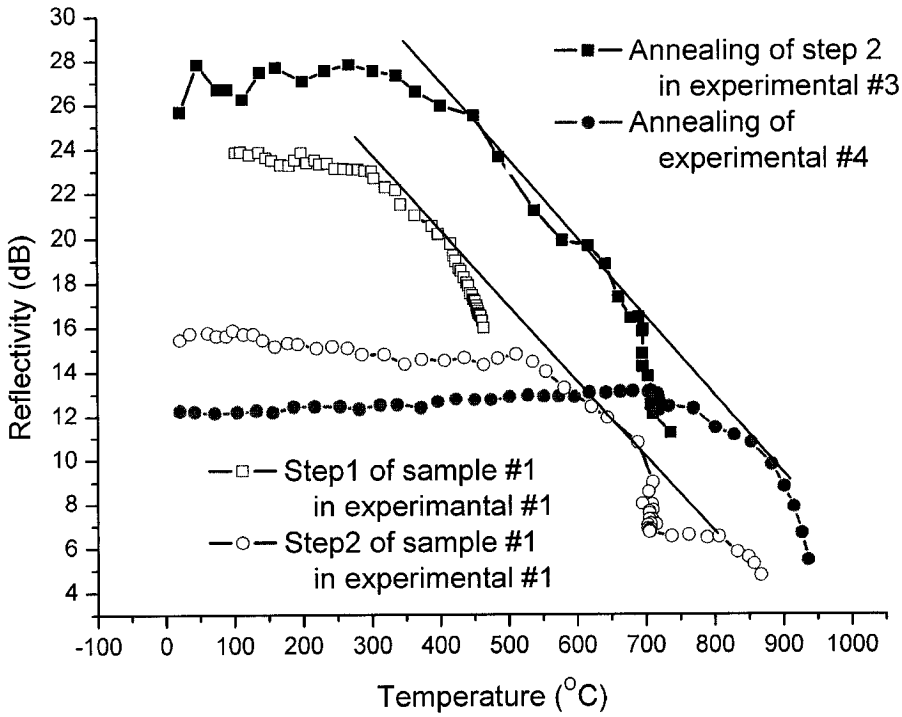

Figure 5.22 *The combination results of grating sample #1 and sample #3 in thermal annealing process.*

Combining Figure 5.19 and Figure 5.21 together, the recorded results of grating sample #1 and sample #3 plotted in Figure 5.22. The reason of making this combination is because of our interest in the thermal decays for the different index modulation. The hollow symbols are the recorded results in experimental #1 of the thermal decays of grating sample #1. The measurand data in experimental #3 and #4 were plotted as solid symbols in Figure 5.22.

Grating sample #1 and sample #3 were from different companies and have different Bragg wavelength (1550 nm and 1480 nm), but they both have the common characteristics. All of the gratings are hydrogen loaded conventional optical fiber with strong reflectivity (near 100%). In Figure 5.22, the recorded data show the similarity of the thermal decay rates of the two grating samples (grating sample #1 and sample #3) (in

dB level). At the same time, we also noticed the differences in reflectivity of the grating sample #1 and sample #3 (5dB different). The results in Figure 5.22 can be probably described as following: Fiber Bragg gratings with the same characteristic (hydrogen loaded fiber Bragg grating with near 100% reflectivity) provide with the same thermal decay characters. The best thermal stability of the fiber Bragg grating of the three grating samples should be the one that has the biggest rejected ability or largest index modulation of the grating samples. These results notarize the correctness of our theory (second and third hypotheses) discussed in chapter 4.

At the same time, we compared the thermal stability of grating sample #1 and sample #3; we also compared the thermal stability of grating sample #2 and sample #3. The combination results exhibit in Figure 5.23.

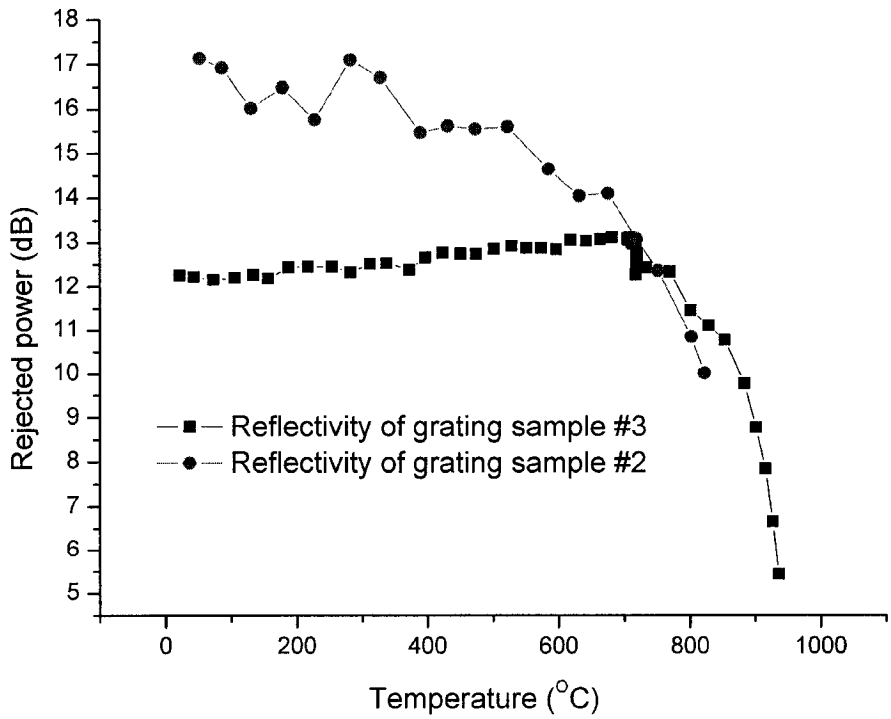

Figure 5.23 *The combination results of grating sample #2 and sample #3 in thermal annealing process.*

In the experimental grating annealing tests (experimental #2, #3, and #4), the tested gratings were heated in the different way to achieve the temperature above 800 °C. The recorded results of grating sample #2 show the grating sample #2 has the reflectivity of 10.84 dB at temperature of 802 °C. In contrast, the reflectivity of grating sample #3 at temperature 801 °C is 11.45 dB. The difference of the thermal stability between grating sample #2 and sample #3 is 0.6 dB. This difference is too trifling to be ignored. The practical results tally with theoretical forecasting.

The primary result, which is explained in this section, is the reflectivity-remembrance of the fiber Bragg grating. The phenomenon of reflectivity-remembrance can be described as following: If the fiber Bragg grating was annealed at a fixed temperature for a sufficiently long time, the grating structure becomes stable and the thermal decay could be ignored. Afterwards, if operating temperatures are lower than the annealing temperature, the grating generally does not experience any thermal decay. Thus it can be seen that the experimental results attest to our three hypotheses and the design of high temperature grating sensor (see chapter 4). The thermal stability of hydrogen loaded fiber Bragg grating is related to the amount of the index modulation of the grating. If the gratings have similar characteristics, they will have the same thermal stability.

Chapter 6
Conclusions and future direction

6.1 Conclusions

The theme of this research has been related to hydrogen loaded fiber Bragg grating high temperature sensor. The research has brought us significantly better understanding of the underlying mechanism of the refractive index modulation, which has been attributed to the changes at high temperature. The mechanisms regarding thermal stability/decay of fiber Bragg gratings at high temperatures have also been studied.

As we introduced in chapter 4, fiber Bragg gratings are compact intrinsic temperatures sensing elements. Although fiber Bragg gratings are often referring to permanent refractive index structures, exposure to increased temperature environment usually results the decay of the refractive index modulation. Basically, an important criterion of fiber Bragg grating for high temperature sensor applications is that the grating's strength is stable at high temperature. The design of fiber Bragg grating for high temperature sensor applications needs to solve the problems involving thermal decay of the gratings at high temperature. In this thesis, three hypotheses based on the Erdogan's "power law" were proposed. The result of three hypotheses can be summarized as following: thermal treatment can increase the thermal stability of hydrogen-loaded fiber Bragg grating. Increasing index modulation of grating makes it possible that the grating temperature sensor works at higher temperature.

To justify these hypotheses, three hydrogen-loaded fiber Bragg grating were designed and tested. A basic setup built in our lab to examine the performance of the

point temperature sensor based on the hydrogen-loaded fiber Bragg grating. Until now, a grating has been shown to stabilize at temperatures in excess of 700°C and to survive at temperatures in excess of 930°C. The evaluations show the tested operation gratings around temperature of 700°C retain up to 94% reflectivity after two hours annealing. The experiments show that the thermal treatment of the tested hydrogen loaded fiber Bragg gratings can enhance effectively the grating's thermal stability. Our experimental results provide a better understanding of thermal response to the hydrogen-loaded fiber Bragg gratings and their decay behavior at elevated temperatures.

The experimental results have proved the three hypotheses, which were described in chapter 4. If the fiber Bragg grating was annealed at a fixed temperature for a sufficiently long time, the grating structure becomes stable and the thermal decay could be ignored. Afterwards, if the operating temperatures lower than the annealing temperatures, the grating generally will not experience any thermal decay. The thermal stability of hydrogen loaded fiber Bragg grating is related to the amount of the index modulation of the grating. In other words, if the gratings have similar characteristics, they will have the same thermal stability.

Our evaluations of devices show that the thermal responsivity at zero strain of grating is not constant. The thermal responsivity, which is the normalized change of the Bragg wavelength with environment temperature, is increased from 10 pm/°C to 17 pm/°C at temperature range from room temperature to 700 °C.

6.1 Future direction

Although the research outcomes presented in this thesis give us the gratifying explanations about several properties of hydrogen loaded fiber Bragg grating temperature

sensors, there are other issues that need to study. For instance, how does the sensitivity of the annealed hydrogen loaded fiber Bragg grating change in lower temperature range? In what way does annealing impact the blue shift of Bragg wavelength and what shall we do to find an improved method to reduce the thermal treatment etc.?

Reference

1. Stephen R. Baker, Howard N. Rourke, Vernon Baker, and Darren Goodchild, "Thermal decay of fiber Bragg gratings written in boron and germanium codoped silica fiber," J. Lightwave Technol. 15(8), 1470-1477,(1997)
2. Sungchul Kim, Seungwoo Kim, Jaejoong Kwon, and Byoungho Lee,"Fiber Bragg Grating Strain Sensor Demodulator Using a Chirped Fiber Grating," IEEE Photonics Technology Letters, 13, 839-841, (2001)
3. P. Anderegg, R. Brönnimann, M. Stahl, "Langzeit- und Fernüberwachung von Bauwerken," VDI, BERICHTE NR. 1463, 475-482, (1999)
4. http://www.fft.com.au/original/backgrnd.shtm
5. Byoungho Lee, "Review of the present status of optical fiber sensors," Optical Fiber Technology 9, 57–79 (2003)
6. R. Kashyap, *Fiber Bragg Gratings*, Academic Press (1999).
7. A. Othonos and K. Kalli, *Fiber Bragg Gratings: Fundamentals and Applications in Telecommunications and Sensing*, Artech House, (1999).
8. N.M. Theune, M. Kaufmann, P. Krämmer, M. Willsch, T. Bosselmann, "Applications of Fiber Optical Sensors in Power Generators: Current and Temperature Sensors," Proceedings OPTO 2000 Conference, 22-25 May 2000.
9. Lars Gruener-Nielsen, Joerg Hueber, "Photosensitive fiber for highly reflective Bragg gratings," WL16, Technical Digest, Optical Fiber Comminication Conference (OFC97), 1997.
10. D.K.W. Lam and B.K. Garside, "Characterization of single-mode optical fiber

filters." Applied Optics, 20 (3), 440-445 (1981).

11. G. Meltz, W. W. Morey, W. H. Glenn, "Formation of Bragg gratings in optical fibers by transverse holographic method," Opt. Lett., **14** (15), 823-825 (1989).
12. P. St. J. Russell, J. L. Archambault, L. Reekie, "Fibre gratings," Physics World, pp. 41-46 October (1993).
13. K. O. Hill, Y. Fujii, D. C. Johnson, B. S. Kawasaki, "Photosensitivity in optical fiber waveguides: Application to reflection filter fabrication," Appl. Phys. Lett., **32**(10), 647-649 (1978).
14. I. Riant, "UV-photoinduced fibre gratings for gain equalisation," Opt. Fiber Technol., **8**, 171-194, (2002).
15. M. Vengsarkar, P. J. Lemaire, J. B. Judkins, V. Bhatia, T. Erdogan, J. E. Sipe, "Long-period fiber gratings as band-rejection filter," J. Lightwave Technol., **14**(1), 58-65 (1996).
16. S. Choi, K. R. Kim, and K. Oh, "Interferometric inscription of surface relief gratings on optical fiber using azo polymer film," Appl. Phys. Lett. **83**, 1080-1082 (2003).
17. J.-L. Archambault, L. Reekie, P. St. J. Russel, "100% reflectivity Bragg reflectors produced in optical fibres by single excimer laser pulses," Electron. Lett., **29**, 453-455 (1993).
18. D. Wiesmann, J. Hübner, R. Germann, I. Massarek, H.W.M. Salemink, G.L. Bona, M.Kristensen and H. Jäckel, "Large UV-induced negative index changes in germanium-free nitrogen-doped planar SiO2 waveguides," Electron. Lett., **34**(4) (1998).
19. M. Douay, W. X. Xie, T. Taunay, P. Bernage, P. Niay, P. Cordier, B. Poumellec, L.

Dong, J. F. Bayon, H. Poignant, E. Delevaque, "Densification involved in the UV-based photosensitivity of silica glasses and optical fibers," J. Lightwave Technol., **15**, 1329-1342 (1997).

20. Akifumi Sakoh, Masahide Takahashi, Toshinobu Yoko, Junji Nishii, Hiroaki Nishiyama, Isamu Miyamoto, "Photochemical process of divalent germanium responsible for photorefractive index change in GeO_2-SiO_2 glasses." Optics Express, **11** (21), 2679-2688 (October 2003).
21. R. M, Atkins, V. Mizrahi, and T. Erdogan, "248 nm induced vacuum UV spectral changes in optical fibre preform cores: support for a color centre model of photosensitivity," Electron. Lett., **29**, 385 –387 (1993).
22. R. M, Atkins, and V. Mizrahi, "Observations of changes in UV absorption bands of signal mode germamosilicate core optical fibres on writing and thermally erasing refractive index gratings," Electron. Lett., **28**, 1743-1744 (1992).
23. D. S. Starodubov, V. Grubsky, J. Feinberg, B. Kobrin, S. Juma, "Bragg grating fabrication in germanosilicate fibers by use of near-UV light: a new pathway for refractive index changes," Opt. Lett., 22, 1086-1088 (1997).
24. B. Malo, J. Albert, K.O. Hill, F. Bilodeau, and D.C. Jonson, "Effective index drift from molecular hydrogen diffusion in hydrogen-loaded optical fiber and its effect on Bragg grating fabrication," Electron. Lrtt. **30**(5), 442-444, (1994)
25. P. J. Lemaire, A. M. Vengsarkar, W. M. Reed, D. J. DiGiovanni, "Thermally enhanced ultraviolet photosensitivity in GeO2 and P2O5 doped optical fibers," Appl. Phys. Lett., **66**, 2034-2036 (1995).
26. E. Salik, D. S. Starodubov, V. Grubsky, and J. Feinberg "Increase of photosensitivity

in Ge-doped fibers under strain," TuH5 - Fiber Bragg Gratings, Optical Fiber Comminication Conference (OFC2000), March 5-10, 2000.

27. D. L. Williams, B. J. Ainslie, J. R. Armitage, R. Kashyap, and R. Campbell, "Enhanced UV photosensitivity in boron codoped germanosilicate fibres," Electron. Lett., **29**(1), 45-47 (1993).
28. H.G. Limberger, P.Y. Fonjallaz,; R.P. Salathe, "Spectral characterisation of photoinduced high efficient Bragg gratings in standard telecommunication fibres," Electron. Lett., **29**(1), 47-49 (1993).
29. P. J. Lemaire, R. M. Atkins, V. Mizrahi and W. A. Reed, "High-pressure H2 loading as a technique for achieving ultrahigh uv photosensitivity and thermal sensitivity in GeO2 doped optical fibers," Electron. Lett., **29**, 1191-1193 (1993)
30. T Sun, S Pal, J Mandal, K T V Grattan, "Fibre Bragg grating fabrication using fluoride excimer laser for sensing and communication applications," School of Engineering, City University, Northampton Square, London, UK, Central Laser Facility Annual Report 147-149, (2001/2002)
31. Bragg Photonics Inc. 880 Selkirk, Pointe-Claire (QC) Canada
32. K. Noguchi, N. Shibata, N. Uesugi, and Y. Negishi, "Loss Increase for Optical Fibers Exposed to Hydrogen Atmosphere." Journal of Lightwave Technology, VOL. LT-3, NO. 2, APRIL 1985
33. Koichi Awazu, Hiroshi Kawazoe, and Masayuki Yamane, "Simultaneous generation of optical absorption bands at 5.14 and 0.452 eV in 9 SiO_2 :GeO_2 glasses heated under an H_2 atmosphere." Journal of Applied Physics, **68**(6) pp. 2713-2718 (1990).
34. V. Grubsky, D. S. Starodubov, J. Feinberg, "Photochemical reaction of hydrogen with

germanosilicate glass initiated by 3.4-5.4-eV ultraviolet light," Opt. Lett., 24, 729-731 (1999).

35. J. Stone, "Interactions of Hydrogen and Deuterium with Silica Optical Fibers: A Review," Journal of Lightwave Technology, LT-5, 712-733 (1987).
36. T. A. Nguty and R. J. Potton, "Photochemical changes in hydrogen-loaded optical fibres with application to Bragg grating formation," Meas. Sci. Technol. 8, 1055–1058 (1997).
37. G. Brambilla, and H. N. Rutt, "Fiber Bragg gratings with enhanced thermal stability," Applied Physics Letters 80, 3259-3261 (2002).
38. Tsung-Ein Tsai, Glen M. Williams, and E. Joseph Friebele, "Index structure of fiber Bragg gratings in Ge–SiO2 fibers," Optics Letters 22, 224-226 (1997).
39. R.J. Egan, H.G. Inglis, P. Hill, Peter A. Krug, F. Ouellette, "Effects of hydrogen loading and grating strength on thermal stability of fiber Bragg gratings," in Technical Digest series on Conference on Optical Communications, OFC´96, Paper TuO3, 83-84 (1996).
40. T. Erdogan, V. Mizrahi, P. J. Lemaire, and D. Monroe, "Decay of ultraviolet induced fiber Bragg gratings," J. Appl. Phys., 1, 73-80 (1994).
41. S. Kannan, J. Z. Y. Guo, P. J. Lemaire, "Thermal stability analysis of UV-induced fiber Bragg gratings," J. Lightwave Technol., **15**, 1478-1483 (1997).
42. A.D. Kersey, M.A. Davis, H.J. Patrick, M. LeBlanc, K.P. Koo, C.G. Askins, M.A. Putnam, and E.J. Friebele, "Fiber Bragg grating sensors," J. Lightwave Technol., 15, pp.1442 (1997)
43. Bowei Zhang, Mojtaba Kahrizi, "Wide range periodic waveguide temperature

sensor," Proceeding of the Canadian Conference on Electrical and Computer Engineering (CCECE) 2003, pp. 117-121, Montreal, Canada, 2003

44. Francis T.S. Yu and Shizhuo Yin, ***Fiber Optic Sensors***, the Pennsylvania State University, University Park, PA, U.S.A., 2002

45. A. D. Kersey, T. A. Berkoff, and W. W. Morey, "High-resolution fibre-grating based strain sensor with interferometric wavelength-shift detection," Electron. Lett. 28, pp. 236–238 (1992).

46. G. Brambilla, "High-temperature fibre Bragg grating thermometer," Electron. Lett. 38, pp. 954-955 (2002)

47. H. Patrick and S. L. Gilberta, "Annealing of Bragg gratings in hydrogen-loaded opticall fiber," Journal of Applied Physics, 78, pp. 2940-2945 (1995).

48. Youlong Yu and Hwayaw Tam, A technique for enhancing the thermal stability of hydrogen-loaded fiber Bragg grating, Chinese Opt. Lett. 1, pp. 256-258 (2003)

49. Suchandan Pal, Jharna Mandal, Tong Sun, Kenneth T. V. Grattan, "Analysis of Thermal Decay and Prediction of Operational Lifetime for a Type I Boron-Germanium Codoped Fiber Bragg Grating," Applied Optics, 42, pp. 2188-2197 (2003).

50. Arif Hidayat, Qinglin Wang, Pierre Niay, Marc Douay, Bertrand Poumellec, Farid Kherbouche, I. Riant, "Temperature-Induced Reversible Changes in the Spectral Characteristics of Fiber Bragg Gratings," Applied Optics, 40, pp. 2632-2642 (2001).

51. Qinglin Wang, Arif Hidayat, Pierre Niay, Marc Douay, "Influence of Blanket Postexposure on the Thermal Stability of the Spectral Characteristics of Gratings Written in a Telecommunication Fiber Using Light at 193 nm," Journal of Lightwave

Technology, 18, pp. 1078-1083 (2000).

52. Stephen J. Mihailov, Christopher W. Smelser, Ping Lu, Robert B. Walker, Dan Grobnic, Huimin Ding, and George Henderson, "Fiber Bragg gratings made with a phase mask and 800-nm femtosecond radiation," Optics Letters, 28, pp. 995-997 (2003).

53. B. Malo, J. Albert, F. Bilodeau, T. Kitagawa, D. C. Johnson, K. O. Hill, K. Hattori, Y. Hibino, and S. Gujrathi, "Photosensitivity in phosphorus-doped silica glass and optical waveguides," Applied Physics Letters, 65, pp. 394-396 (1994).

54. L. Dong, J.L. Cruz, L. Reekie, M.G. Xu y D.N. Payne, "Enhanced photosensitivity in Tin-codoped germanosilicate optical fibers," IEEE Photonics Technology Letters, 7, pp.1048-1050 (1995).

55. W.F. Liu, L. Dong, L. Reekie, D.N. Payne, "Complex decay behavior of fiber Bragg gratings: further evidence of three-energy-level system of photosensitivity in germanium-doped optical fibers," Proc. Conference on Optical Fiber Communications OFC'97, Technical Digest Thj7, pp.287-288 (1997).

56. Kevin P. Chen, Peter R. Herman, and Robin Tam, "Strong Fiber Bragg Grating Fabrication by Hybrid 157- and 248-nm Laser Exposure," IEEE Photonics Technology Letters, 14, pp. 170-172 (2002).

57. G. Brambilla and H. N. Rutt, "Fiber Bragg gratings with ultra-high temperature-stability," In Proceedings of Optical Fiber Communications Conference (OFC) 2002, Anaheim, USA (2002).

58. Bowei Zhang, Mojtaba Kahrizi, "High-Temperature Bragg Grating Waveguide Sensor," Sensor Letters, submitted.

59. Bowei Zhang, Mojtaba Kahrizi, "High-Temperature Bragg Grating Waveguide Sensor," International Conference on MEMS, NANO and Smart Systems (ICMENS'03), pp. 400-404, Banff, Alberta, Canada, 2003